UNIVERSITY OF CALGARY

Seismic Performance of Masonry Walls with GFRP and Geogrid Bed Joint Reinforcement

by

Husam Adnan Sadek

A THESIS

SUBMITTED TO THE FACULTY OF GRADUATE STUDIES

IN PARTIAL FULFILLMENT OF THE REQUIREMENTS FOR THE

DEGREE OF MASTER OF SCIENCE

DEPARTMENT OF CIVIL ENGINEERING

CALGARY, ALBERTA

September, 2009

Your file Votre référence
ISBN: 978-0-494-54567-6
Our file Notre référence
ISBN: 978-0-494-54567-6

ABSTRACT

Masonry is a highly durable material used in construction since hundreds of years ago. The durability of the overall masonry construction depends generally on the workmanship skills and how the units are built. In addition, masonry elements are relatively quick to construct and low in cost, and have a beautiful final appearance. It is now commonly accepted that Unreinforced Masonry (URM) structures are the most vulnerable during earthquakes. The poor performance of URM walls subjected to lateral loads is due to insufficient shear and flexural capacity. In this thesis, the results from tests on a total of eight squat concrete masonry unit (CMU) walls under simulated seismic load are reported. The first specimen is an URM control wall and one specimen was horizontally reinforced with steel-ladder shaped bed joint reinforcement. Three walls were horizontally reinforced with different configurations of GFRP material and the last three were reinforced with different configurations of Geogrid material. No vertical reinforcement was provided. The results showed that the seismic performance of URM walls due to cyclic in-plane loads can be enhanced by using GFRP or Geogrid materials when used as bed joint reinforcements. However, the level of enhancement varies due to the configuration and properties of material and also due to the distribution of the horizontal reinforcement (every course/every 2nd course). The significance of this experimental study is that it examines both FRPs and a new material, Geogrid, along with a new configuration/shape of bed joint reinforcement, grid shape.

ACKNOWLEDGEMENTS

I need to express my gratitude and thanks to Dr. Shelley Lissel for her continuous encouragement, support, and guidance.

Also, I wish to thank Dr. Nigel Shrive for his support and help to enhance this work. I would like to extend my gratitude to Dr. Ezz Sayed-Ahmed who helped me to join the program and helped me a lot to be a good student and engineer.

Many thanks to the technical staff of the Department of Civil Engineering, University of Calgary for their patience and cooperation in the experimental work. Thanks a lot to Dan Tilleman, Don Anson, Terry Quinn, Mirsad Berbic, Don McCullough. It was great to work with you all.

The financial support provided by Natural Sciences and Engineering Research Council of Canada (NSERC), and the Masonry Contractors Association of Alberta (Southern Region) is appreciated.

In addition, I wish to thank Bruce Borstmayer from Qualicase Ltd. (FRP bed joint reinforcement), George Larocque (masonry specimens construction) and all the staff in the department office for their help and support.

Finally, I would like to thank all my colleagues and friends Monica Guzman, Jason Moroz, Mark Hagel, Badr Abozeid, Casie Yuen, Ahmed Oan and Hani Zaki for their support and encouragement.

Thanks to everybody who helped me to accomplish this work.

DEDICATION

To my family and friends who offered me continuous and unconditional love and support throughout the time of my studying and doing this work.

TABLE OF CONTENTS

LIST OF TABLES

LIST OF FIGURES

LIST OF SYMBOLS

$\%$	Percentage
A_e	Effective cross-sectional area (mm^2)
A_{env}	Area under idealized envelopes (kN·mm)
A_g	Gross cross-sectional area (mm^2)
A_{uc}	Uncracked cross-sectional area (mm^2)
A_v	Cross-sectional area of horizontal shear reinforcement (mm^2)
b_w	Overall web width of masonry unit (mm)
d_{cr}	Wall displacement at initial cracking or cracking at $0.7H_{max}$ (mm)
d_e	Wall displacement at idealized elastic limit (mm)
d_{Hmax}	Wall displacement at maximum horizontal load (mm)
d_{max}	Maximum wall displacement (mm)
d_u	Ultimate idealized wall displacement (mm)
d_v	Effective depth of the wall (mm)
f'_m	Compressive strength of masonry normal to the bed joint (MPa)
f_u	Ultimate strength of steel reinforcement (MPa)
f_y	Yield strength of steel reinforcement (MPa)
H	Applied horizontal load (kN)
H_{cr}	Horizontal load at initial cracking or $0.7H_{max}$ (kN)
H_{max}	Maximum horizontal load (kN)
H_u	Ultimate idealized horizontal load (N)
h_w	Height of the wall (mm)
I	Second moment of area (mm^4)

K_e	Effective wall stiffness (kN/mm)
l_w	Length of the wall (mm)
M_n	Nominal moment (kN·m)
P	Axial load corresponding to the lateral load at failure (kN)
P_l	Compression force perpendicular to the sliding force (kN)
P_d	Axial compressive load on the section under consideration (kN)
P_f	Factored axial load (kN)
s	Spacing between horizontal reinforcement (mm)
V_m	Shear strength attributed to the masonry (kN)
V_n	Nominal shear resistance (kN)
V_r	Shear resistance (kN)
γ_g	Factor to account for partial grouted or ungrouted walls that are constructed of hollow or semi-solid units
μ	Friction coefficient
μ_u	Ultimate ductility factor
ρ	Horizontal reinforcement ratio
y	Half the length of the wall (mm)
ϕ_m	Material resistance factor for masonry
ϕ_s	Material resistance factor for steel

LIST OF ABBREVIATIONS

AAC	Autoclaved Aerated Concrete
AFRP	Aramid Fibre Reinforced Polymer
BJR	Bed Joint Reinforcement
CFRP	Carbon Fibre Reinforced Polymer
CMU	Concrete Masonry Unit
COV	Coefficient of Variation
CSA	Canadian Standards Association
DL	Dead Load
eqn.	Equation
FRCC	Fibre-Reinforced Cement Composite
FRP	Fibre Reinforced Polymer
GFRP	Glass Fibre Reinforced Polymer
LSCs	Linear Strain Converters
NSM	Near Surface Mounted
RC	Reinforced Concrete
URM	Unreinforced Masonry
UV light	Ultraviolet light

CHAPTER ONE:

INTRODUCTION

1.1 General Background

Unreinforced masonry (URM) walls are masonry walls which are constructed of clay, calcium silicate, or concrete units and mortar, and are not reinforced at all. URM walls are commonly used on their own in many countries and also as infill wall panels in reinforced concrete and steel frame structures because they offer several advantages, including low cost, ease of construction, and environmental efficiency [Sanada *et al.* 2006]. "*URM infills fulfill architectural and other functional requirements, such as forming a significant portion of building envelope, partitioning, temperature and sound barriers, while also providing adequate compartmentalization against fire hazard*" [Saatcioglu *et al.* 2005].

Fibre Reinforced Polymers (FRP), which are fibres in a polymer resin matrix, have been used extensively for many years in the aerospace and sporting goods industries. The advantages of these materials (light weight, high strength, high durability and non-corrodibility) have been recognized relatively recently to provide many advantages and many possible applications to civil engineering (especially structural). Hence, applications of FRPs in concrete or steel structures have been the theme of much research and experimental studies especially in the last decade. However, the use of FRPs in masonry structures has not been studied to the same extent as for concrete structures, but due to the

fact that most of the historical structures in the world are constructed with masonry, the use of FRPs in the retrofitting and strengthening of these structures has been studied recently.

1.2 Objective of the Research Programme

The aim of this experimental study is to investigate and evaluate the improvement of the in-plane load carrying capacity of ungrouted masonry walls reinforced horizontally by different materials, configurations and spacing of bed joint reinforcement. The significance of this experimental study is that it examines both FRPs and a material new to structural engineering, Geogrid, along with a new configuration/shape of bed joint reinforcement, grid shape.

1.3 Thesis Organization

- **Chapter 2:**

This chapter contains the literature review, where the relevant literature related to the use of FRPs, bed joint reinforcement, and other methods for improving the performance of masonry walls under in-plane or seismic loads will be explored.

- **Chapter 3:**

In this chapter, the properties and configurations of the materials used, description of the test setup, loading system and testing procedure will be discussed.

- **Chapter 4:**

In this chapter, the observations and the primary results of the tests will be presented and discussed.

- **Chapter 5:**

In this chapter, the test results will be further discussed and analyzed and then compared to the theoretical results obtained using the equations of the Canadian design code to support conclusions obtained from this study.

- **Chapter 6:**

In this final chapter of the thesis, conclusions and recommendations drawn from the results of this experimental study are presented.

CHAPTER TWO:

LITERATURE REVIEW

2.1 Introduction

In some seismic zones, Unreinforced Masonry (URM) walls have a poor history in construction and buildings, perhaps because of the quality of workmanship and perhaps due in part to the magnitude of earthquakes in those areas. During the last 10 years, many buildings with URM walls collapsed due to seismic loading resulting from earthquakes as shown in Figure 2.1 [El-Gawady *et al.* 2005, Li *et al.* 2001]. This led some to conclude that URM walls cannot resist dynamic loads at all despite evidence to the contrary. For example, it has been reported that URM walls can resist and sustain seismic loading if used properly, as observed in Italy, Greece and other Mediterranean countries [Tomaževič 1999]. In any case, there are many reports on ways in which URM walls can be reinforced, strengthened or retrofitted to increase the stiffness and the strength of the structures and the resistance to seismic loads [El-Gawady *et al.* 2005, Shrive 2005].

Figure 2.1: Destruction of Building [Blondet *et al.* 2004]

Magenes and Calvi [1997] addressed the problems of the evaluation of the strength, deformability, and energy dissipation capacity of URM walls subjected to in-plane seismic loads. They discussed the possible approaches to simplified strength evaluation on the basis of experimental and numerical data. In addition, the principal failure mechanisms of masonry walls subjected to seismic actions were summarized by the authors as follows:

1. *Rocking (Flexural) Failure*: as lateral load or displacement demand increase, bed joints crack in tension and shear is carried by the compressed masonry; final failure occurs by overturning of the wall and simultaneous crushing of the compressed corner.
2. *Shear Cracking (Diagonal) Failure*: peak resistance is governed by the formation and development of inclined diagonal cracks, which may follow the path of bed- and head-joints or may go through the units, depending on the relative strength of mortar joints, unit-mortar interface, and units.
3. *Sliding Failure*: due to the formation of tensile horizontal crack in the bed joints, subjected to reversed seismic action, potential sliding planes can form along the cracked bed joints; this failure mode is possible for low levels of vertical load and/or low friction coefficients [Magenes and Calvi 1997].

To improve the performance of URM structures, especially walls, in resisting the in-plane seismic forces resulting from earthquakes, much research and many tests have been conducted. Researchers have explored two main methods to improve the seismic

performance of URM walls: using Fibre Reinforced Polymer (FRP) and using interlocking masonry units, bricks and concrete blocks.

Over the past 15 years, FRP materials have been increasingly considered for civil construction applications around the world [Fig. 2.2]. FRP bars, rods, and prestressing tendons are being used for new structures. Additionally, FRP plates, sheets, and wraps are being used for strengthening and retrofitting of structural members [ISIS Design Manual No. 3 2007, Shrive 2005, Zhuge 2008].

Figure 2.2: Available Shapes of FRP Products [ISIS Design Manual No. 3 2007]

Reinforcing is considered here to be the placement of reinforcement during the construction of structural elements, while strengthening is considered to be the external application of any material, such as FRP, to enhance and increase the strength capacity of the element some time after construction. Retrofitting is considered here to be the rehabilitation or treatment of damaged structural elements to handle the current and future load regardless of the damages.

In general, FRP materials have many important advantages. They are easy to handle due to their lightweight which also speeds the construction process. They have up to five times the strength of steel, and are corrosion resistant which leads to durable structures, while they are also highly versatile and suit any kind of project [ISIS Design Manual No. 3 2007].

A review of research in the area of FRP retrofitted URM walls under in-plane loading, was presented by Zhuge [2008]. It was mentioned that "*if FRP applies on seismic retrofitting applications, these materials can absorb tensile stress and increase overall stiffness and ductility and bearing capacity*". In addition, the author presented two failure modes that are common for shear: shear sliding and diagonal tension cracking. The experimental study indicated that the strength of the retrofitted masonry walls depends on controlling the modes of failure. Also, the modes of failure were affected by the strength, orientation and anchorage length of FRP. Generally, in the study presented by Zhuge [2008], when FRP was bonded to the wall, compressive crushing type of failure (Flexural Failure) was still observed, but tension or shear failure modes may be prevented by the application of FRP [Fig. 2.3].

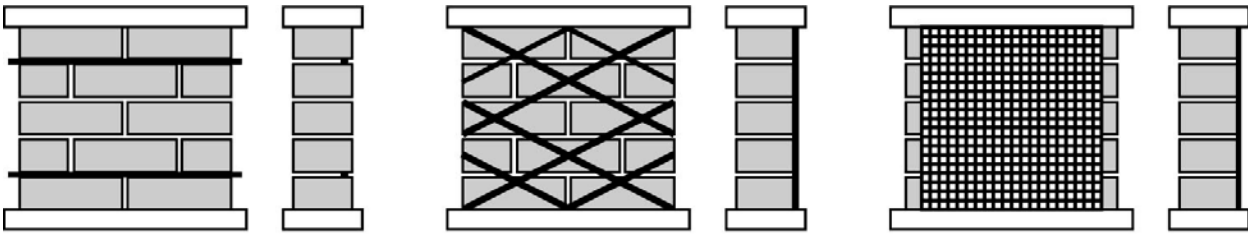

Figure 2.3: Strengthening Masonry using FRP [Zhuge 2008]

2.2 Reinforcing, Strengthening and Retrofitting with FRP

The relevant literature related to the FRP method of improving the performance of masonry walls under in-plane or seismic loads will be explored in this section.

2.2.1 Reinforcing, Strengthening and Retrofitting with FRP Sheets or Laminates

FRP laminates are a uniting of two or more sheets of FRP. Fibre Reinforced Polymer (FRP) sheets or laminates are used for retrofitting, strengthening and reinforcing URM walls to improve their in-plane and out of plane load capacity.

It has been shown in many experimental programs and studies that the application of Fibre Reinforced Polymer (FRP) sheets/laminates to URM walls significantly improves the stiffness and lateral strength of the URM walls and their ability to resist in-plane seismic loading.

El-Gawady *et al.* [2005] conducted dynamic in-plane tests on six slender URM walls with dimensions of 1570 mm long × 1600 mm high, and five squat URM walls with dimensions of 1570 mm long × 700 mm high. All specimens were tested and then retrofitted on one side only with different types and configurations (fully covered or in X shape) of FRP sheets (CFRP, GFRP and AFRP) and retested. The specimens were subjected to a series of seismic loadings on a uni-axial earthquake simulator driven by a 100 kN servo-hydraulic actuator [Fig. 2.4].

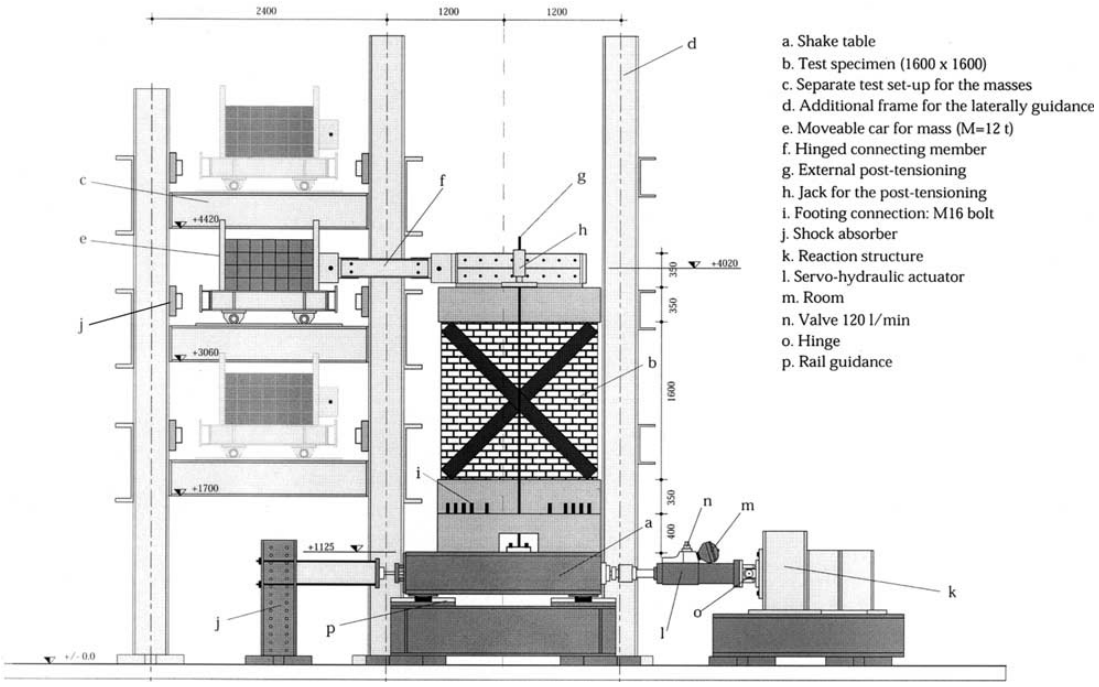

Figure 2.4: Test Setup [El-Gawady *et al.* 2005]

As a result, the lateral strength of the slender walls retrofitted with GFRP as well as the squat wall retrofitted with AFRP on one face fully covered was increased by a factor of 2.9. However, the lateral strength of the slender and squat walls retrofitted with GFRP or CFRP in X shape was increased by a factor of about 1.5. This indicates that some of the retrofitted walls achieved about 3 times their original strength.

At the University of Auckland in New Zealand, Mahmood *et al.* [2008] conducted in-plane laboratory tests on two URM walls, one with and the other without retrofitting by application of unidirectional GFRP sheets. The test was displacement-controlled and the lateral cyclic force was applied to the top of the specimen using a hydraulic actuator. Then, a vertical load was simulated using four external stressing tendons, two on each side of the wall. The tendons were anchored to the strong floor [Fig. 2.5]. The test walls were

constructed with bricks, obtained from demolished buildings and cleaned for use in this study, and a weak mortar mix (Type O) which was selected to simulate decayed mortar in old URM structures. The two walls were 1970 mm long × 1970 mm high × 240 mm thick. The test wall was externally strengthened on one face only by two layers of GFRP sheets (laminate thickness is 1.3 mm) in shear only (the glass fibres oriented horizontally) to allow the wall to fail in flexural mode. The ultimate tensile strength (f_u) of the GFRP sheets was 575 MPa and the modulus of elasticity was 26.1 GPa. As a result, the retrofitted wall was deformed by rocking at the base because the FRP sheet held together the upper masonry courses. The first crack appeared in a pull cycle at a displacement of 2 mm and the corresponding lateral load was 79.5 kN. The V_r for the retrofitted wall was only about 15% higher than the unretrofitted wall. This low improvement in the lateral capacity may be due to the weakness of the mortar used and bricks collected from demolished buildings. It could also be because the strengthening was on one face only.

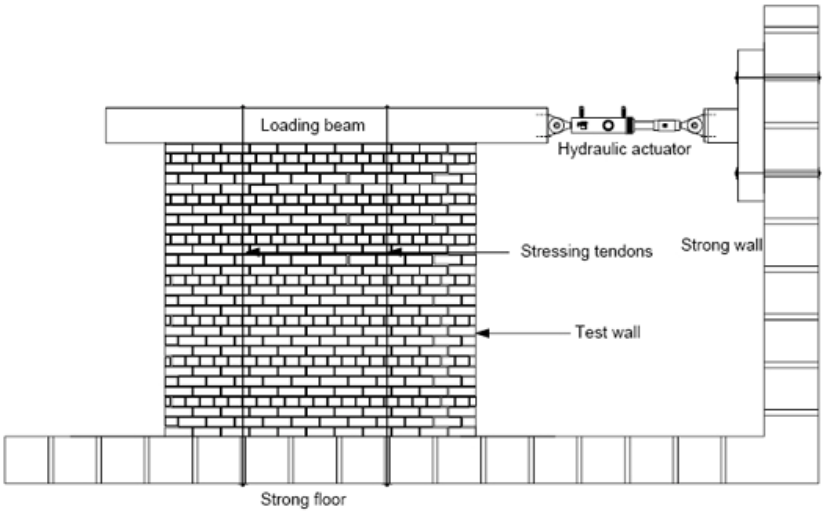

Figure 2.5: Test Setup [Mahmood *et al.* 2008]

In addition, Foster *et al.* [2005] from University of North Carolina talked about FRP repair methods for URM buildings subjected to lateral cyclic loading. A full-scale URM building with dimensions of 2.48 m high × 3.25 m wide × 4.47 m long was constructed and tested under a constant vertical load of 667 kN, simulating the weight of two additional floors, and quasi-static lateral loading at a rate of 3.5 kN/sec. After failure, it was repaired with externally applied wet lay-up GFRP laminates. The results proved that repairing the damaged CMU building with GFRP laminates resulted in a 67% increase in strength and 550% increase in energy dissipation.

Furthermore, Saatcioglu *et al.* [2005] from University of Ottawa tested two half-scale reinforced concrete frames, infilled with concrete masonry blocks, with and without seismic retrofitting diagonally on one face with CFRP sheets (two plies per sheet). The two walls were 1825 mm long × 1825 mm high. The ultimate tensile strength (f_u) of the CFRP sheets was 785 MPa and the thickness was 0.8 mm/ply. The walls were subjected to a constant vertical load of 400 kN on the columns and three concentrated loads applied at an equal spacing on the beam, each having a magnitude of 40 kN. Then, an incrementally increasing cyclic lateral load was applied by an actuator in deformation control mode. The tests indicated that the CFRP sheets controlled cracking, increased the lateral capacity by three times and improved the elastic capacity of the overall structural system.

According to Yu *et al.* [2007], grids of GFRP were used to reinforce a fast setting polyurea spray to strengthen eleven URM walls [Fig. 2.6]. Six of the walls, with overall dimensions of 1626 mm high × 1626 mm long, were constructed from concrete masonry blocks and the rest from clay bricks. Two concrete walls and also two brick walls were

reinforced horizontally and another two concrete walls and two brick walls were reinforced vertically. The walls were subjected to in-plane diagonal compressive load as shown in Figure 2.6. The tests were stopped when the failure occurred.

Figure 2.6: Test Setup (left) and Spraying Polyurea to one URM Wall (right) [Yu *et al.* 2007]

It was concluded that the failure mode of the strengthened URM walls was directly affected by the strengthening schemes (orientations) and the lateral capacity increased in the order of 10 to 43% in comparison with unreinforced brick walls and 10 to 60% in comparison with unreinforced concrete walls.

Recently, Corradi *et al.* [2008] tested twenty-five walls (1.2 m long × 1.2 m high) reinforced by five different methods; GFRP and Polypropylene jacketing (on both sides) were two of these methods. The aim of the work was to study the effectiveness of seismic-upgrading methods both on un-damaged and damaged walls. Two types of GFRP were used: unidirectional GFRP sheets (thickness of 0.23 mm) and GFRP mesh (thickness of 0.67 mm). The GFRP sheets tensile strength used was 1778 MPa and they were applied

as one sheet per face on six walls. However, the Polypropylene net has a mesh size of 30 × 45 mm and tensile strength of 17 kN/m. The results indicated that the GFRP jackets, in general, increased the lateral resistance of the masonry walls by 186%. However, Polypropylene jackets didn't enhance the strength of masonry under lateral load.

Haroun *et al.* [2005] from University of California conducted cyclic in-plane shear tests on six fully grouted concrete masonry walls, 1830 mm high × 1830 mm long, which were internally reinforced with 20M vertical steel bars ($\rho = 0.0054$). One of the walls was a control wall. Then, the second wall was tested as-built and then repaired/retrofitted with a single sheet of CFRP (thickness of 0.23 mm) on each side of the wall and tested again. Another two walls, one strengthened with a single layer of CFRP laminate on one side and the other strengthened with a single layer of CFRP laminate on each side. The fifth wall was strengthened with a double layer of GFRP laminate on each side. The last wall was strengthened with horizontal CFRP strips on one side. Each specimen was subjected to a constant vertical load and an increasing cyclic lateral load (displacement control). The test results indicated that the weak compressive strength properties of the masonry units, especially at the wall toes, were the limiting parameter that affected the strength gain of the FRP strengthened walls. However, the tests showed that the lateral capacity of the repaired wall increased by 120%. In addition, the capacity of the wall strengthened with a single layer of CFRP laminate on both sides increased by 130%, while the capacity of the wall strengthened on one side increased by only 115%. Then, the capacity of the wall strengthened with a double layer of GFRP laminate on each side increased by 128%. Finally, the capacity of the wall strengthened with horizontal CFRP strips on one side

increased by 118%. The enhancement in the ductility ranged from 3.4 times that of unstrengthened walls in case of double-side CFRP strips strengthen to 6 times in the case of horizontal CFRP strips.

2.2.2 Reinforcing, Strengthening and Retrofitting with FRP Strips

In an experimental study conducted at the University of Sannio in Italy [Marcari *et al.* 2007], the in-plane shear performance of fifteen masonry walls built with tuff masonry units and strengthened with GFRP and CFRP strips were tested. The specimens' dimensions were 1570 mm high, 1480 mm wide and 530 mm deep. "*Tuff is a rock composed of volcanic particles, compacted, cemented or welded into a firm, consolidated state*" [Marcari *et al.* 2007]. The mean compressive strength of the tuff units was 2.1 MPa. The ultimate tensile strength of the GFRP and CFRP strips was 1320 MPa and 3450 MPa respectively. Four walls were strengthened with cross pattern CFRP strips, four walls with grid pattern CFRP strips, three walls with cross pattern GFRP strips and finally four walls with grid pattern GFRP strips. The strengthened specimens were tested under an axial load of 400 kN equal to a vertical pre-stress of 0.5 MPa on the top of the panel and a monotonic shear load (displacement control) applied up to failure at a loading rate of 2 mm/sec [Fig. 2.7].

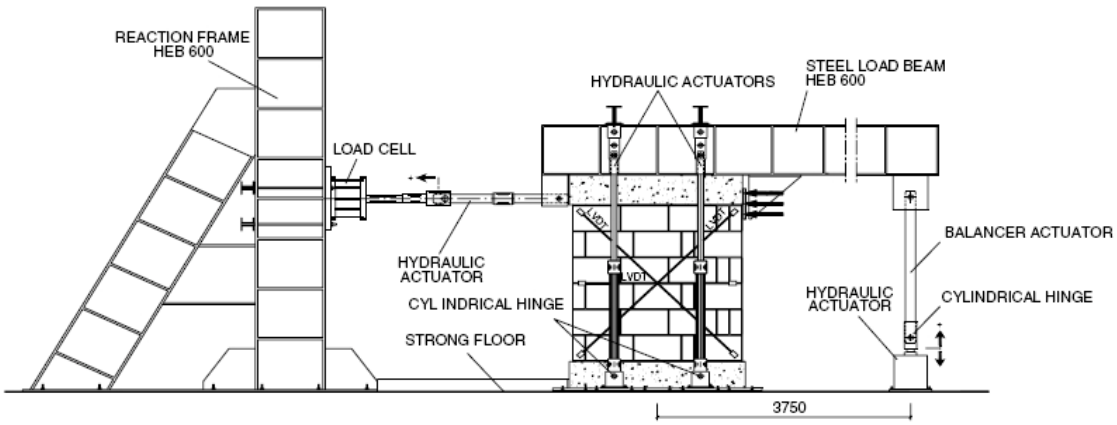

Figure 2.7: Apparatus for Testing Panels [Marcari *et al.* 2007]

The results showed that the maximum shear capacity of the as-built panel was 120 kN. However, the maximum shear capacity provided by both CFRP and GFRP grid pattern was 190 kN, while the lowest shear capacity, provided by the panel strengthened with GFRP cross pattern, was about 142 kN. In general, the shear strength of the masonry walls was improved significantly by using the FRP strips. However, the elastic stiffness of the retrofitted walls was not substantially modified by the external reinforcement.

In another experimental study at The University of Zagreb, Croatia, conducted by Soric *et al.* [2008], brick walls (1030 mm long × 1060 mm high × 120 mm wide) strengthened with one layer of GFRP strips (one side only) were subjected to a constant vertical compression load of 79 kN (0.64 MPa) and a monotonically increasing horizontal load. Results from these walls were compared with those from unstrengthened walls. The tests specimens were divided into three groups: a) Unreinforced-unstrengthened walls, b) walls strengthened on one side only with horizontal and diagonal GFRP strips, and c) walls

strengthened on one side only with horizontal and vertical GFRP strips. The results showed that strengthening the walls with diagonal GFRP strips increased the shear resistance by 83% compared with unstrengthened walls while with horizontal GFRP strips the shear resistance of the walls increased by 86%. In addition to the insignificant difference in the percentage increase of V_r, horizontal strips were much simpler to apply than diagonal strips.

2.2.3 Reinforcing, Strengthening and Retrofitting with FRP Bars or Rods

Li *et al.* [2001] from University of Missouri discussed the retrofitting of URM walls with Near Surface Mounted (NSM) GFRP rods. One of the objectives of the work reported was to improve analytical models to predict the performance of URM walls under in-plane loading and minimize the stiffening effect of retrofitted URM walls by allowing some level of damage to occur in the specimens. Three concrete masonry walls (2235 mm high × 1219 mm long) were tested; a wall retrofitted with vertical NSM GFRP rods, a wall retrofitted with horizontal NSM GFRP rods, and a control wall. The results showed that no significant difference was registered between the wall that was retrofitted with horizontal rods [Fig. 2.8] and the other wall retrofitted with vertical rods before debonding of the vertical rods occurred. However, the ultimate load capacities of the retrofitted walls were approximately three and six times higher than that of the control wall for the vertical and horizontal rods, respectively.

Figure 2.8: Ultimate State of the Wall Retrofitted with Horizontal GFRP Rods [Li *et al.* 2001]

In another study by Li *et al.* [2005], six full-scale rectangular concrete masonry walls (2032 mm high × 2032 mm long × 152 mm wide) with rectangular openings occupying 16% of the wall area were tested under cyclic lateral load to obtain diagonal shear failure. The strengthening method consisted of adding NSM GFRP bars on both faces of the specimens. The GFRP bars were embedded with either epoxy or cementitious-base paste in precut grooves along the mortar joints. There were two control walls, two walls strengthened with horizontal NSM GFRP bars, one wall strengthened with vertical NSM GFRP bars and the last wall strengthened with horizontal NSM GFRP bars and wide vertical GFRP strips. All panels were tested under two concentrated compressive loads of about 70 kN each (0.45 MPa) and a cyclic horizontal load was applied along the axis of a steel beam located on the top of the test wall. The authors concluded that it was not efficient to improve the load capacity of URM walls with openings by strengthening with

horizontal NSM FRP bars in the spandrels because the lateral capacity didn't increase more than 8%. However, the lateral capacity of the wall with horizontal NSM GFRP bars and wide vertical GFRP strips was increased by 20% and the stiffness and the energy dissipation of the URM walls were enhanced significantly, though the authors did not quantify this.

In another experimental study by Tinazzi *et al.* [2000] in a collaborative project between the University of Missouri - Rolla and the University of Padua, fourteen clay masonry walls were tested under diagonal compression load (shear test). The dimensions of these walls were 600 mm long × 1200 mm high and the compressive strength was 28.1 MPa for clay bricks. The walls were strengthened with NSM GFRP rods embedded with epoxy mortar horizontally into the bed joints and vertically into grooves. For wall panels strengthened on one side only, vertically or horizontally, the shear capacity increased by 45% with respect to the unreinforced specimens. More than 120% increase was obtained when rods were applied on the front-side and the back-side of the wall panels.

Foster *et al.* [2005] from the University of North Carolina also tested two full-scale URM buildings (brick structures) with dimensions of 2.48 m high × 3.25 m wide × 4.47 m long under a constant vertical load of 667 kN, simulating the weight of two additional floors, and quasi-static lateral loading at a rate of 3.5 kN/sec. These brick buildings were repaired with NSM GFRP rods and NSM CFRP rods to be compared with the results of the reference buildings. The repairing with NSM CFRP resulted in a 100% increase in strength and 300% increase in energy dissipation. However, NSM GFRP resulted in only a 70% increase in strength and 100% increase in energy dissipation.

Yu *et al.* [2005] from the University of Missouri - Rolla and the University of California-San Diego presented an experimental study on in-plane strengthening of URM walls with prestressed GFRP bars (tensile strength of 1024 MPa). Six URM walls with dimensions of 1626 mm high × 1626 mm long were constructed with concrete masonry blocks, with compressive strength of 16.8 MPa, and five of them were strengthened with seven 6.35 mm diameter NSM GFRP bars (one wall was without prestress) along the horizontal bed joints. The bars were placed inside horizontal square grooves and filled with epoxy. Then, the prestressing system was fixed to the specimen by tightening one steel nut with a regular wrench and by using a torque wrench and strain gauges installed on the bar, the applied load was controlled to the desired strain level. The walls were tested under a diagonal compressive loading. Two hydraulic jacks were connected in parallel and positioned at the upper left corner of the wall to apply the desired load. The results showed that the shear capacity of the URM walls strengthened with the prestressed GFRP bars increased by an average of 55%.

Tumialan *et al.* [2001] tested three concrete masonry walls with dimensions of 1220 mm high × 610 mm long and strengthened with GFRP rods having a diameter of 6.35 mm using NSM technique; one with a GFRP rod in every horizontal joint on one side, a second with a GFRP rod in every horizontal and vertical joint on one side, and a third with a GFRP rod in every horizontal joint on one side and every vertical joint on the other side. The walls were subjected to diagonal loads and compared with a control wall [Fig. 2.9]. The results demonstrated that the lateral capacity of the walls improved 100% compared to the control wall and that the walls were stable after failure.

This latter is important as retained integrity can avoid injuries or loss of human life due to catastrophic failures. In addition, it was stated that strengthening the walls in one or two faces doesn't affect the behaviour of the wall. This contradicts the work of Tinazzi *et al.* [2000] who showed that nearly three times more shear strength was achieved when rods were applied on both the front-side and the back-side of the wall panels.

Figure 2.9: Test Setup (left) and Installation of GFRP Bars (right) [Tumialan *et al.* 2001]

There is a large variation in the results from the studies presented in the preceding sections. The enhancement from strengthening or retrofitting with FRP ranges from 21% over the original lateral strength to 6 times the original strength. This variation occurs because of the different types of FRP application, because of the differences in the performance of the GFRP or CFRP materials, and also because of the differences in the properties and strength of the masonry units themselves.

2.3 Other Methods to Improve Seismic Performance of URM

There are other methods that can be used to improve the lateral capacity of Unreinforced Masonry Walls (URM). Bed joint reinforcement is believed to contribute to shear strength and therefore it is common in Canada and the USA to use steel bed joint reinforcement though other materials such as geotextiles and FRPs have been investigated for this purpose. The use of Interlocking Masonry Units, bricks and concrete blocks, to construct URM walls has also been shown to improve the in-plane load capacity significantly. Here, some studies regarding these two methods will be discussed.

2.3.1 Steel Bed Joint Reinforcement

According to Schultz *et al.* [1998], six partially grouted concrete masonry shear walls with steel bed joint reinforcement were tested. The height of the specimens was 1422 mm for all the walls but three aspect ratios were considered, two walls of each; 0.5, 0.7 and 1. "*Bed joint reinforcement comprising welded wire grids in a "ladder" configuration [was] placed in all bed joints of all specimens, and two different wire sizes were used to fabricate the grids*". The wire sizes were grids with 3.76 mm diameter Gauge longitudinal wires and grids with 5.26 mm diameter Gauge longitudinal wires to achieve horizontal reinforcement ratios, ρ, of 0.056% and 0.11% respectively. The six masonry walls were subjected to vertical compression stress and in-plane cyclic load while the bottom of every wall was fixed. The results suggested that partially-grouted masonry walls with steel bed joint reinforcement are a feasible lateral-load resisting structural system for seismic design. Furthermore, the lateral load resistance of the walls generally decreased with increasing aspect ratio (h_w/l_w) and the horizontal reinforcement ratio did not affect the

lateral load resistance significantly. In addition, "*Resistance of partially-grouted masonry shear walls to the seismic drift histories was found to be stable and featured high initial stiffness and ample energy dissipation*".

Gouveia *et al.* [2007] and Lourenço *et al.* [2008] at University of Minho, Portugal, conducted an experimental study on sixteen specimens (1150 mm high × 1020 mm long) tested under cyclic in-plane lateral loading applied to the mid-height of the wall and a constant vertical stress of 0.9 MPa [Fig. 2.10].

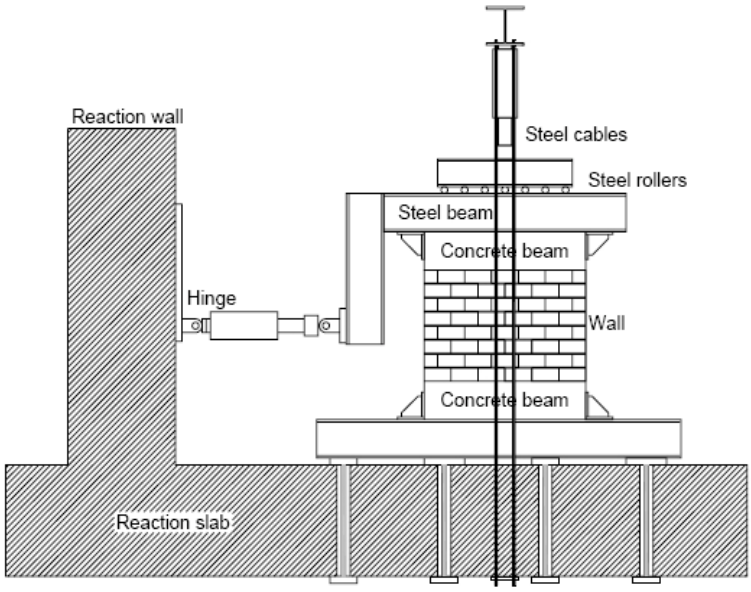

Figure 2.10: Test Setup [Lourenço *et al.* 2008]

The lateral load was applied to the wall via controlled displacement at a rate of 60 μm/sec. Two types of masonry units were used, hollow lightweight concrete blocks and hollow normal weight concrete blocks. The specimens were divided into two groups, walls that were horizontally reinforced with steel bed joint reinforcement of truss shape Murfor® RND/Z (bars of 5mm with f_y = 550 MPa and ρ = 0.09%) (unconfined) and

walls that were confined. The possibility of eliminating the need for filling of the vertical joints by using horizontal bed joint reinforcement, the need for filling vertical joints in confined masonry solutions and reinforced masonry elements based on vertical and horizontal truss reinforcement were the main aspects of this study. The results showed that the addition of steel bed joint reinforcement (truss shape) in the standard unreinforced masonry unconfined wall increased the shear resistance by 5 to 10% only, while in the confined walls capacity increased by 20%.

Penna *et al.* [2008] conducted an experimental study to assess the seismic behaviour of bearing slender and squat walls. Nine walls were built using Autoclaved Aerated Concrete (AAC) units with a mean compressive strength of 2.2 MPa and reinforced with horizontal steel truss-type bed joint reinforcement every second course or with horizontal steel rebar lodged in grooved blocks as shown in Figure 2.11.

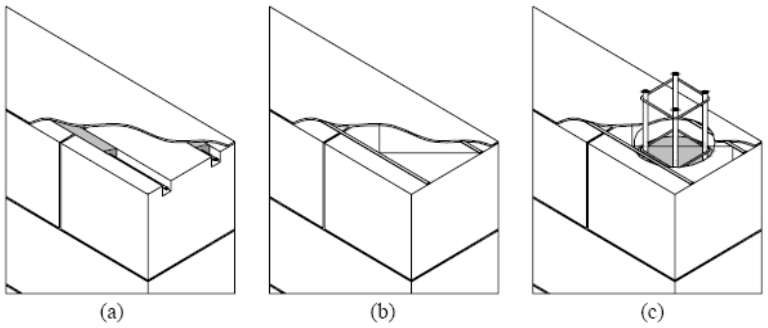

Figure 2.11: (a) Horizontal Rebars Lodged in Grooved Blocks; (b) Flat Truss Bed-Joint Reinforcement; (c) Flat Truss Reinforcement and Cast in Place Confining RC Columns [Penna *et al.* 2008]

All the specimens were 2.75 m high while the length was 1.5 m for four walls, 3 m for another four walls and 4.5 m for one wall. The test setup was a cantilever system with the horizontal load applied by a displacement-controlled horizontal hydraulic actuator and

a constant vertical load applied at the top by hydraulic jacks and distributed by a reinforced concrete beam. All the slender walls exhibited a clear flexural behaviour while the unreinforced squat wall exhibited a clear shear failure, the horizontally reinforced one a flexural failure and for the confined wall a mixed failure mode was observed. The results proved that the bed joint reinforcement in slender walls increased the strength and it was concluded that the strength increased with the wall length, with the maximum strength obtained for the 4.5 m wall. The lateral displacement capacity was also increased by about 60% to 70% for squat walls.

2.3.2 FRP Bed Joint Reinforcement

Lissel *et al.* [2000] presented the results of a study conducted using the ASTM E519 Diagonal Tension (Shear) test to examine the use of FRP bed joint reinforcement to improve the in-plane shear strength of masonry walls. The study compared the performance of clay brick wall panels reinforced with two different types of GFRP bed joint reinforcement and a nylon geo-textile fabric to traditional steel joint reinforcement. The results indicated that the GFRP reinforcement used was not very effective due to its smooth nature, and the geo-textile fabric, as joint reinforcement, worked very well.

2.3.3 Use of Interlocking Masonry Units

Some studies have sought to improve the in-plane capacity of URM walls by changing the shape of the masonry units themselves. Researchers found that if they construct the walls with masonry units that interlock with each other, the performance of URM walls under in-plane loading will be enhanced.

Thanoon *et al.* [2007] investigated the behaviour of twelve full-scale Dry-Stack (mortarless) interlocking walls (1.2 m long × 3 m high) subjected to concentric and eccentric compressive loads as shown in Figure 2.12. However, because this experimental study is not directly related to the study in this thesis, it will be discussed only briefly. The specimens were divided into three groups; A, B and C. Group A specimens were constructed by simply assembling the block units (compressive strength 17 MPa) with no mortar or reinforced concrete (RC) stiffeners. Group B and C walls were constructed the same as walls in Group A but with RC stiffeners located at the perimeter of the wall in group B and at the perimeter and at the mid height in group C. "*The interlocking mechanism of the block relies on the insertion of the protrusions of the block to that of the next course*" [Thanoon *et al.* 2007].

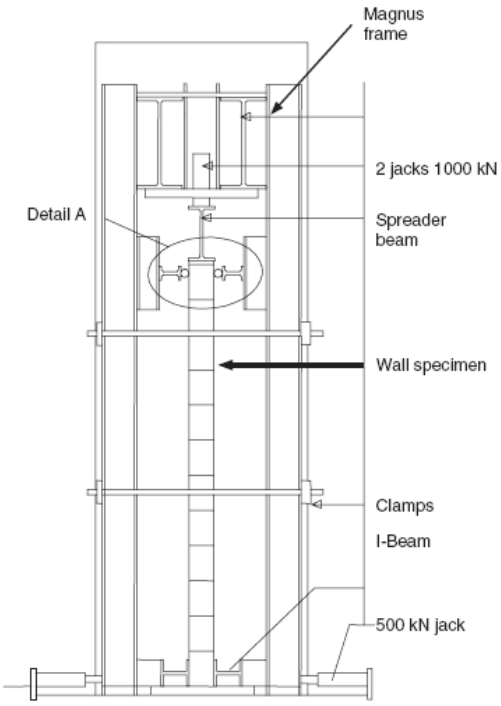

Figure 2.12: Test Setup [Thanoon *et al.* 2007]

The results indicated that the interlocking walls showed a superior response under eccentric load compared to the conventional walls. The absence of mortar layers in the interlocking walls provided more flexibility and allowed tolerated movement in all the joints.

Sanada *et al.* [2006], at the University of Tokyo, tested two types of brick interlocking walls (500 mm high × 870 mm long) under simulated seismic loads compared with a conventional masonry wall [Fig. 2.13]. The units of the first wall were cut out from typical bricks with a compressive strength of 7.62 MPa and the units of the second wall were made of Fibre-Reinforced Cement Composite (FRCC) with a compressive strength of 7.48 MPa [Fig. 2.14]. The two walls and the conventional wall were subjected to cyclic antisymmetric bending and shear under constant axial load of 20 kN (≈ 0.23 MPa).

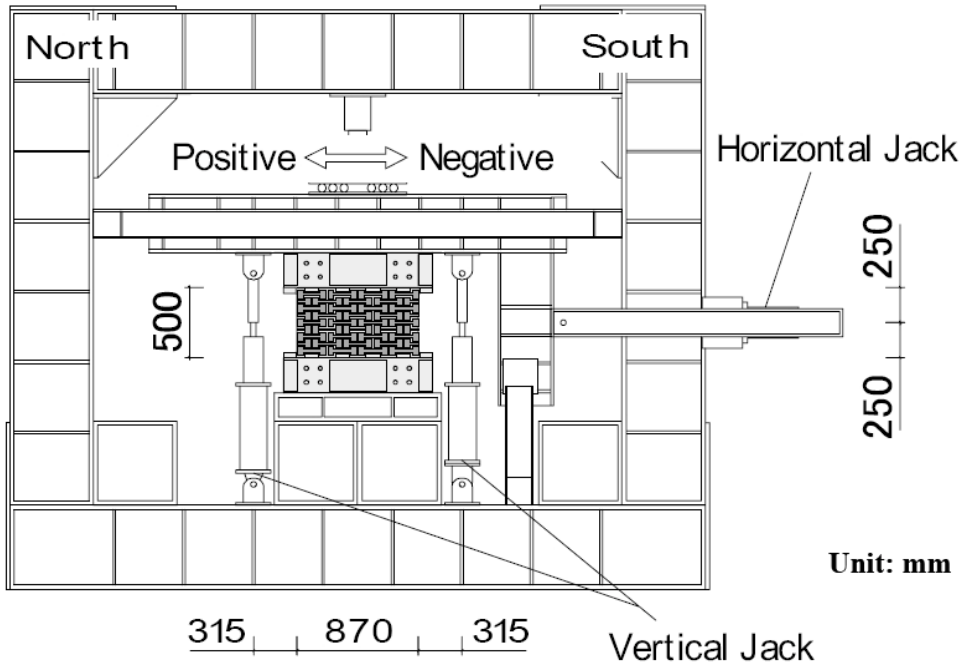

Figure 2.13: Loading System [Sanada *et al.* 2006]

The strength of the first wall constructed with interlocking bricks was 1.5 times higher than that of the control wall. However, in the case of the FRCC wall, the strength was only 1.1 times higher than that of the first wall constructed with interlocking bricks.

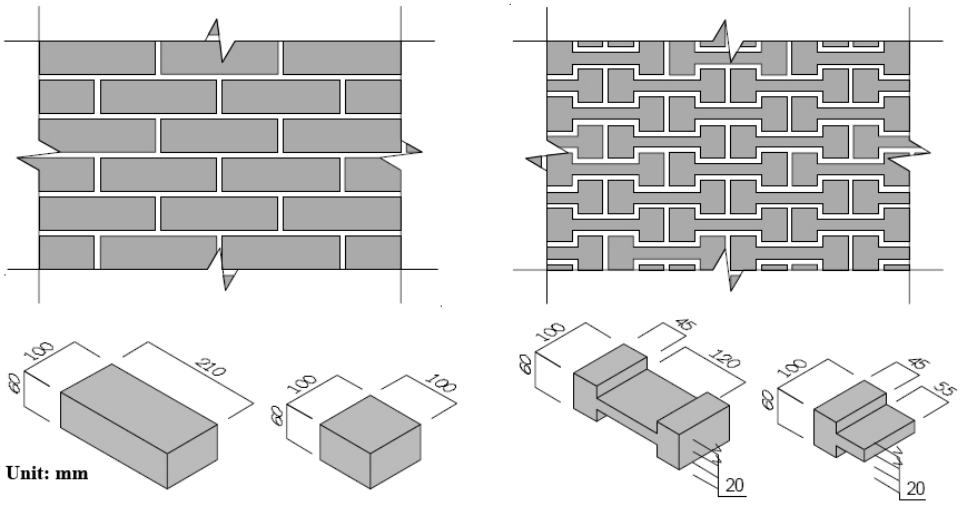

Figure 2.14: Theme Structures; Conventional Type (left), Interlocking Type (right) [Sanada *et al.* 2006]

2.4 Discussion

Various studies have demonstrated that the use of FRP, steel reinforcements and interlocking units can enhance the performance of URM walls under in-plane loading resulting from earthquakes. Most studies are experimental in nature and the results varied between them.

Applications of FRPs in masonry structures have focused mainly on the retrofit of existing structures due to the fact that a large proportion of the world's building stock is masonry buildings. FRPs lend themselves quite well to this purpose due to their light

weight, ease of external application, corrosion resistance, and the fact that they do not add significant mass to an existing structure.

However, the disadvantages of using external FRPs are the adverse effects of UV light on FRPs, lack of fire resistance and the effect on the appearance of the masonry. With the development of new UV and fire resistant materials, the main disadvantage remains the aesthetic effect of externally applied FRPs. Therefore, other researchers have concentrated on investigating the use of FRP bars or rods, which are usually near-surface-mounted (NSM), for strengthening masonry structures. This method has been shown to increase the load capacity by 3 to 6 times depending on the orientation of the bars [Li *et al.* 2001].

FRP sheets, as strengthening or retrofitting material, have been studied more extensively than other techniques, perhaps because it is easier to apply or more common than FRP bars or rods (no need to make grooves), and it was proved that they can significantly improve the lateral capacity and stiffness of the masonry walls. Some studies tested the role of FRP sheets in improving the lateral capacity by applying it on one side of the masonry wall and others on both sides.

FRP rods and bars have not been studied as much. However, all studies proved that using FRP rods or bars (NSM or horizontal reinforcements) can increase the in-plane shear capacity by at least 55%.

Using interlocking masonry units was also shown to be effective and enhanced the lateral capacity of walls. Dry stacked and mortared interlocking walls require professional workmanship but it was stated that it improves the in-plane capacity of masonry walls in

some cases by 50% or more. In the studies discussed in this chapter, the lateral capacity of the walls constructed with interlocking units was increased by an average of 40%.

It is worth mentioning that the properties and the strength of the masonry units used in constructing the masonry walls are also very influential on the amount of capacity increase that was obtained in the presented studies.

Regarding bed joint reinforcement, there are variations in the shape of bed joint reinforcement, the properties and the characteristics of the material used and the spacing between them (every course or every second course). The use of bed joint reinforcements as a method to improve the lateral capacity of the masonry walls has not been studied extensively in literature. Moreover, there has apparently been no previous study to compare materials and configurations of bed joint reinforcements and no previously reported experimental study, except Lissel *et al.* [2000], that examined the use of Geogrid or Geotextile materials as bed joint reinforcement. So, it will be valuable to examine or compare materials and configurations of bed joint reinforcements in enhancing the ability of masonry walls to resist in-plane loads.

It is worth mentioning that the effectiveness of bed joint reinforcement depends mainly on the type of mortar and the bond between the mortar and the longitudinal wires. The better the bond strength, the more efficient the reinforcement is in controlling cracking, and in-service experience has shown that only types S and N mortars should be used with bed joint reinforcement [Hatzinikolas and Korany 2005].

2.5 Summary

In general, there exist many ways in which masonry walls can be strengthened or improved to safely resist in-plane loads resulting from earthquakes, as panels in reinforced concrete and steel frame structures or as standalone masonry structures. The strengthened masonry walls are much more capable of resisting earthquakes than the unstrengthened ones.

Most of the studies reviewed in this chapter concluded that bed joint reinforcement has a moderate effect on the shear strength of the masonry walls with an average of 50% increase in the original lateral capacity perhaps because it doesn't bond well. However, it is very effective in increasing the stiffness and the energy dissipation of walls. In order to decrease the lack of bonding and its smooth surface, bed joint reinforcement can be manufactured in truss or grid shape instead of ladder shape.

Geogrid (Geotextile) is a unique material. It is light in weight, resists corrosion, and is recyclable which is considered a very important characteristic. The properties of this material will be introduced in the next chapter in further detail.

In the work presented in this thesis, investigations of the difference and the effect of the use of bed joint reinforcements (Steel, GFRP, and Geogrid) in different configurations and spacing as a method to improve the in-plane capacity of unreinforced ungrouted masonry walls will be discussed.

CHAPTER THREE:

EXPERIMENTAL PROGRAM

3.1 Introduction

To examine the effect of using Glass Fibre Reinforced Polymer (GFRP) and Geogrid as bed joint reinforcement in improving the performance of ungrouted masonry walls under in-plane lateral load, eight ungrouted masonry walls (1.6 m long × 1.4 m high) were constructed for this experimental study. The test setup and the experimental program were chosen based on similar types of experimental programs and studies of testing horizontally reinforced, strengthened or retrofitted masonry walls reported in the literature such as Haroun *et al.* [2005], Li *et al.* [2005] and Schultz *et al.* [1998]. The walls were tested under incremental cyclic lateral load combined with axial load to evaluate the effect of bed joint reinforcement on masonry wall performance under lateral cyclic load.

In this chapter, the properties and configurations of the materials used, description of the test setup, loading system and testing procedure are discussed.

3.2 Materials

The specimens were constructed with hollow concrete masonry blocks and type-S mortar. Three different materials were tested as bed joint reinforcement (BJR) to improve the in-plane load capacity and the strength of the ungrouted masonry walls; Steel wire, GFRP, and Geogrid. These materials will be discussed in further detail here.

3.2.1 Masonry Units and Mortar

All test walls and prisms were face shell bedded and ungrouted. The lightweight concrete block units (190 mm wide × 190 mm high × 390 mm long) used in this study were from the same batch of blocks used by M. Guzman who reported mean prism strength as 18.6 MPa in her experimental study [Guzman 2008]. Two-high ungrouted face shell bedded prisms were also constructed along with the walls in this study to determine compressive strength (Clause 5.1.2 of the CSA S304.1-04). Three prisms were built for Wall-C, three for Wall-S, three for Wall-G(G), three for WallG(L) and G(T) and three prisms for the walls reinforced with geogrid BJR. It is accepted that, similarly to concrete, the compressive strength of masonry increases with age, especially in the first 28 days. Since the walls were tested at different ages, the compressive strength was determined from these prisms at the time the walls were tested. The average compressive strength at testing age for all prisms was 13.6 ± 1.9 MPa. Figure 3.1 shows two of the prisms and a compression test for one of them.

Figure 3.1: Compression Test (left) and Two-High Ungrouted Face Shell Bedded Prisms (right)

Type-S mortar (1 part cement: 1/2 part lime: 4½ parts sand by volume), mixed in the lab, was used in constructing the walls. The mortar joints were 10 mm thick. Based on Drysdale and Hamid [2005], Type-S mortar is for general uses and when high lateral strength is required. However, Type-N (1 part cement: 1 part lime: 6 parts sand by volume) is used when high compressive or lateral strength are not required. The walls were built by a professional mason, with each wall being constructed in approximately one hour.

3.2.2 Steel Bed Joint Reinforcement

Steel wire is commonly used in Canada and the USA as bed joint reinforcement. In order to compare the effect of this reinforcement with those of other materials, GFRP and Geogrid, in improving the lateral load capacity of concrete masonry walls, steel bed joint reinforcement was used in one wall [Fig. 3.2].

Figure 3.2: Steel Bed Joint Reinforcement (Ladder shape)

The steel ladder shaped reinforcement is 0.18 m wide × 1.5 m long and the mean tensile strength, f_y, of the steel BJR was determined in the laboratory as shown in

Figure 3.3 by A. Oan to be 560 MPa [Oan *et al.* 2009]. The diameter of each wire is 3.5 mm and the cross-sectional area is 9.6 mm^2. The main disadvantages of steel are corrosion, which occurs when it is exposed to moisture, oxygen and chlorides penetrate through cracks or concrete, and the cost, which is higher than GFRP and Geogrid [Fallis 2008 and ISIS Design Manual No. 3 2007].

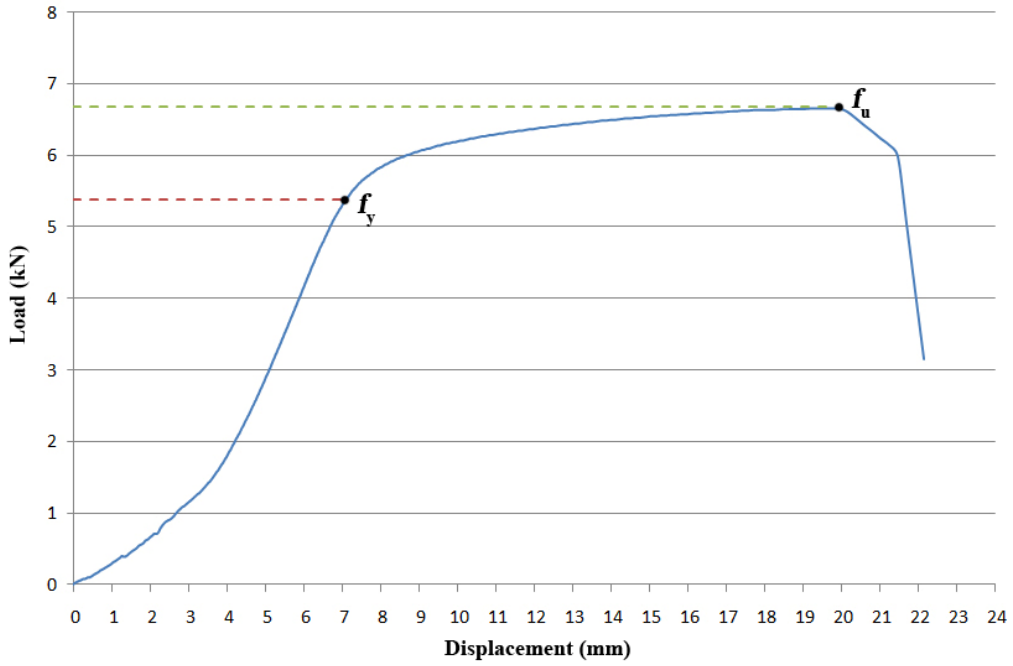

Figure 3.3: Steel BJR Load-Displacement Graph (data obtained from Oan *et al.* 2009)

3.2.3 GFRP Bed Joint Reinforcement

The main advantages of Glass Fibre Reinforced Polymer (GFRP) are its ease of application, corrosion resistance, and lightweight. Three different configurations of GFRP were produced by Qualicase for use as bed joint reinforcement in this study; grid, truss and ladder shape [Fig. 3.4]. The typical aperture size for the grid shape is about 40 × 40 mm, the diameter of each wire is 3 mm and the cross-sectional area is 7.1 mm^2. Many attempts

were made to determine the tensile strength of the GFRP used in this experimental program. However, none of these tests were successful. While the tensile strength of the fibres is reported as 278 mN/Tex on the manufacturer's datasheet, neither the manufacturer nor the literature provide the conversion factor to convert mN/Tex into MPa for this fibre type. However, a conversion factor was found in the literature for polypropylene fibres of 1 mN/Tex ≈ 0.9 MPa [Vinidiktova *et al.* 2006]. So, the tensile strength for GFRP used here is estimated to be 250 MPa.

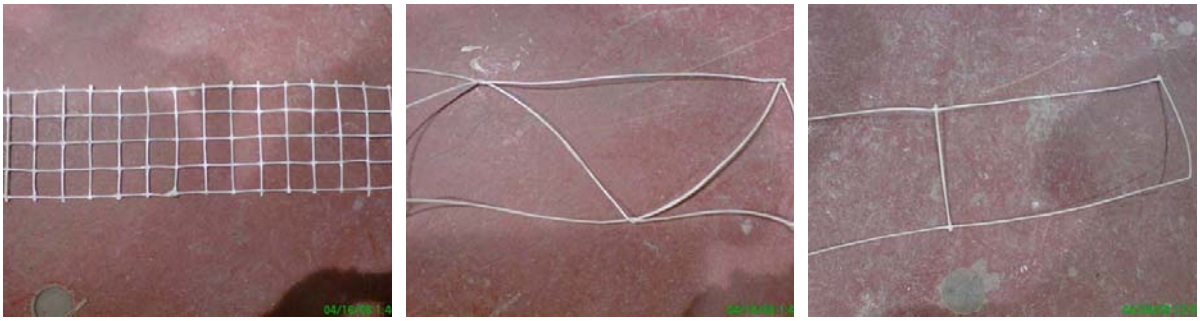

Figure 3.4: GFRP Bed Joint Reinforcement (Grid, Truss, and Ladder Shapes)

3.2.4 Geogrid Bed Joint Reinforcement

Geogrid bed joint reinforcement was used in three test specimens. Geogrid is a biaxial polypropylene geogrid (bi-axial PP geogrid, E'GRID 2020), from Layfield Geosynthetics and Industrial Fabrics Ltd. and is commonly used as base earth reinforcement for roads, storage yards and parking lots. The typical aperture size is 40 × 40 mm; the roll size is 3.9 × 100 m. The mean tensile strength of the Geogrid (E'GRID 2020) was determined in the laboratory to be 202 ± 4.5 MPa. The diameter of each wire is 2.4 mm and the cross-sectional area is 4.5 mm^2. Geogrid was used in both a ladder shape and a grid shape (every course and every 2^{nd} course) [Fig. 3.5]. The main advantage of this

material is that it can be made from recycled materials or recycled itself. In addition, it is light weight and resists corrosion.

Figure 3.4: Geogrid Bed Joint Reinforcement Grid (left) and Ladder (right) Shapes

3.3 Specimens

Eight concrete masonry walls (1.6 m long × 1.4 m high), were constructed and tested in this experimental study using the materials described above. The aspect ratio of all specimens is $\frac{h_w}{l_w} = \frac{1.0}{1.6} = 0.625$ because the effective tested height of the wall is only 1.0 m due to the horizontal actuator which is located at the first two courses (-400 mm) from the top of the wall [Fig. 3.6]. So, they are all squat CMU walls. All test specimens were constructed by the same professional mason in an attempt to reduce differences between specimens, minimize the effect of workmanship, and try to concentrate on the effect of bed joint reinforcement and the materials used. Each specimen was constructed in approximately one hour and cured for at least 28 days at the Civil Engineering Department Mike Ward laboratory at The University of Calgary, Alberta, Canada.

The first two conventional walls consisted of the URM control wall and the concrete masonry wall reinforced with steel bed joint reinforcement. Then, three masonry walls reinforced with GFRP bed joint reinforcement with different configurations and finally, three masonry walls reinforced with Geogrid bed joint reinforcement with different configurations. According to clause 10.15.2.6 of the CSA S304.1-04, for seismic reinforcement, bed joint reinforcement should be located every 2nd course (spacing = 400 mm) as shown in Figure 3.6. Each wall will be described in the following section.

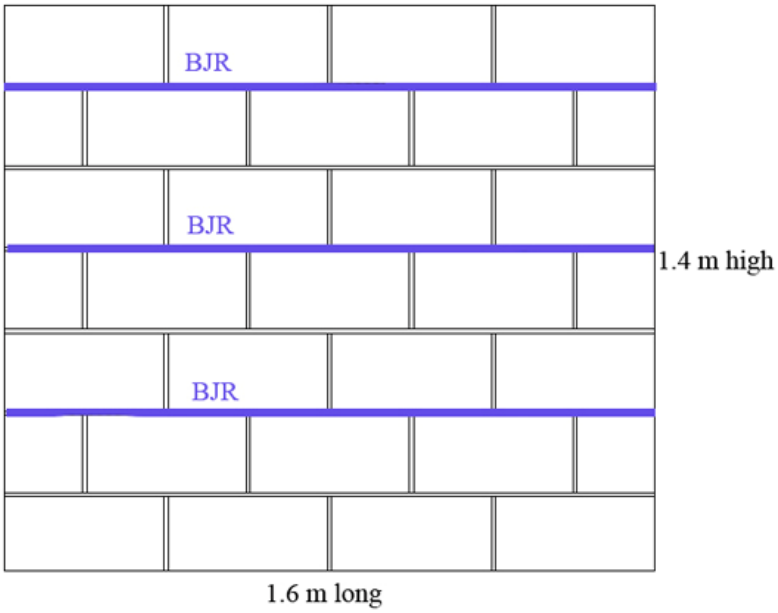

Figure 3.6: Dimensions of the Test Walls and Bed Joint Reinforcement Locations

3.3.1 Conventional Walls

- **Wall-C:** a typical ungrouted URM control wall specimen [Fig. 3.7].

Figure 3.7: The Typical Control Wall "Wall-C"

- **Wall-S:** an ungrouted masonry wall with Steel ladder reinforcement in every second bed joint [Fig. 3.8].

Figure 3.8: Steel Bed Joint Reinforcement in Wall-S

3.3.2 Walls with GFRP Bed Joint Reinforcement

- **Wall-G(G):** an ungrouted masonry wall with GFRP grid reinforcement in every second bed joint [Fig. 3.9].

Figure 3.9: GFRP Bed Joint Reinforcement (Grid Shape) in Wall-G(G)

- **Wall-G(L):** an ungrouted masonry wall with GFRP ladder reinforcement in every second bed joint [Fig. 3.10].

Figure 3.10: GFRP BJR (Ladder Shape) in Wall-G(L) (left) and (Truss Shape) in Wall-G(T) (right)

- **Wall-G(T):** an ungrouted masonry wall with GFRP truss reinforcement in every second bed joint [Fig. 3.10].

3.3.3 Walls with Geogrid Bed Joint Reinforcement

- **Wall-E(L):** an ungrouted masonry wall with Geogrid (E'GRID 2020 type) ladder reinforcement in every second bed joint [Fig. 3.11].

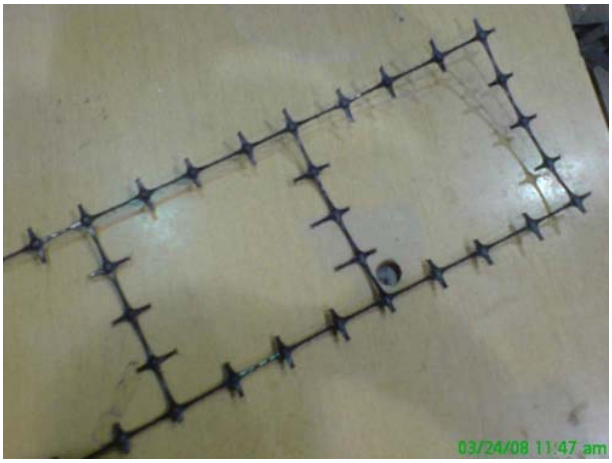

Figure 3.11: Geogrid Bed Joint Reinforcement (Ladder Shape) used in Wall-E(L)

- **Wall-E(G1):** an ungrouted masonry wall with Geogrid grid reinforcement in every bed joint [Fig. 3.12].

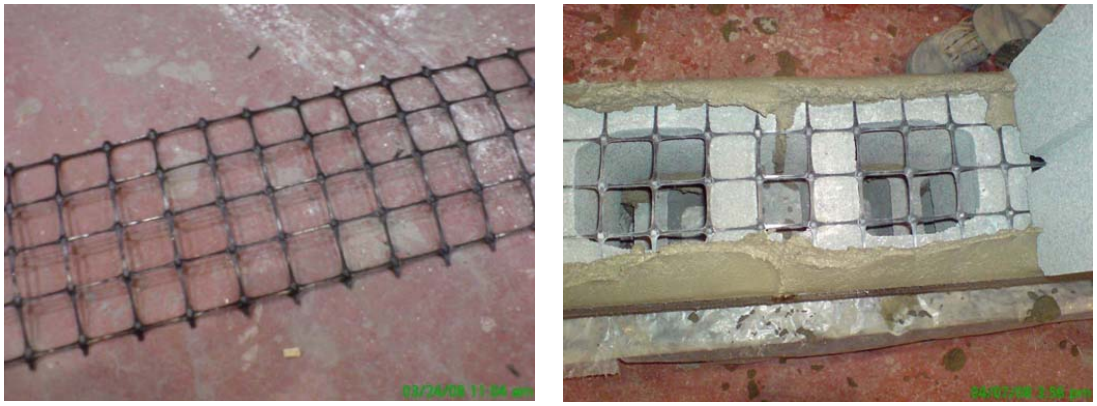

Figure 3.12: Geogrid BJR (Grid Shape) in Wall-E(G1) and E(G2)

- **Wall-E(G2):** an ungrouted masonry wall with Geogrid grid reinforcement in every second bed joint [Fig. 3.12].

It is important to mention that the surface finish of the steel wires, FRP or geotextile bed joint reinforcement is a basic factor in improving the lateral capacity of the CMU walls. Rough surfaces increase the friction in the mortar joints between and the mortar and the reinforcing and increase the lateral capacity of the masonry walls.

In Table 3.1, a summary of all specimens constructed for this experimental study, reinforcement configurations and properties, is shown.

Table 3.1: Characteristics of Specimens

Test Specimen	**Wall-C**	**Wall-S**	**Wall-G(G)**	**Wall-G(L)**	**Wall-G(T)**	**Wall-E(L)**	**Wall-E(G1)**	**Wall-E(G2)**
Type of BJR	N/A	Steel Ladder	GFRP Grid	GFRP Ladder	GFRP Truss	Geogrid Ladder	Geogrid Grid	Geogrid Grid
Cross-sectional Area, A_v, mm^2	N/A	19.2	14.1	14.1	14.1	9.0	9.0	9.0
Frequency of BJR	N/A	Every 2nd course	Every 2nd course	Every 2nd course	Every 2nd course	Every 2nd course	Every course	Every 2nd course

3.4 Test Setup and Loading System

The loading system and test set-up used are shown schematically in Figure 3.13. A vertical load of 60 kN (500 kN capacity actuator) was applied to the top of the walls distributed by a steel beam as a uniform load of about 40 kN/m (0.2 MPa) to the wall including the weight of the steel beam [Fig. 3.13].

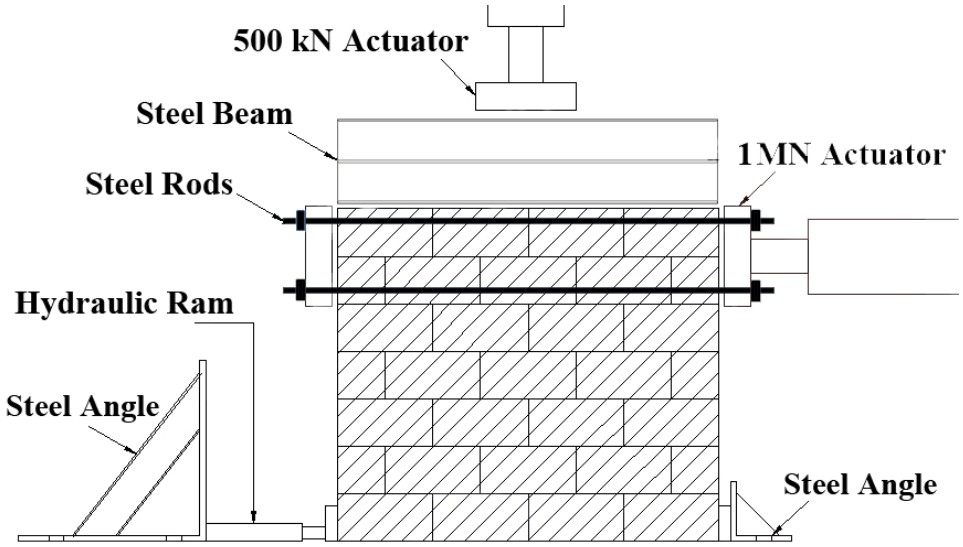

Figure 3.13: A Schematic Drawing of the Test Setup

Moreover, a small hydraulic ram was provided with minimal load (≈ 10 kN) at the base on the left side of the wall to prevent sliding while the right side rested on a steel angle as shown in Figure 3.13. In addition, the specimens were supported from the sides by steel rods and plates to prevent them from kicking out [Fig. 3.14]. Six Linear Strain Converters (LSCs) were used, three on each side, to measure the displacement of the walls at various heights as shown in Figure 3.14. The LSCs were placed at 285 mm, 665 mm and 1300 mm from the base of the specimen. The bottom LSC on the left side was used to feed data in the program to allow compensation for any sliding.

The specimens were subjected to an incremental cyclic in-plane displacement (pull then push, two cycles at each displacement level) applied to the top of the specimen using a horizontal actuator (1 MN capacity) at a rate of 1 mm/sec. The laterally applied cyclic load history is shown in Figure 3.15.

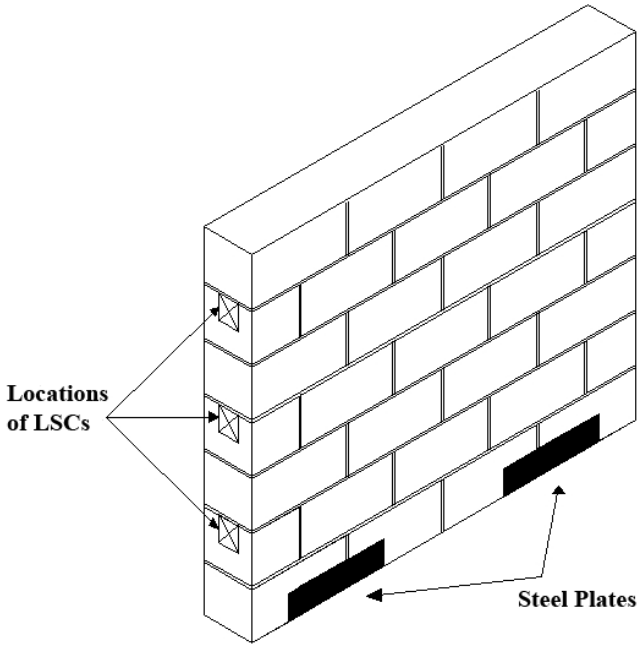

Figure 3.14: Locations of LSCs on the West and East Sides of the Wall and Steel Plates

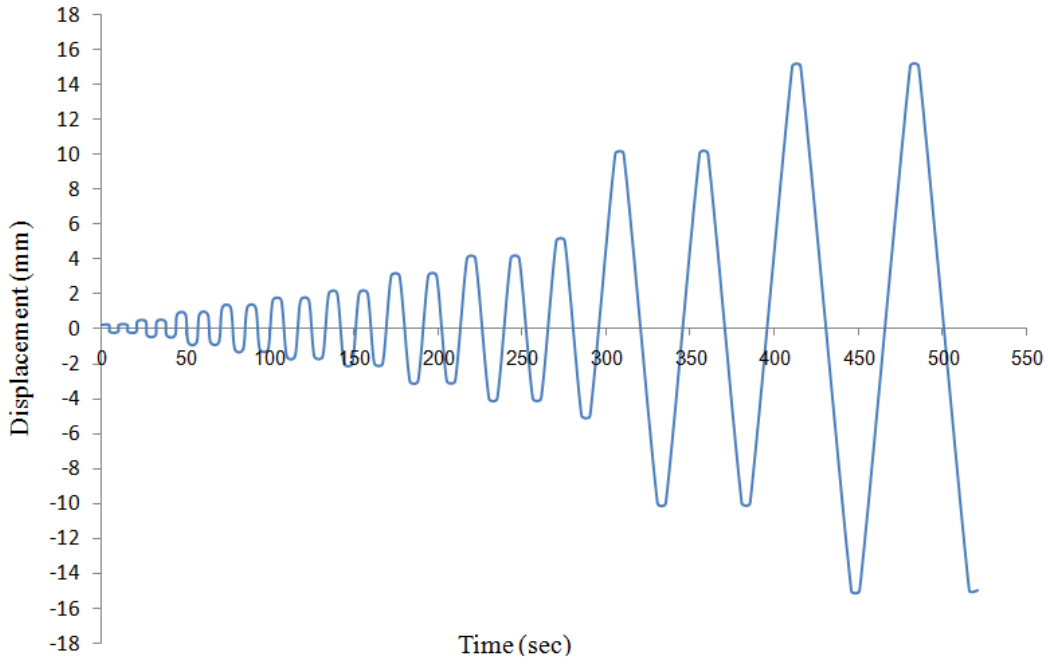

Figure 3.15: Time-Displacement History

Once the test began, the vertical actuator was held in displacement control to prevent lifting of the wall. Despite this, the heel of the walls lifted by about 6 to 10 mm during the tests. As a result, the value of the vertical load applied on the top of the wall varied during the tests, increasing with increasing horizontal load. The effect of this variation will be discussed more in the next chapter.

3.5 Experimental Procedure

Each wall was set in place using a special steel lifting frame [Fig. 3.16] to align it with the centre of the actuator and then plaster was placed beneath the wall to ensure a level and even connection between the bottom of the wall and the lab strong floor.

Figure 3.16: The Steel Frame Manufactured to Lift Walls

After that, fibreboard and the steel I-beam was placed on the top of the wall while the vertical actuator was placed in contact with the top of the steel beam [Fig. 3.17]. The horizontal actuator was then aligned and a second thick steel plate placed at the other end of the wall and tightened to the horizontal actuator by long steel rods. The centre of the

horizontal actuator was located at 1200 mm from the base of the wall. Then, the hydraulic pump at the base of the wall was pumped to the 10 kN to hold the wall and eliminate movement at the base during the test [Fig. 3.17].

Figure 3.17: Steel Rods, I-Beam (left) and the Hydraulic Pump (right)

After that, side rods and plates were placed at the base of the specimen from both sides and tightened to prevent the walls from kicking out [Fig. 3.18].

Figure 3.18: Rod and Steel Plates used on the Side of the Wall to Prevent Kicking Out

The LSCs were placed and connected to the data acquisition system to measure the displacements during the tests [Fig. 3.19].

Figure 3.19: Locations of LSCs on the Left Side of the Wall

3.6 Summary

The test set-up was prepared and fine-tuned over a period of several months in collaboration with fellow MSc. student Jason Moroz. Mr. Moroz carried out his testing first during which time several problems in the setup and programming were encountered, leading to the implementation of many changes and improvements in the setup. His final test set-up is the one that was used for the testing described here. Calibration and checking of the actuators and load cells was done before carrying out the tests in this study to make sure that they were working accurately. Every test was prepared in an average of three hours: plastering and aligning the specimen, setting up the transducers and actuators, and finally checking the test program. Each test took about 20 minutes to complete.

CHAPTER FOUR:

OBSERVATIONS AND EXPERIMENTAL RESULTS

4.1 Introduction

In this chapter of the thesis, the observations and the data from the tests described in the previous chapter will be discussed and analyzed to support the conclusions obtained from this experimental study.

4.2 Test Observations

The eight walls were subjected to the lateral cyclic load (pull then push) and the tests were stopped when the walls had cracked, experienced a significant decrease in sustained load and it was deemed they were about to collapse and/or it was deemed unsafe to continue loading. Moreover, it was observed that the push cycles (negative values on the load-displacement graphs in this chapter) are the more accurate readings and will be relied upon in the calculations. The pull cycles do not give the exact displacement applied because some of the input deformation was taken up by the stretching of the steel rods that connected the thick steel plates of the actuator together. In this section, the observations and what happened in the tests are thoroughly discussed.

- **Wall-C:**

This wall was tested 28 days after construction and the mean prism compressive strength was 12.7 MPa. The maximum lateral load resisted by this wall (see the red dot on the graph), considering the push cycles only, was about 60 kN at a displacement of 2 mm [Fig. 4.1]. The first visible crack appeared at a displacement of 3 mm. There, the wall started to absorb energy (see the starting of the dotted line in the figure below) and the load resistance decreased gradually till a complete failure happened at the end of the first pull cycle of 4 mm when the right side of the wall started to have step failure also as shown in Figure 4.2. The test was stopped when the wall was about to collapse at the second cycle of 5 mm displacement.

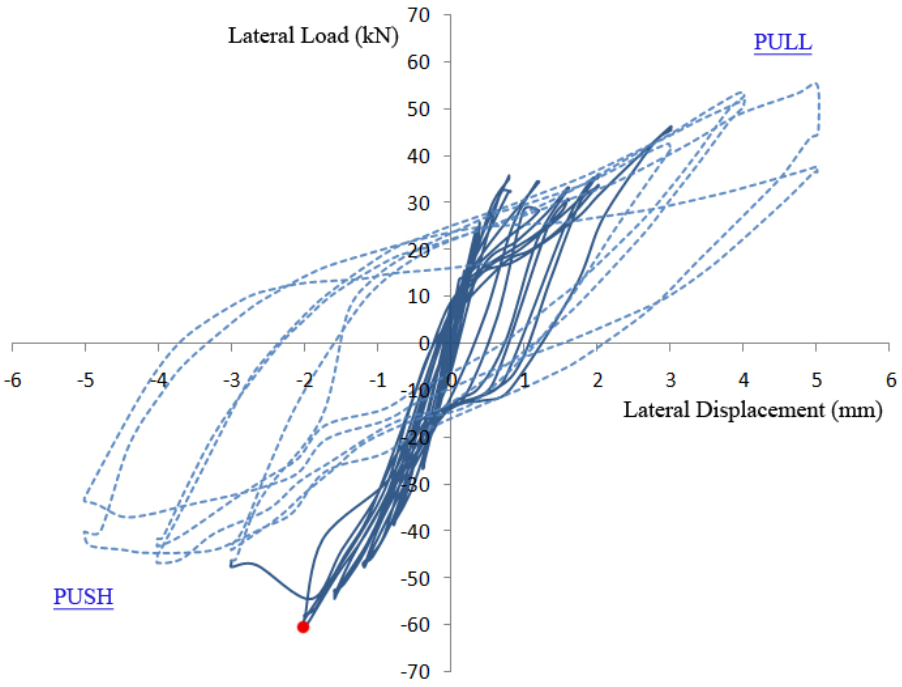

Figure 4.1: Load-Displacement Graph of Wall-C

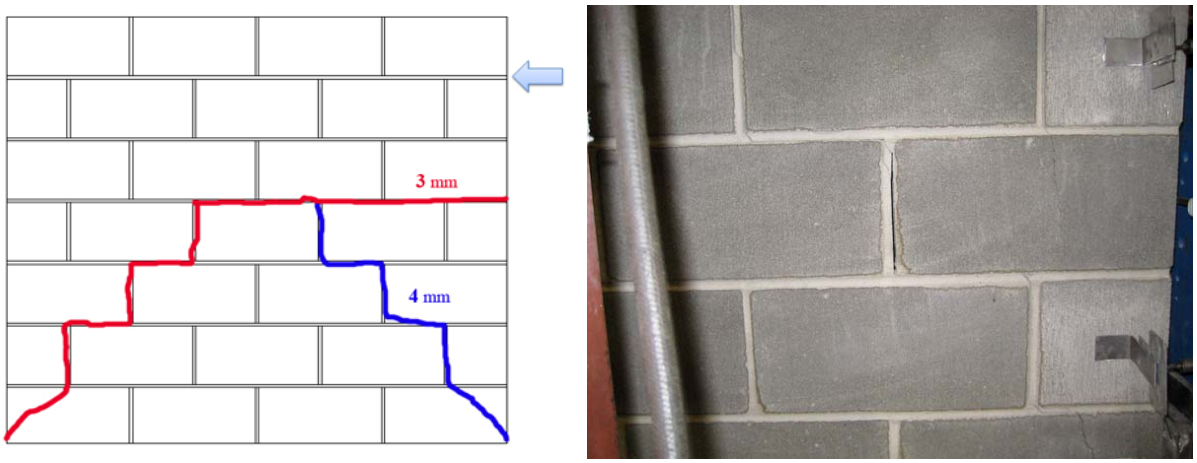

Figure 4.2: Cracks and Corresponding Displacement Cycles in Wall-C

- **Wall-S:**

  This wall was tested 58 days after construction and the mean prism compressive strength was 12.0 MPa. The maximum lateral load resisted by Wall-S was about 68 kN occurring at a displacement of 3 mm [Fig. 4.3]. Then, a visible crack appeared at the bottom course of the wall at a displacement of 4 mm where no bed joint reinforcement was present and at the toes as shown in Figure 4.4. There, the wall started to absorb energy and the load resistance decreased gradually. At the end of push cycle 4 mm the whole mortar joint at the bottom was cracked (debonding) and the upper part of the wall started to move separately (sliding) without any further cracking. The test was stopped when cycle 4 mm completed because the wall was about to collapse.

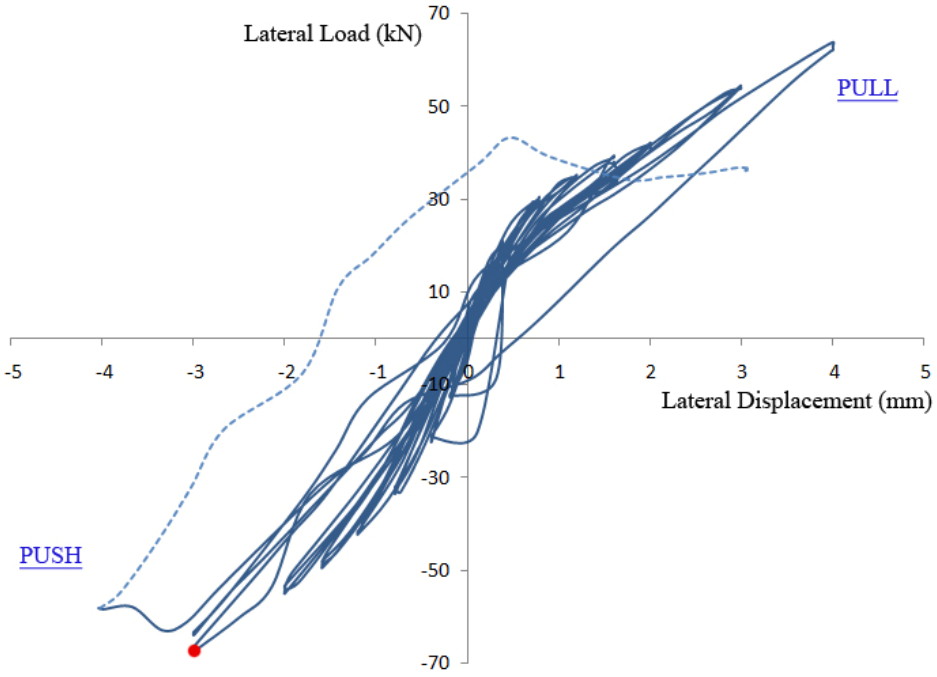

Figure 4.3: Load-Displacement Graph of Wall-S

Figure 4.4: Cracks and Corresponding Displacement Cycle in Wall-S

- **Wall-G(G):**

  Wall-G(G) was tested 32 days after construction and the mean prism compressive strength was 12.2 MPa. The maximum lateral load resisted by

Wall-G(G) was about 105 kN at a displacement of 5 mm [Fig. 4.5]. The first visible cracks appeared at the bottom course at a displacement of 5 mm where no bed joint reinforcement was present and at the toes as shown in Figure 4.6. At this stage, the wall began to absorb energy and the load resistance decreased gradually. At the end of the second cycle of 5 mm, another crack appeared along the mortar joint in the second course. Then, at the first push cycle of 10 mm, the whole mortar joint at the two bottom courses was cracked (debonding) and the upper part of the wall started to move separately (sliding) without any further cracking. The test was stopped when the second push cycle of 10 mm completed because the wall was about to collapse.

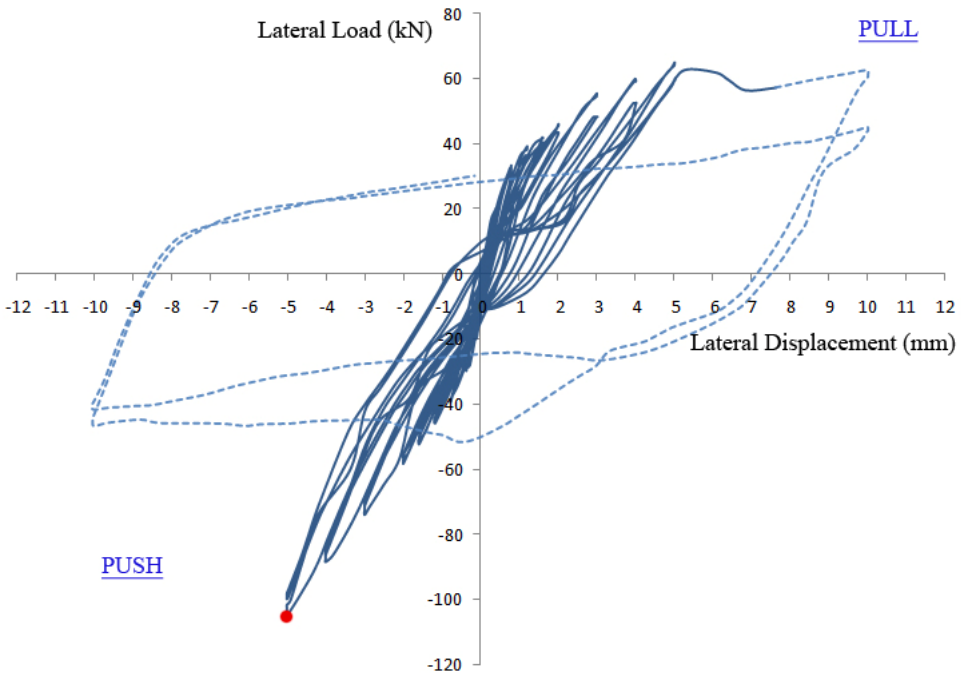

Figure 4.5: Load-Displacement Graph of Wall-G(G)

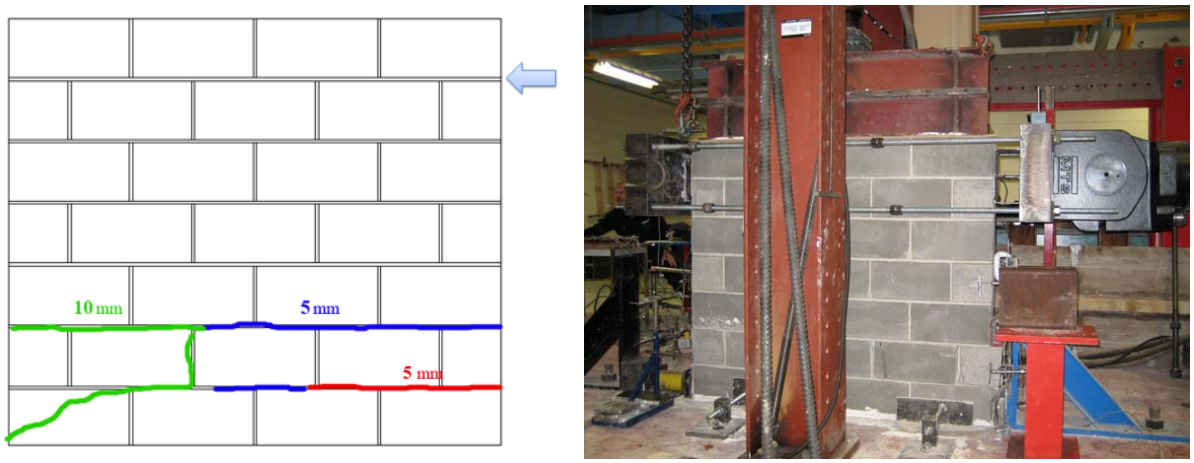

Figure 4.6: Cracks and Corresponding Displacement Cycles in Wall-G(G)

- **Wall-G(L):**

  This wall was tested 30 days after construction and the mean prism compressive strength was 14.4 MPa. The maximum horizontal load resisted by this test specimen was about 96 kN at a displacement of 5 mm [Fig. 4.7]. The first visible cracks appeared at a displacement of 5 mm at a joint where no reinforcement is present when the wall started to absorb energy and the lateral load resistance decreased gradually. The failure crack was stepped as shown in Figure 4.8. At the end of the second pull cycle of 10 mm the left side of the wall started to have step failure also. The test was stopped when the second cycle of 10 mm completed because it was deemed unsafe to continue loading.

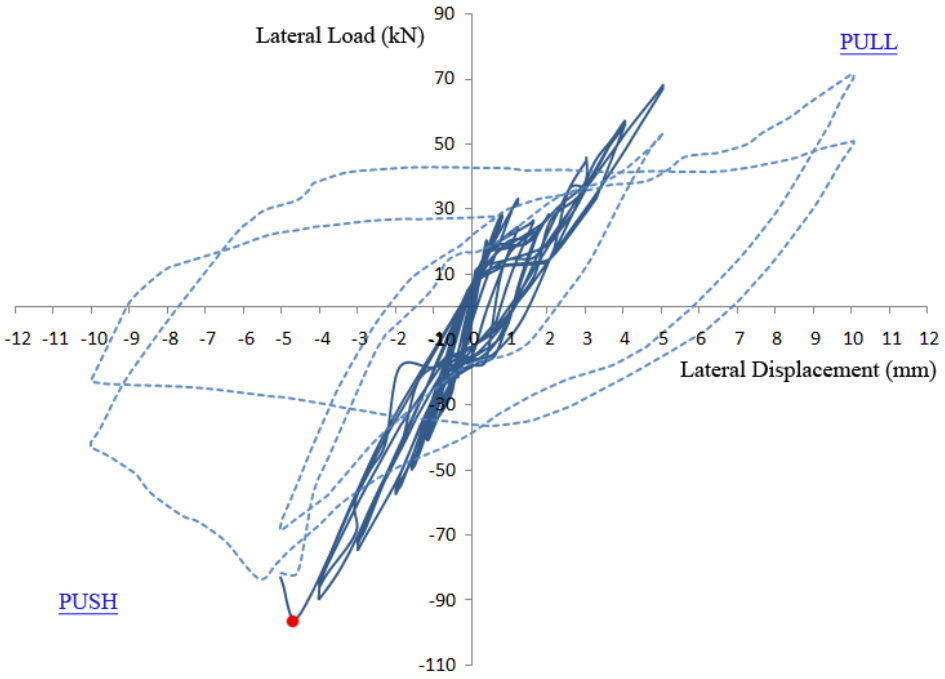

Figure 4.7: Load-Displacement Graph of Wall-G(L)

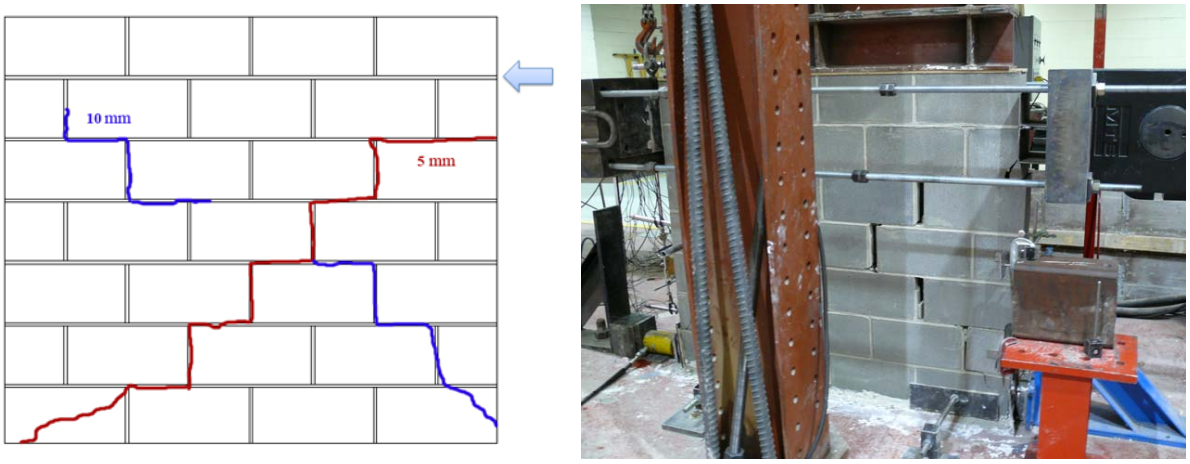

Figure 4.8: Cracks and Corresponding Displacement Cycles in Wall-G(L)

- **Wall-G(T):**

Wall-G(T) was tested 35 days after construction and the mean prism compressive strength was 14.4 MPa. The maximum lateral load resisted by the

wall was 100 kN at a displacement of 5 mm as shown in Figure 4.9. The first cracks appeared at a displacement of 5 mm at the bottom course where no reinforcement was present when the wall started to absorb energy and the lateral load resistance decreased gradually. At the end of the second push cycle of 5 mm, the half unit in the second course separated due to the cracks in the mortar joints [Fig. 4.10]. Then, the whole mortar joint at the bottom was cracked (debonding) and the wall's upper part started to move separately (sliding) without any further cracks. The test was stopped when the second push cycle of 10 mm completed because it was deemed unsafe to continue loading.

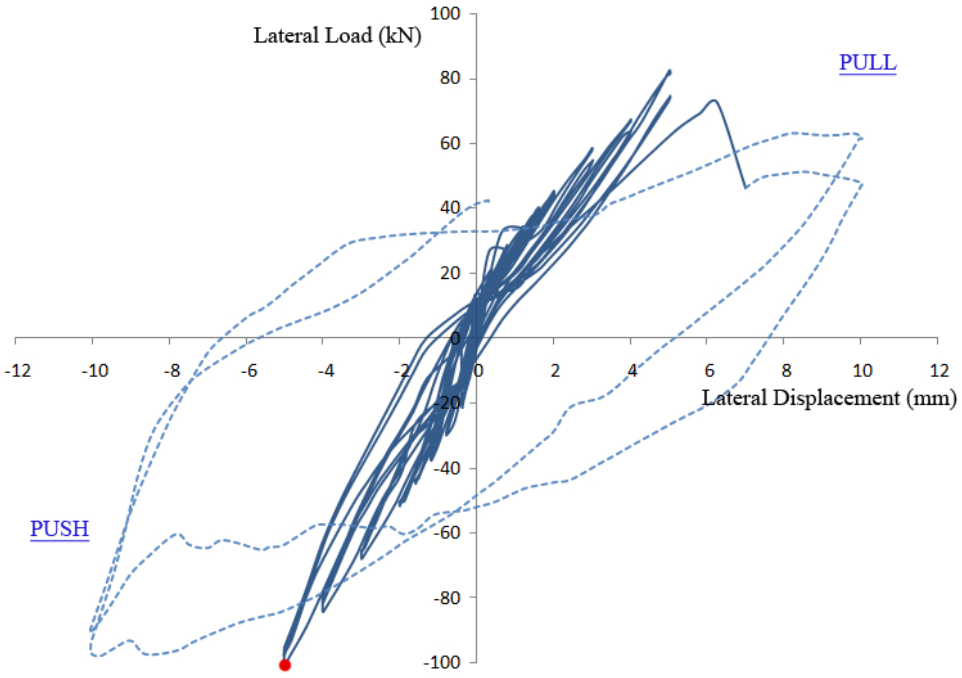

Figure 4.9: Load-Displacement Graph of Wall-G(T)

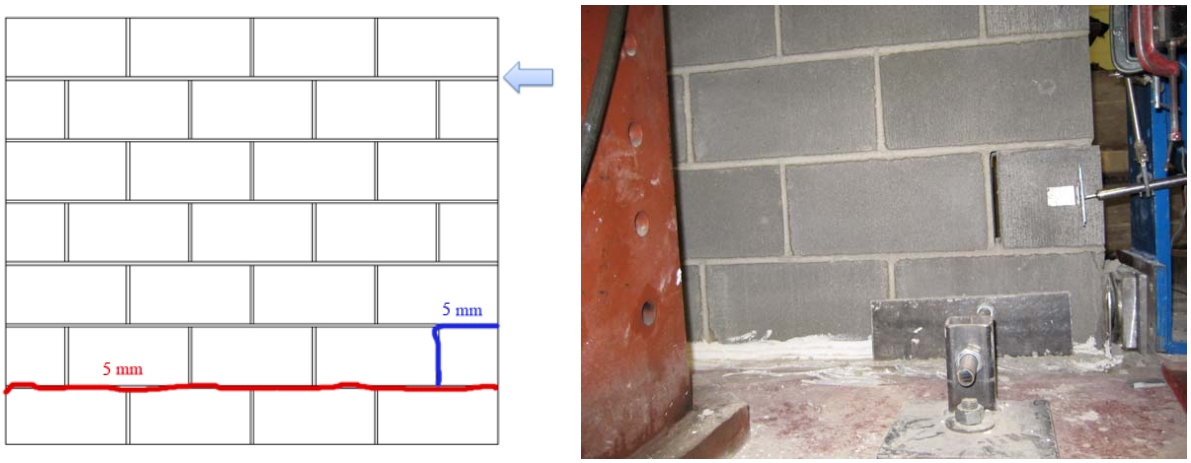

Figure 4.10: Cracks and Corresponding Displacement Cycles in Wall-G(T)

- **Wall-E(L):**

Walls E(L), E(G1) and E(G2) were all tested 30 days after construction and the mean prism compressive strength for these walls was 17 MPa. For the specimen Wall-E(L), the maximum lateral load resisted was about 70 kN occurring at a displacement of 4 mm [Fig. 4.11]. However, the first visible crack appeared at a displacement of 4 mm where a ladder shaped Geogrid BJR was located. At this stage the wall started to absorb energy and the lateral load resistance decreased gradually. Then, a crack appeared at the bed joint of the fourth course on the right side of the wall and propagated to form a step failure in the 4 mm displacement pull cycle. As shown in Figure 4.12, other cracks appeared in the left side and the left bottom corner of the wall in the 5 mm cycle. The test was stopped when the second cycle of 10 mm completed because the wall was about to collapse.

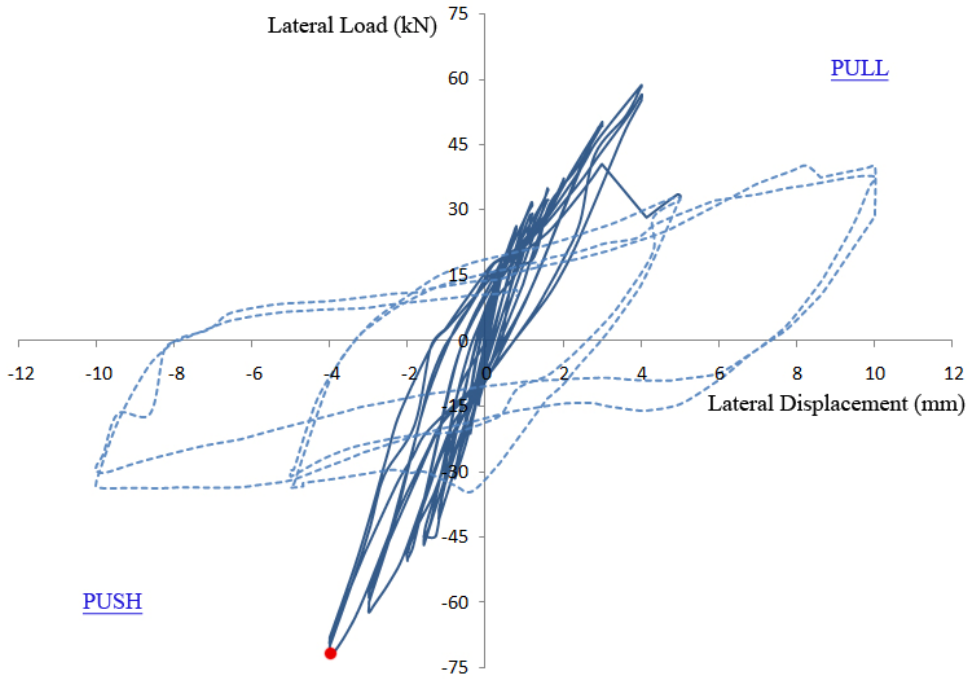

Figure 4.11: Load-Displacement Graph of Wall-E(L)

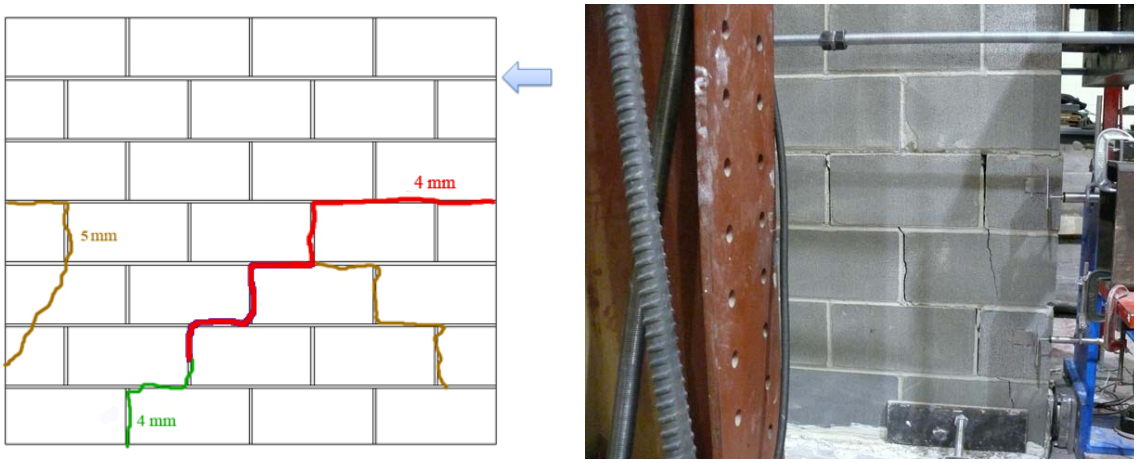

Figure 4.12: Cracks and Corresponding Displacement Cycles in Wall-E(L)

- **Wall-E(G1):**

The maximum lateral load resisted by Wall-E(G1) before any visible cracks was about 111 kN at a displacement of 10 mm [Fig. 4.13]. The wall remained

uncracked until the second cycle of 10 mm displacement. At that point, a crack appeared at the bottom course as shown in Figure 4.14 where no reinforcement was present when the wall started to absorb energy and the lateral load started to decrease gradually. At the end of the second pull cycle of 15 mm the toes of the wall were crushed and the whole mortar joint at the bottom was cracked (debonding). Then, the upper part of wall started to move separately (sliding) without any further cracking. The test was stopped when the second push cycle of 20 mm completed because the wall was about to collapse.

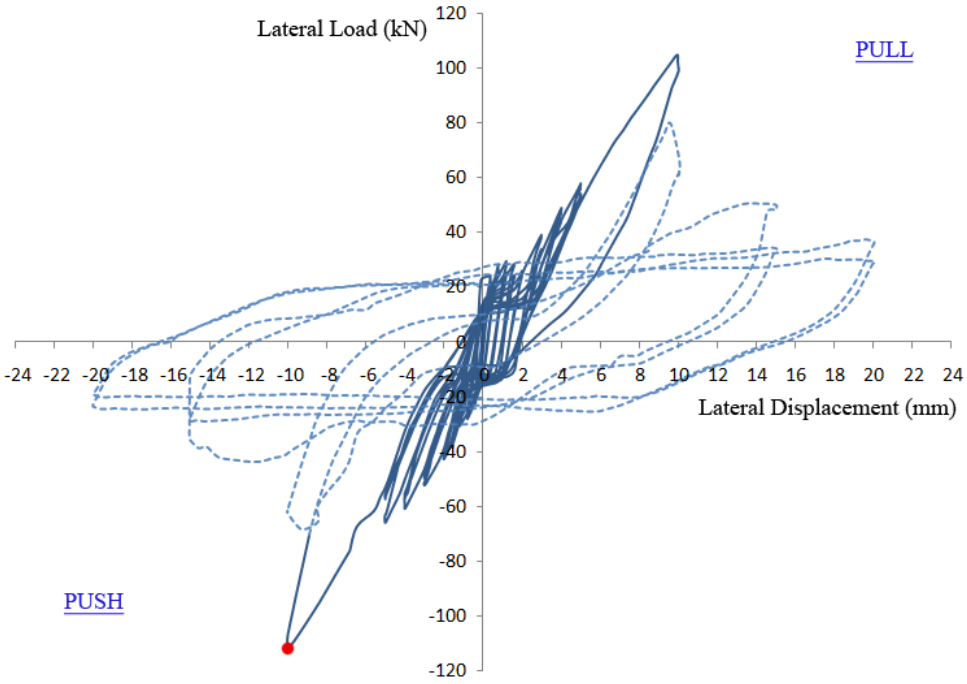

Figure 4.13: Load-Displacement Graph of Wall-E(G1)

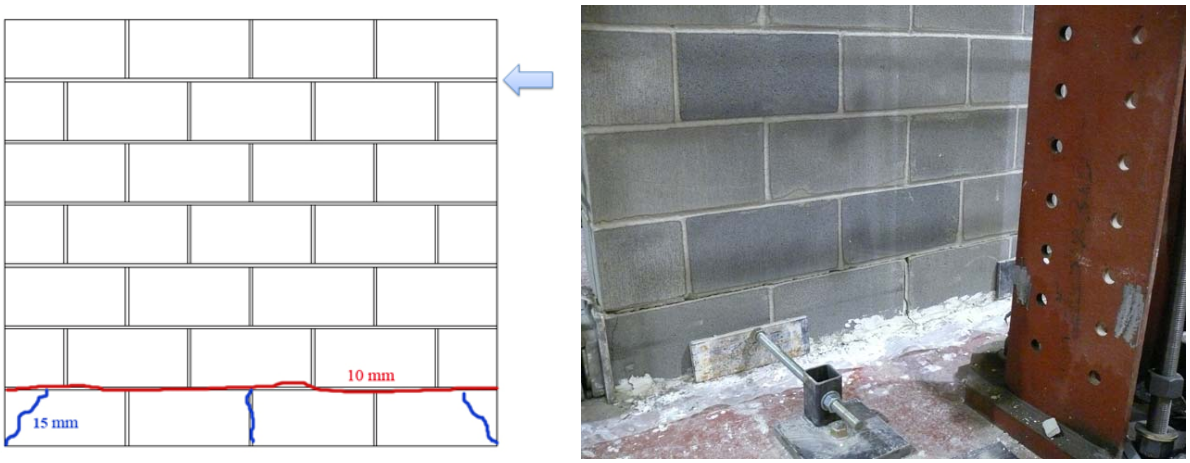

Figure 4.14: Cracks and Corresponding Displacement Cycles in Wall-E(G1)

- **Wall-E(G2):**

  The maximum lateral load resisted by Wall-E(G2) was about 80 kN at a displacement of 5 mm [Fig. 4.15]. This wall remained uncracked until a displacement of 6 mm. The first visible cracks appeared at the bottom course where no reinforcement was present and the toes as shown in Figure 4.16 when the wall started to absorb energy and the load resistance decreased gradually. At the end of the second pull cycle of 10 mm, the half units in the second course separated due to the crack in the mortar joints. Subsequently, the whole mortar joint at the bottom was cracked (debonding) and the upper part of the wall started to move separately (sliding) without any further cracking. The test was stopped when the first push cycle of 15 mm completed because the wall was about to collapse.

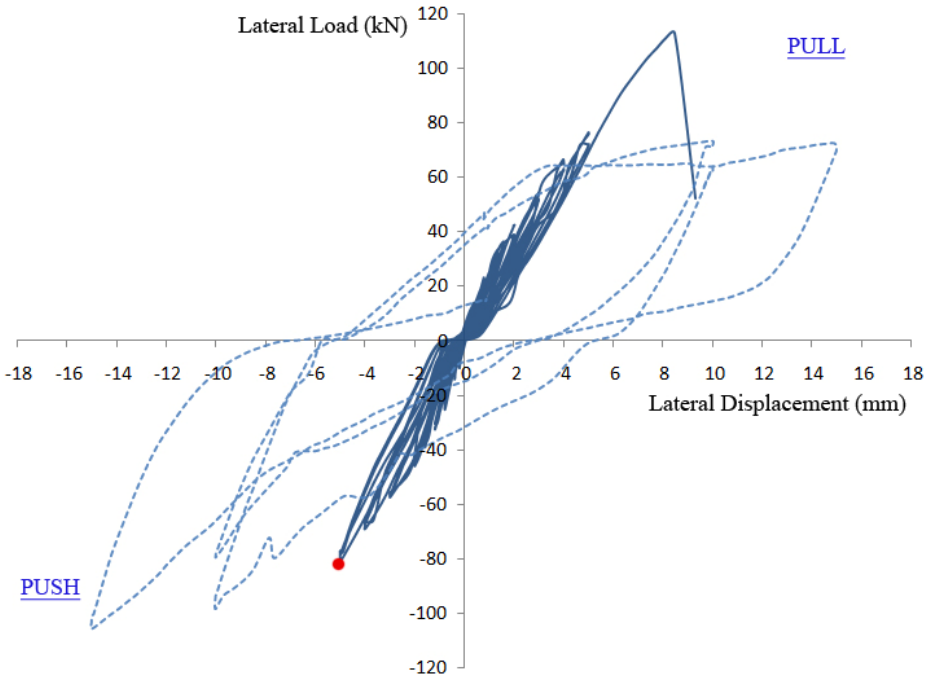

Figure 4.15: Load-Displacement Graph of Wall-E(G2)

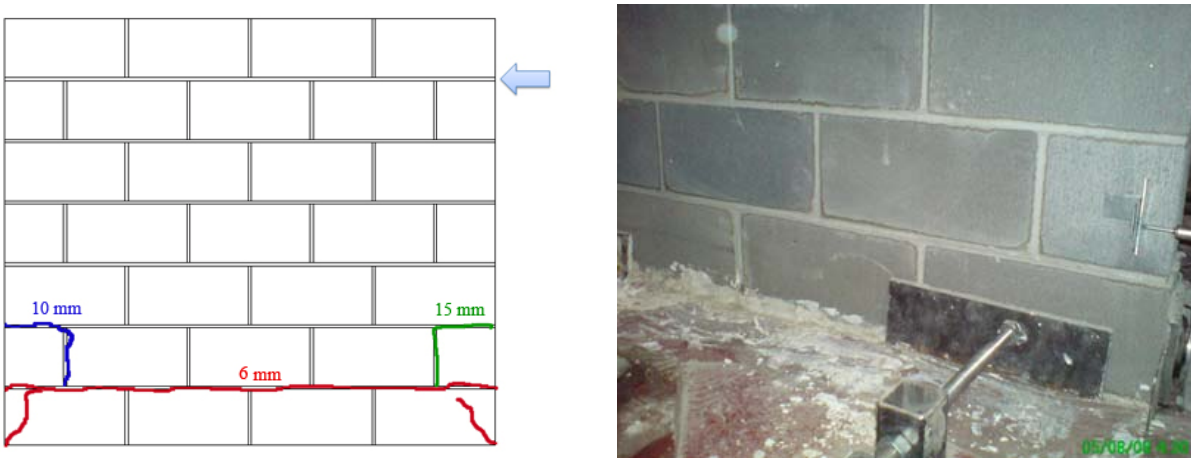

Figure 4.16: Cracks and Corresponding Displacement Cycles in Wall-E(G2)

4.3 Discussion

As mentioned earlier, the vertical load (60 kN) applied to the top of the wall varied during the tests because the walls were not fixed on the ground and could rotate slightly due to the use of a spherical seat with the vertical actuator. The variation in the value of the vertical load applied would affect the lateral load capacity of the specimens. When the vertical load increases the lateral load capacity increases and vice versa. As a result, at maximum lateral load, the heel of the walls lifted by about 6 to 10 mm and the vertical load was higher than 60 kN. So, in the next chapter, the vertical load corresponding to the failure will be considered in the calculations and analysis. This makes comparison between the specimens more challenging, however; several observations and conclusions can still be made.

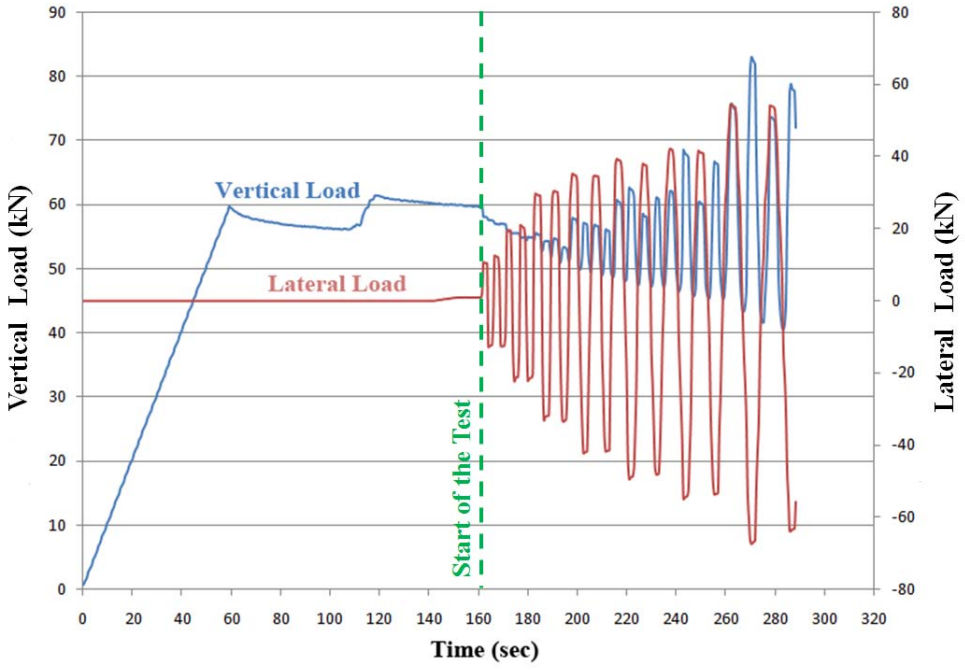

Figure 4.17: Variation in Vertical Load and Corresponding Lateral Load for Wall-S

Figure 4.17 shows the variation in vertical load and corresponding lateral load for one of the tests as a typical example to demonstrate the changes in the value of the axial load. As shown in Figure 4.17, from a time of 60 seconds up to 130 seconds, the vertical load dropped below 60 kN and then increased again to this target. This drop in load occurs in part due to the initial elastic shortening of the wall but mainly due to the slow initial compression of the fiberboard placed between the top of the wall and the steel beam..

Table 4.1: Summary of the Test Specimens and the Modes of Failure

Specimen	**Wall-C**	**Wall-S**	**Wall-G(G)**	**Wall-G(L)**	**Wall-G(T)**	**Wall-E(L)**	**Wall-E(G1)**	**Wall-E(G2)**
Mean Prism Compressive Strength, MPa	12.7	12.0	12.2	14.4	14.4	17.0	17.0	17.0
Type of BJR	N/A	Steel Ladder	GFRP Grid	GFRP Ladder	GFRP Truss	Geogrid Ladder	Geogrid Grid	Geogrid Grid
Cross-sectional Area, A_v , mm^2	N/A	19.2	14.1	14.1	14.1	9.0	9.0	9.0
Frequency of BJR	N/A	Every 2nd course	Every 2nd course	Every 2nd course	Every 2nd course	Every 2nd course	Every course	Every 2nd course
Failure Mode	Step	Sliding	Sliding	Step	Sliding	Step	Sliding	Sliding
Maximum Lateral Load Reached, kN *	60	68	105	96	100	70	111	80
Corresponding Displacement, mm *	2	3	5	5	5	4	10	5
Displacement of 1st Visible Crack, mm	3	4	5	5	5	4	10	6
1st Crack went through the BJR	N/A	No	No	No	No	Yes	No	No
% Increase in lateral load over Wall-C	-	13.3%	75%	60%	66.7%	16.7%	85%	25%

* Only "Push" values were considered as mentioned in Section 4.2.

Generally and based on the primary results, it can be stated that the use of bed joint reinforcement increased the lateral load capacity of CMU walls by between 13.3% and 85% of the original capacity. For example, the lateral capacity of Wall-E(L) and Wall-G(G) increased over the capacity of Wall-C by 16.7% and 75% respectively. In addition, the first visible crack in all specimens except Wall-E(L) occurred in a joint where no bed joint reinforcement was present which shows that the joints without reinforcement have less resistance to lateral loads than the reinforced joints.

In addition, GFRP ladder bed joint reinforcement increased the lateral capacity of the masonry walls by about 45% more than steel while the GFRP has a smaller cross-sectional area than steel (≈ 36% less) [Table 4.1]. This as a primary result shows how GFRP is more effective and economical than the conventional BJR material.

As shown in Table 4.1, the variation of the mean prism compressive strength (12 to 17 MPa) is quite large which affects the failure mode and the capacity of the tested walls significantly.

In the next chapter, results and output data obtained from the tests of the eight walls will be examined more in depth, analyzed, discussed and then compared to the theoretical results obtained from the equations of the Canadian design code.

CHAPTER FIVE:

ANALYSIS OF EXPERIMENTAL RESULTS

5.1 Introduction

In this chapter, data collected and results obtained from the experimental tests of the eight specimens will be analyzed, discussed and then compared to the theoretical results obtained from the equations of the CSA Standard (S304.1-04) to support the conclusions and recommendations.

5.2 Analysis of Experimental Results

In general, the maximum enhancement in strength compared to the control wall was observed for the wall reinforced with grid shape Geogrid bed joint reinforcement (BJR) every course (Wall-E(G1)); where the lateral load capacity increased by 85% as shown in Table 5.1. However, the minimum enhancement was in Wall-S where there was only a 13.3% increase which is not significant due to the high variation in just the strength of the masonry itself as determined from the prism compression tests (COV = 14%).

Figure 5.1 shows the load-displacement envelopes for the push cycles of the load-displacement hysteresis loops shown in the previous chapter. In the following section, each load-displacement envelope will be idealized and analyzed to facilitate comparison between the BJR configurations and materials used in the tested walls.

Table 5.1: Summary of Results of the Test Specimens

Specimen	Wall-C	Wall-S	Wall-G(G)	Wall-G(L)	Wall-G(T)	Wall-E(L)	Wall-E(G1)	Wall-E(G2)
Mean Prism Compressive Strength, MPa	12.7	12.0	12.2	14.4	14.4	17.0	17.0	17.0
Type of BJR	N/A	Steel Ladder	GFRP Grid	GFRP Ladder	GFRP Truss	Geogrid Ladder	Geogrid Grid	Geogrid Grid
Frequency of BJR	N/A	Every 2nd course	Every 2nd course	Every 2nd course	Every 2nd course	Every 2nd course	Every course	Every 2nd course
Maximum Lateral Load Reached, kN *	60	68	105	96	100	70	111	80
% increase in lateral load cap. compared to Wall-C	-	13.3%	75%	60%	66.7%	16.7%	85%	25%

* Only "Push" cycles were considered as mentioned in section 4.2.

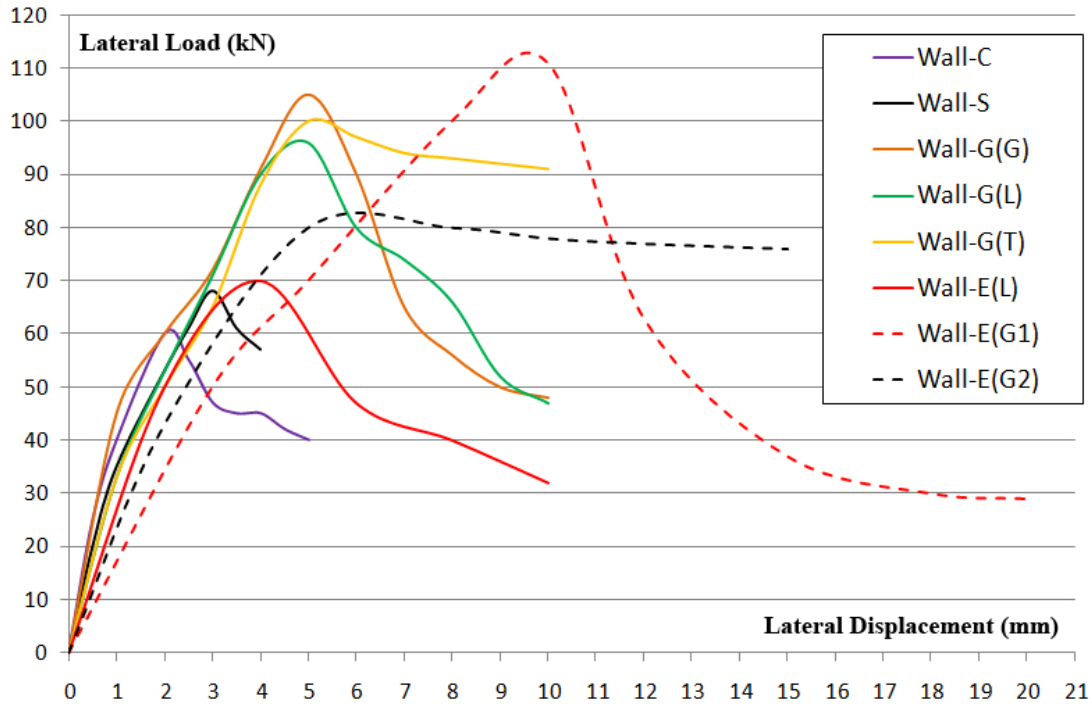

Figure 5.1: Load-Displacement Envelopes for Tested Walls (push cycles)

To simplify these envelopes, a common method used is the bilinear idealization for which some observations and results from the experimental tests are used in the equations.

Gouveia *et al.* [2007], Lourenço *et al.* [2008] and Tomaževič [1999] present the equations and explain the steps of obtaining the idealized envelopes [Fig. 5.2].

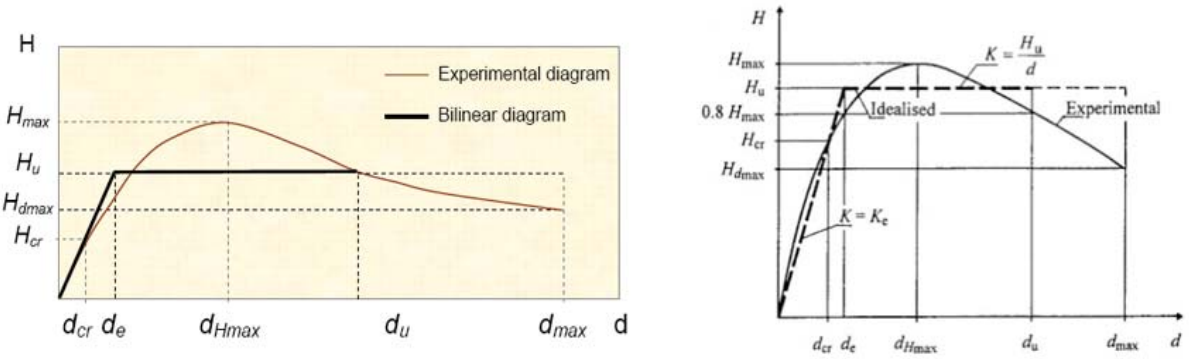

Figure 5.2: Idealization of Load-Displacement Envelopes from Gouveia *et al.* [2007] (left) and Tomaževič [1999] (right)

The value of H_{cr} is $0.7H_{max}$ and d_{cr} is the corresponding value of displacement for H_{cr}. Then, d_e is the deflection at the end of the elastic stage of the idealized curve. The value of the initial slope which is the effective stiffness, K_e, is given by:

$$K_e = \frac{H_{cr}}{d_{cr}} \qquad [5.1]$$

,the value of the ultimate idealized lateral resistance, H_u, is given by:

$$H_u = K_e\left[d_{\max} - \sqrt{d_{\max}^2 - \frac{2A_{env}}{K_e}}\right] \qquad [5.2]$$

and the ultimate ductility, μ_u, is given by:

$$\mu_u = \frac{d_u}{d_e} \qquad [5.3]$$

The energy absorption of the walls was estimated by first idealizing the load-displacement envelopes and then calculating the area, A_{env}, under each idealized curve. The different values obtained from all tested walls are given in Table 5.2 below while Figure 5.3 shows a typical example of an idealized curve obtained from the experimental envelope. Figures for the other walls can be found in Appendix B.

Table 5.2: Calculation Results for Bilinear Idealization and Ductility of the Test Specimens

Wall	H_{max} (kN)	$0.7H_{max}$ (kN)	d_{cr} (mm)	K_e (kN/mm)	$0.8H_{max}$ (kN)	d_e (mm)	d_u (mm)	d_{max} (mm)	A_{env} (kN.mm)	H_u (kN)	H_u/H_{max}	μ_u
Wall-C	60.0	42.0	1.1	38.2	48.0	1.30	3.60	5.0	139.3	47.2	0.79	2.8
Wall-S	68.0	47.6	1.6	29.8	54.4	2.00	4.00	4.0	155.1	51.8	0.76	2.0
Wall-G(G)	105.0	73.5	3.1	23.7	84.0	3.60	8.00	10.0	513.4	82.8	0.79	2.2
Wall-G(L)	96.0	67.2	2.8	24.0	76.8	3.20	8.00	10.0	491.5	76.0	0.79	2.5
Wall-G(T)	100.0	70.0	3.2	21.9	80.0	3.55	10.00	10.0	658.0	79.1	0.79	2.8
Wall-E(L)	70.0	49.0	2.0	24.5	56.0	2.40	7.50	10.0	346.5	55.0	0.79	3.1
Wall-E(G1)	111.0	77.7	5.8	13.4	88.8	6.80	13.00	20.0	839.0	87.4	0.79	1.9
Wall-E(G2)	80.0	56.0	2.9	19.6	64.0	3.50	15.00	15.0	830.8	62.7	0.78	4.3

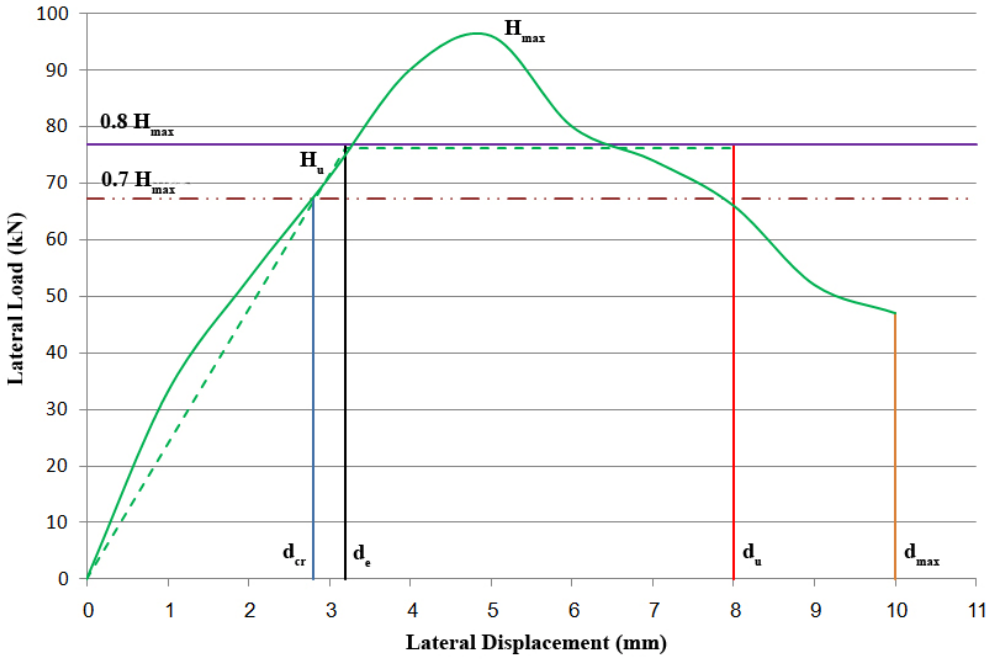

Figure 5.3: Typical Idealization Example of Experimental Envelope (Wall-G(L))

The idealized envelopes for all of the tested walls are shown below in Figure 5.4.

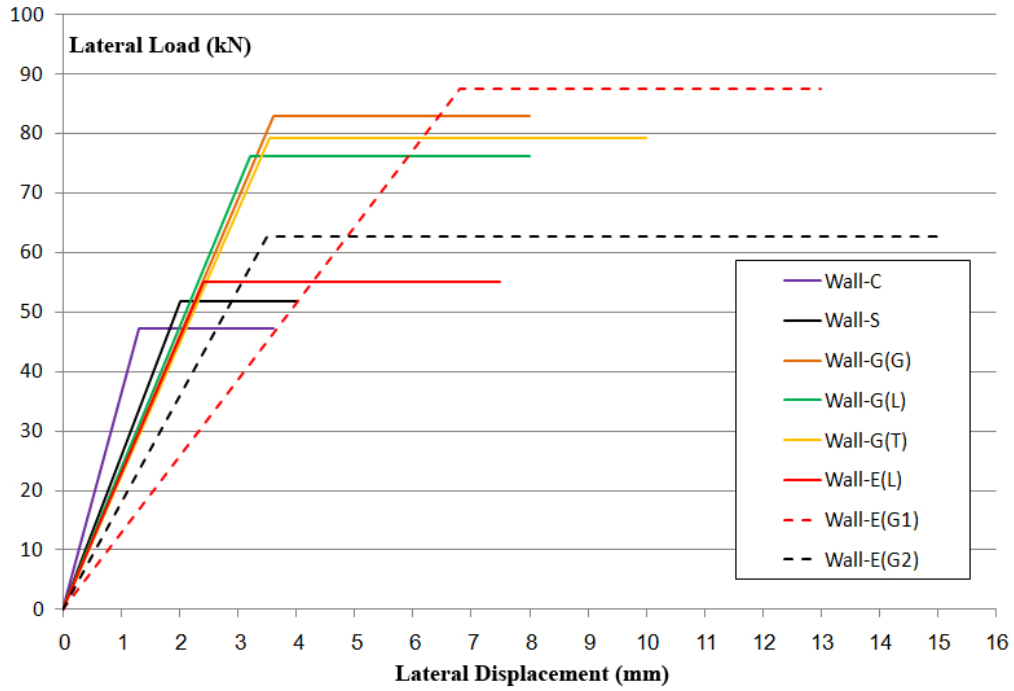

Figure 5.4: Idealized Experimental Envelopes for all Walls

The energy-absorbing properties are not restricted to the wall behaviour leading up to the ultimate strength and there may be additional energy absorption beyond the peak load [Drysdale and Hamid 2005]. Therefore, ductility, μ_u, which is indicated by the deformation after yielding and describes the extent to which materials can be deformed plastically without fracture, is a measure of this desirable quality. So, by comparing the area under the idealized envelopes, which indicates the dissipation of the energy absorbed, and ductility values from Table 5.2, the more ductile material and wall will be identified. However, generally from Table 5.2, it can be seen that the ductility value for the unreinforced masonry control wall, 2.8, is within the limitation stated by Tomaževič [1999] for seismic design for URM walls, 2.0 – 3.0. Also, the highest value for ductility is 4.3 for

Wall-E(G2) and this corresponds well with Figure 5.4 where Wall-E(G2) has the 2nd lowest stiffness and the largest displacement value. However, even though Wall-E(G1) has the lowest stiffness and the 2nd largest displacement value among the walls, it has the lowest ductility value, 1.9, due to the rapid decrease in load resistance beyond the peak point as shown in Figure 5.1.

In addition, large displacement with high load resistance increased the energy absorbed by the walls significantly. The ductility is also still affected by the increase in displacement and load capacity but is more directly related to the difference between the ultimate displacment resisted and the displacement at the end of the elastic stage of the idealized curve.

Hatzinikolas and Korany [2005] stated that unreinforced masonry walls are very stiff and their elastic response during intense earthquakes can be very high. This is shown clearly in the slopes for the idealized envelopes in Figure 5.4 and the stiffness value, K_e, in Table 5.2 where Wall-C has the highest K_e, 38.2 kN/mm.

5.2.1 Ladder Shape Bed Joint Reinforcement

By comparing the idealized load-displacement envelopes shown in Figure 5.5 between the control wall (Wall-C) and the walls with ladder shape bed joint reinforcement (Wall-S, Wall-E(L) and Wall-G(L)) and the results in Table 5.1, it can be stated that the use of Steel, Geogrid and GFRP bed joint reinforcement increased the lateral capacity of the masonry walls by 13.3%, 16.7% and 60%, respectively. There is apparently a huge difference between the increase in lateral capacity by using GFRP BJR versus Steel

or Geogrid. This means that GFRP was much more effective than Geogrid and steel when ladder shape is used as BJR.

However, the stiffness of the walls with Geogrid and GFRP ladder bed joint reinforcement is lower compared to the other specimens (Wall-C and Wall-S) as indicated by the lower slope of the idealized load-displacement curves of those walls [Fig. 5.5] and the K_e values in Table 5.2. However, the stiffness of the wall with ladder shape of GFRP bed joint reinforcement is slightly more than the wall with ladder shape of Geogrid.

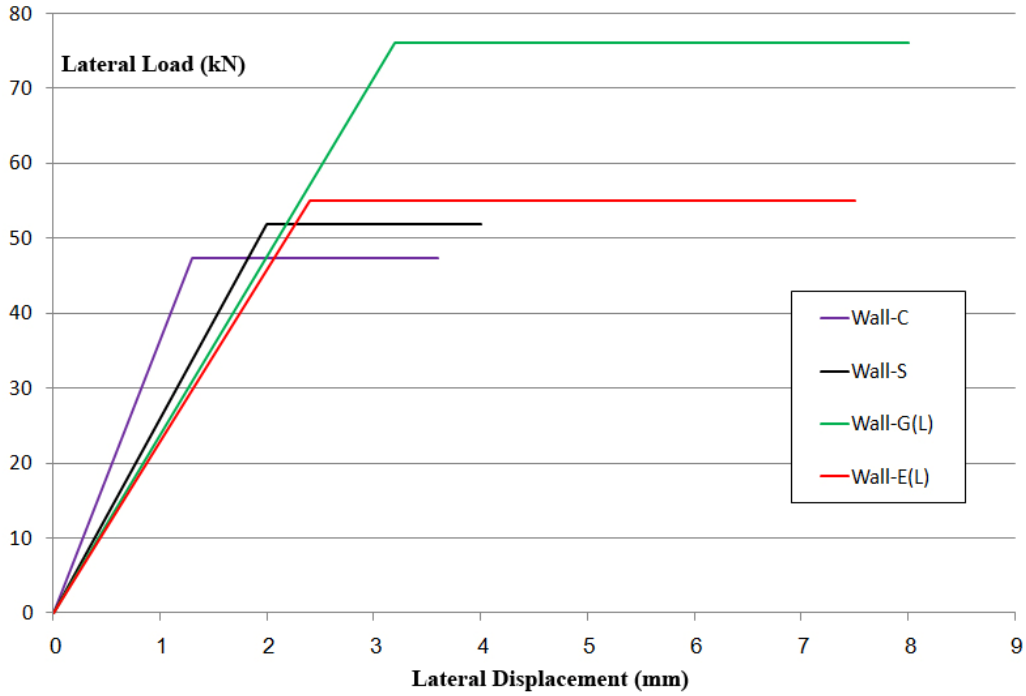

Figure 5.5: Idealized Load-Displacement Envelopes for Walls with Ladder Shape BJR

On the other hand, it can be concluded from Figure 5.5 that the use of Geogrid and GFRP bed joint reinforcement (ladder shape) increased the energy absorption of the walls significantly by 149% and 253% respectively compared to the control wall while steel BJR in Wall-S increased the energy absorption by only 11.4%. Based on Table 5.2, Wall-E(L)

and Wall-G(L) also have high values of ductility, 3.1 and 2.5 respectively, while Wall-S has the lowest ductility value, 2.0, which indicates how GFRP and Geogrid increased the ductility of the walls.

5.2.2 Grid Shape Bed Joint Reinforcement

By comparing the idealized load-displacement envelopes [Fig. 5.6] between Wall-C and the walls with grid shape BJR (Wall-E(G1), Wall-E(G2) and Wall-G(G)) and results shown in Table 5.1, it can be stated that the use of Geogrid and GFRP bed joint reinforcement increased the lateral load capacity of the CMU walls by 85%, 25% and 75%, respectively. In contrast with the ladder shape bed joint reinforcement comparison, the enhancement of Geogrid is more than that of GFRP. The Geogrid grid shape provides more strength to the walls compared to the ladder shape.

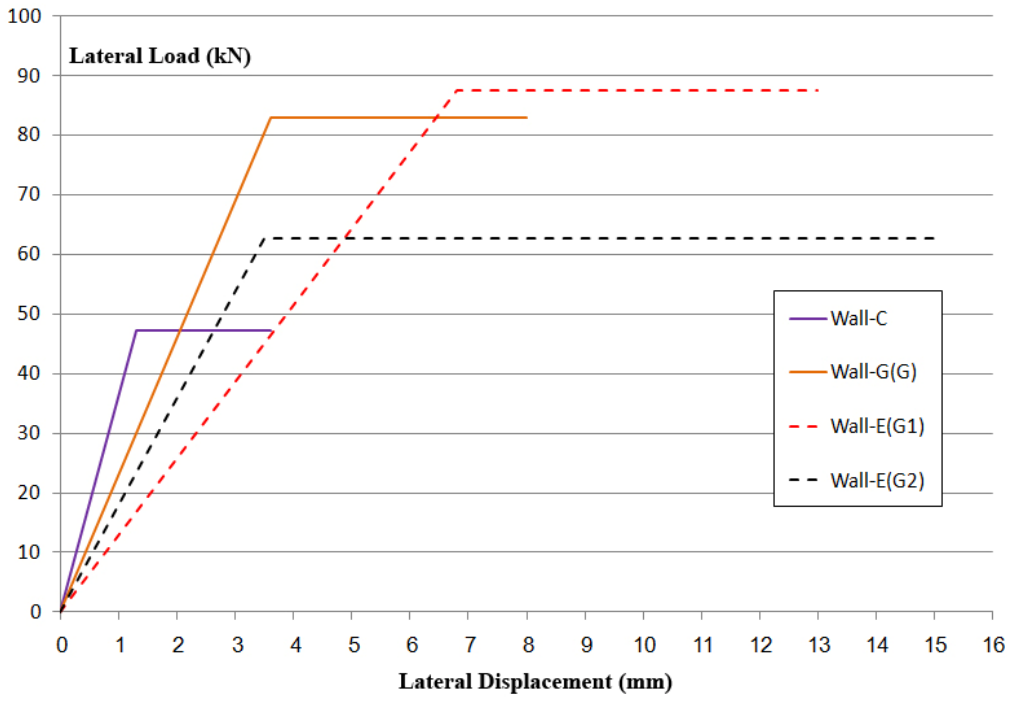

Figure 5.6: Idealized Load-Displacement Envelopes for Walls with Grid Shape BJR

As shown in Figure 5.6 and from Table 5.2, the stiffness of the wall with grid shape of GFRP bed joint reinforcement, Wall-G(G), is again higher than the walls with grid shape of Geogrid, Wall-E(G1) and Wall-E(G2), but all of them are lower in stiffness than the control wall (Wall-C) as expected according to Hatzinikolas and Korany [2005]. In fact, all walls with BJR have lower stiffness than the control wall, perhaps due to the presence of the BJR interrupting the mortar in the joints. In addition, Wall-E(G1) with grid BJR in every course has lower stiffness than Wall-E(G2) with grid BJR every 2nd course which shows how the various configurations, thicknesses and spacing of bed joint reinforcement could also affect the stiffness.

Based on the area under the idealized envelopes it can also be concluded that the use of Geogrid and GFRP bed joint reinforcement (grid shape) increased the energy absorption of the walls by 502.6%, 496.7% and 268.7% for Wall-E(G1), Wall-E(G2) and Wall-G(G), respectively, compared to the control wall. However, Wall-E(G2) has the highest ductility value, 4.3, as shown in Table 5.2 while Wall-E(G1) has the lowest ductility value, 1.9.

5.2.3 GFRP Bed Joint Reinforcement

In Figure 5.7, a comparison between the idealized load-displacement envelopes of Wall-C and the walls with GFRP bed joint reinforcement (Wall-G(G), Wall-G(L) and Wall-G(T)) is shown. Then based on the results in Table 5.1, it can be stated that the use of GFRP bed joint reinforcement increased the lateral capacity of the CMU walls by 60% and 66.7% in the case of ladder shape and truss shape respectively, and in the case of grid shape by 75%.

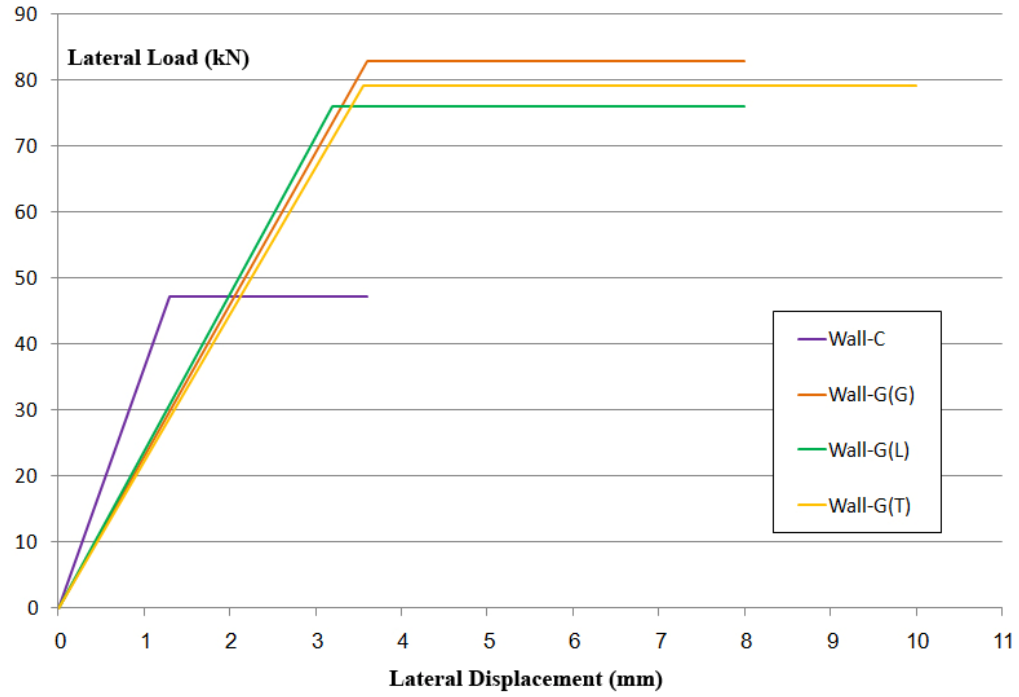

Figure 5.7: Idealized Load-Displacement Envelopes for Walls with GFRP BJR

However, the stiffness of the walls with GFRP bed joint reinforcement is lower than Wall-C as indicated by the lower slope of the idealized load-displacement curves of those walls and K_e values in Table 5.2.

Based on the area under the idealized envelopes in Figure 5.7, the use of GFRP bed joint reinforcement, grid, ladder and truss shapes increased the energy absorption of the walls by almost the same amount; 268.7%, 253% and 372.6%, respectively. This leads to the observation that all of the GFRP walls behaved similarly, as is clearly seen in the figure, but the ductility, μ_u, of Wall-G(T) is the highest compared to the other walls with GFRP bed joint reinforcement as shown in Table 5.2.

5.2.4 Geogrid Bed Joint Reinforcement

Figure 5.8 shows a comparison between the idealized load-displacement envelopes of Wall-C and the walls with Geogrid bed joint reinforcement (Wall-E(L), Wall-E(G1) and Wall-E(G2)). From Table 5.1 it can be stated that the use of Geogrid bed joint reinforcement increased the lateral capacity of the CMU walls by at least 16.7%. However, in the case of grid shape bed joint reinforcement (E(G1) and E(G2)) the lateral load capacity increased by 85% and 25% respectively.

Furthermore, based on the figure below and the K_e values in Table 5.2, the stiffness of the walls with Geogrid BJR is lower than the control wall but Wall-E(L) is the stiffest wall compared to the other two Geogrid walls.

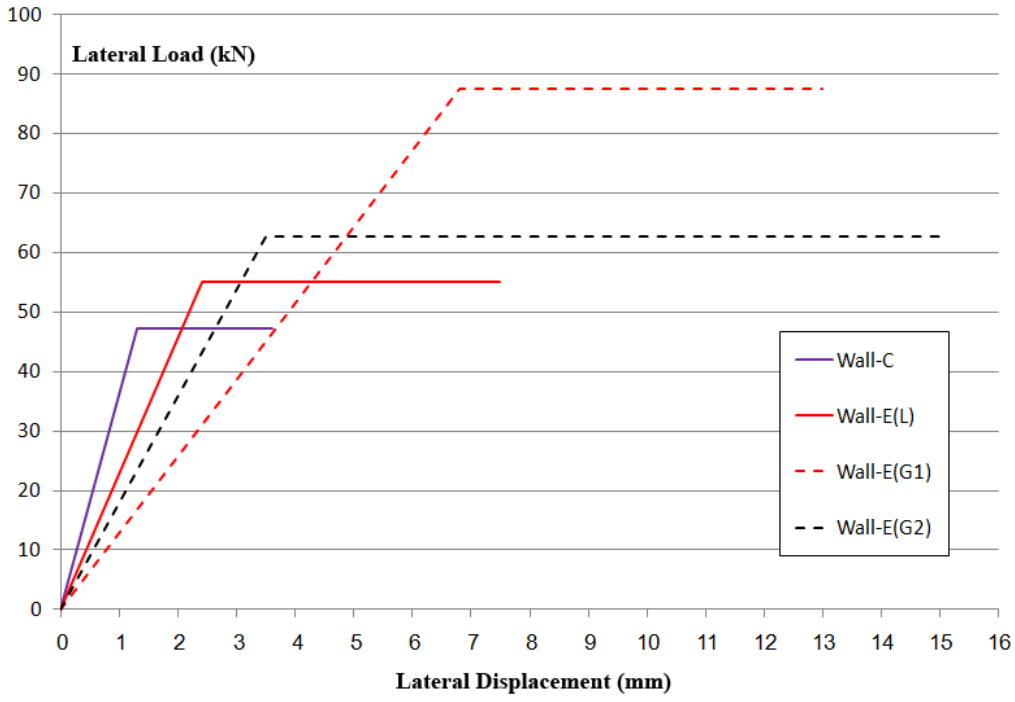

Figure 5.8: Idealized Load-Displacement Envelopes for Walls with Geogrid BJR

It can also be concluded based on the area under the envelopes that the use of Geogrid bed joint reinforcement, ladder and grid shaped (E(G1) and E(G2)) increased the energy absorption of the walls by 149%, 502.6% and 496.7% respectively. Unlike GFRP where there was little difference based on bed joint reinforcement configuration, for this material the grid shape is at least 3 times better in absorbing energy than the ladder shape. And as mentioned before, Wall-E(G2) has the highest ductility value, 4.3, as shown in Table 5.2 while Wall-E(G1) has the lowest ductility value, 1.9. The difference between Wall-E(G1) and Wall-E(G2) in lateral load capacity is 60% and this indicates that using bed joint reinforcement every course compared to every 2^{nd} course significantly affects the lateral capacity of the masonry walls, at least for this material.

From the analysis of the experimental results discussed in the previous sections, it is important to note that the variations within the properties of the concrete masonry units used and the properties of each bed joint reinforcement material used significantly affected the results obtained. This will be one of the major factors that control the improvement in the lateral capacity of the CMU walls generally.

Now, to understand the results more, it is important to compare them with the theoretical equations provided in the codes.

5.3 Theoretical vs. Experimental

Theoretically, the lateral capacity of concrete masonry walls, reinforced and unreinforced, could be calculated according to the provisions for in-plane shear in the CSA Standard S304.1-04.

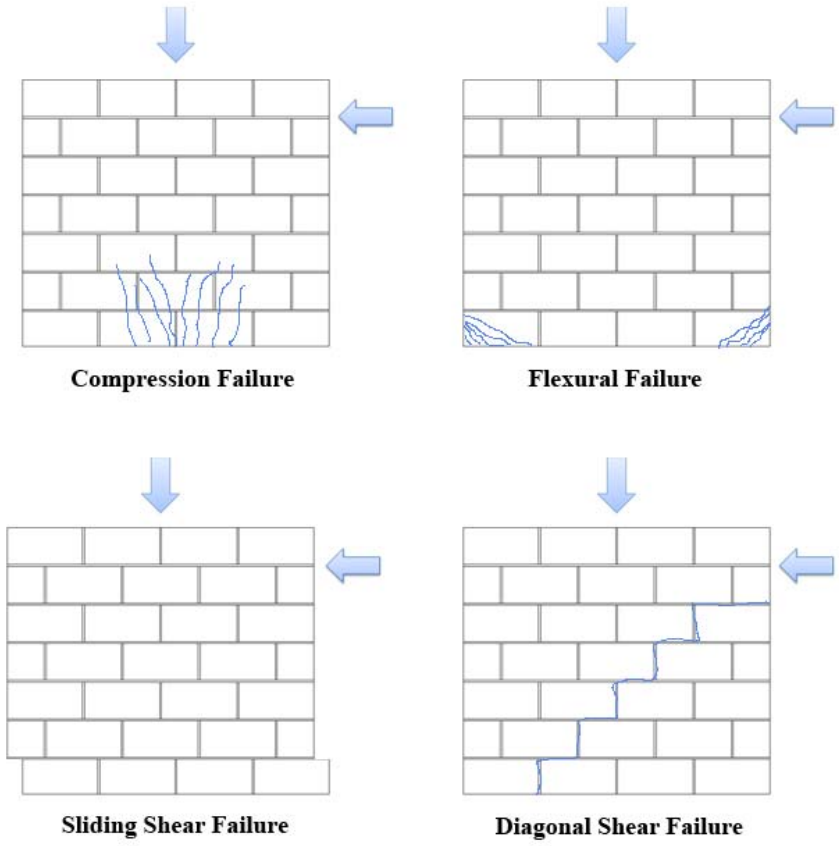

Figure 5.9: Failure Modes for Shear Walls

Basically, the failure mode of a shear wall depends on the combination of applied loads, wall geometry (slender or squat), properties of the materials, and reinforcement details [Drysdale and Hamid 2005]. Four failure modes are stated for shear walls:

compression failure due to axial load, flexural failure due to overturning moment, sliding shear failure along bed joint due to loss of adhesion and finally, diagonal shear failure along joints [Fig. 5.9].

For reinforced masonry walls, flexural and diagonal shear failures are the most common types of failure and the horizontal reinforcement is typically used to prevent diagonal failure. For unreinforced masonry walls, walls having low aspect ratio, walls built using low strength mortar, or walls with low axial load, sliding shear may also be predominant [Hatzinikolas and Korany 2005]. However, the best crack/failure mode and the desired one for shear walls, reinforced and unreinforced, for seismic is the sliding failure which ensures sufficient energy dissipation with only small loss of strength [Drysdale and Hamid 2005]. In contrast, Hatzinikolas and Korany [2005], mentioned that diagonal tension and sliding shear failures are usually considered brittle failure modes characterized by a rapid decrease in capacity and very limited deformation. Thus, they don't provide warning. Hatzinikolas and Korany [2005] suggested designing masonry shear walls to fail in flexural mode. Generally, design must try to account for the various potential modes of failure because energy absorption and potential damage are both considerations in design for seismic.

In this study, an unreinforced wall and walls with BJR were tested and no compression failure was evident in the test results due to the low applied axial load. Therefore, flexural failure, sliding shear failure and diagonal shear failure will be discussed and the theoretical shear strength (V_n) values calculated for those failures will be compared

with the experimental shear values. All material factors (e.g. ϕ_m and ϕ_s) were taken as "1" in order to compare calculated values to results from an experimental study.

5.3.1 Flexural Failure

For the in-plane case, at any section of the wall, the following equations are used for checking compression and tension failure:

$$\frac{P}{A_e} + \frac{M_n y}{I} \leq \phi_m f_m^{'} \qquad \text{Compression} \qquad [5.4]$$

$$\frac{P}{A_e} - \frac{M_n y}{I} \geq 0 \qquad \text{Tension} \qquad [5.5]$$

where,

P is the axial load corresponding to the lateral load at failure.

A_e is the effective cross-sectional area of the tested wall.

M_n is the nominal moment.

y is half the length of the wall ($\frac{l_w}{2}$).

I is the second moment of area.

ϕ_m is the material resistance factor for masonry.

Using these previous two equations [5.4] and [5.5], the value of (V_n) could be calculated by substituting (M_n) by ($V_n \times h_w$) for the eight CMU walls. The detailed calculation is provided in the spreadsheet shown below.

l_w =	1590 mm	y = l_w/2 =	795 mm
A_e =	117660 mm^2	I =	29417925537 mm^4
h_w =	1200 mm	ϕ_m =	1

Compression:

$$\frac{P}{A_e} + \frac{(V_n h_w) y}{I} = \phi_m f'_m$$

Tension:

$$\frac{P}{A_e} - \frac{(V_n h_w) y}{I} = 0$$

			Compression	Tension	
	P, (kN)	f'$_m$, (MPa)	V_n, (kN)	V_n, (kN)	Max. Exp. V_r, (kN)
Wall-C	76.0	12.7	371.7	19.9	60.0
Wall-S	75.0	12.0	350.4	19.7	68.0
Wall-G(G)	141.0	12.2	339.3	37.0	105.0
Wall-G(L)	116.0	14.4	413.6	30.4	96.0
Wall-G(T)	143.0	14.4	406.6	37.5	100.0
Wall-E(L)	86.0	17.0	501.7	22.5	70.0
Wall-E(G1)	84.0	17.0	502.2	22.0	111.0
Wall-E(G2)	147.0	17.0	485.7	38.5	80.0

The difference in the compressive strength (f'_m) of the tested walls obviously had a significant effect on the results and the capacity of the walls to resist the flexural compression failure. When f'_m increases, the compression failure V_n increases. In fact, all

the tested walls, technically, had a flexural tension failure because there was no vertical reinforcement (anchorage) and the axial load was low. So, as soon as the overturning moment exceeded the moment due to the axial load, lifting occurred. Tension failure values V_n are therefore significantly lower than the experimental loads seen here. The compression failure values are also much higher than the experimental values of V_r and compression failure was not observed, so these failure modes should be neglected.

5.3.2 Sliding Shear Failure

The in-plane sliding shear resistance according to clause 7.10.4.1 of the CSA S304.1-04 is:

$$V_r = 0.16\phi_m \sqrt{f'_m} A_{uc} + \phi_m \mu P_1 \qquad [5.6]$$

where,

A_{uc} is the uncracked portion of the effective cross-sectional area of the wall that provides shear bond capacity.

μ is = 1 for a masonry-to-masonry or masonry-to-roughened concrete sliding plane.

= 0.7 for a masonry-to-smooth concrete or bare steel sliding plane.

P_1 is compression force perpendicular to the sliding force.

The detailed calculations for this case for all walls are in the spreadsheet below.

$V_r = 0.16\ \phi_m\ (f'_m)^{\wedge 0.5}\ A_{uc} + \phi_m\ \mu\ P_1$

ϕ_m = 1

$A_{uc} = A_e = 74 \times 1590$ = 117660 mm^2

μ = 1

	P_1, (kN)	f'_m, (MPa)	Sliding Failure V_r, (kN)	Max. Exp. V_r, (kN)	Calc. V_r/Exp. V_r
Wall-C	**76.0**	**12.7**	**143.1**	**60.0**	**2.4**
Wall-S	**75.0**	**12.0**	**140.2**	**68.0**	**2.1**
Wall-G(G)	**141.0**	**12.2**	**206.8**	**105.0**	**1.9**
Wall-G(L)	**116.0**	**14.4**	**187.4**	**96.0**	**1.9**
Wall-G(T)	**143.0**	**14.4**	**214.4**	**100.0**	**2.1**
Wall-E(L)	**86.0**	**17.0**	**163.6**	**70.0**	**2.3**
Wall-E(G1)	**84.0**	**17.0**	**161.6**	**111.0**	**1.5**
Wall-E(G2)	**147.0**	**17.0**	**224.6**	**80.0**	**2.8**

From the spreadsheet above, it can be noticed that most of the values of sliding failure (V_r) are about double the experimental V_r. Significant additional shear resistance comes from the term accounting for the compression force perpendicular to the sliding surface (P_1). In fact, if one considers only the first term ($0.16\ \phi_m\ (f'_m)^{\wedge 0.5}\ A_{uc}$) which depends on the CMU properties and the uncracked portion of the effective cross-sectional area of the wall that provides shear bond capacity (A_{uc}), sliding shear resistance values V_r close to the experimental ones are obtained.

5.3.3 Diagonal Shear Failure

The in-plane diagonal shear resistance according to clause 10.10.1.1 of the CSA S304.1-04 is:

$$V_r = \phi_m (V_m b_w d_v + 0.25 P_d)\gamma_g + \left(0.6 \phi_s A_v f_y \frac{d_v}{s} \right) \quad [5.7]$$

where,

V_m is shear strength attributed to the masonry and is given by:

$$V_m = 0.16 \left(2 - \frac{M_n}{V_n d_v} \right) \sqrt{f_m'} \quad [5.8]$$

d_v is effective depth, which need not be taken less than $0.8 l_w$ for walls with flexural reinforcement distributed along the length.

P_d is axial compressive load on the section under consideration.

γ_g is factor to account for partial grouted or ungrouted walls that are constructed of hollow or semi-solid units.

$= A_e/A_g$, but not greater than 0.5

Based on the experimental study of Miller *et al.* [2005], who suggested that the contribution of the horizontal reinforcement should be increased in calculating shear resistance, especially in squat walls, the factor 0.6 in the equation was varied between 0.6 to 1 to investigate the effect of this factor on the theoretical results for the shear resistance. The value of the effective depth "d_v" was also varied between $0.8 l_w$ and l_w since the CSA standard stipulates only that it shall be "not less than $0.8 l_w$" but there is perhaps more of the

depth that should be considered as effective depth. The detailed calculations for this case for all walls are in Appendix A. An example of the calculations is shown below.

For Wall-S:

$V_r = \phi_m (V_m b_w d_v + 0.25 P_d) \gamma_g + [0.6 \phi_s A_v f_y d_v/s]$

$V_m = 0.16 (2\text{-}M_n/V_n d_v) (f'_m)^{\wedge 0.5}$

$\phi_m = \phi_s =$	**1**	
$f_m' =$	**12.0**	MPa
$\gamma_g = A_e/A_g =$	**0.39**	
$A_v =$	**19.2**	mm^2
$f_y =$	**560.0**	MPa
Vertical load corresp. to $V_r =$	**75000**	N
$s =$	**400**	mm
$b_w =$	**74**	mm
P_d = DL + Vertical load corresp. to $V_r =$	**79668.3**	N
$M_n =$	**81600000**	N.mm
$V_n =$	**68000**	N
$l_w =$	**1590**	mm
Experimental $V_r =$	68.0	kN

$d_v = d_{factor} * l_w$

			Reinf. factor			
d_{factor}	d_v	V_m	0.6	0.75	0.85	1
0.80	1272	0.586	**49.8**	**54.9**	**58.3**	**63.5**
0.81	1287.9	0.592	**50.5**	**55.7**	**59.2**	**64.4**
0.82	1303.8	0.598	**51.3**	**56.6**	**60.1**	**65.3**
0.83	1319.7	0.605	**52.1**	**57.4**	**60.9**	**66.3**
0.84	1335.6	0.611	**52.8**	**58.2**	**61.8**	**67.2**
0.85	1351.5	0.616	**53.6**	**59.1**	**62.7**	**68.1**
0.86	1367.4	0.622	**54.4**	**59.9**	**63.6**	**69.1**
0.87	1383.3	0.628	**55.1**	**60.7**	**64.4**	**70.0**
0.88	1399.2	0.633	**55.9**	**61.5**	**65.3**	**70.9**
0.89	1415.1	0.639	**56.7**	**62.4**	**66.2**	**71.9**
0.90	1431	0.644	**57.4**	**63.2**	**67.0**	**72.8**
0.91	1446.9	0.649	**58.2**	**64.0**	**67.9**	**73.8**
0.92	1462.8	0.654	**59.0**	**64.9**	**68.8**	**74.7**
0.93	1478.7	0.659	**59.7**	**65.7**	**69.7**	**75.6**
0.94	1494.6	0.664	**60.5**	**66.5**	**70.5**	**76.6**
0.95	1510.5	0.668	**61.3**	**67.3**	**71.4**	**77.5**
0.96	1526.4	0.673	**62.0**	**68.2**	**72.3**	**78.4**
0.97	1542.3	0.677	**62.8**	**69.0**	**73.2**	**79.4**
0.98	1558.2	0.682	**63.6**	**69.8**	**74.0**	**80.3**
0.99	1574.1	0.686	**64.3**	**70.7**	**74.9**	**81.2**
1.00	1590	0.690	**65.1**	**71.5**	**75.8**	**82.2**

According to the calculations shown above and by comparing the experimental V_r with the theoretical values of V_r by varying the horizontal reinforcement contribution factor and the effective depth d_v, it can be stated generally that increasing the reinforcement contribution factor and the effective depth value together will get the theoretical V_r much closer to the experimental V_r.

So, for the case of Wall-S, increasing the horizontal reinforcement contribution factor to 0.88 and the effective depth, d_v, to $0.9l_w$ gives a theoretical value for shear strength that closely matched the experimental result. However, for the other walls in this study, using these factors or larger will bring the theoretical V_r values just somewhat closer to the exact values of the experimental ones.

5.3.4 Comparison and Comments on Theoretical V_r

Based on the equations discussed above, the shear resistance of the walls in the flexural case, sliding shear case and diagonal shear case were calculated (with 0.6 for horizontal reinforcement contribution and $0.8l_w$ for the effective depth, d_v, as recommended in the CSA S304.1-04). Table 5.3 shows a summary of the results and the values of V_r in all cases compared with the experimental V_r values.

Table 5.3: Summary and Comparison between the Experimental and the Theoretical Shear Resistance Values for Failure Modes

Specimen		Wall-C	Wall-S	Wall-G(G)	Wall-G(L)	Wall-G(T)	Wall-E(L)	Wall-E(G1)	Wall-E(G2)
Type of BJR		N/A	Steel Ladder	GFRP Grid	GFRP Ladder	GFRP Truss	Geogrid Ladder	Geogrid Grid	Geogrid Grid
Frequency of BJR		N/A	Every 2nd course	Every 2nd course	Every 2nd course	Every 2nd course	Every 2nd course	Every course	Every 2nd course
Failure Mode		Step	Sliding	Sliding	Step	Sliding	Step	Sliding	Sliding
Max. Experimental Load Capacity V_r		60 kN	68 kN	105 kN	96 kN	100 kN	70 kN	111 kN	80 kN
Theoretical	**Flexural Failure V_r (Tension Failure)**	19.9 kN	19.7 kN	37.0 kN	30.4 kN	37.5 kN	22.5 kN	22.0 kN	38.5 kN
	Sliding Failure V_r	143.1 kN	140.2 kN	206.8 kN	187.4 kN	214.4 kN	163.6 kN	161.6 kN	224.6 kN
	Diagonal Failure V_r*	30.0 kN	49.8 kN	42.6 kN	42.0 kN	44.7 kN	37.9 kN	41.2 kN	43.8 kN

* with 0.6 for horizontal reinforcement contribution and $0.8l_w$ for d_v

Some comments could be stated based on the calculations and the values of shear resistance of each mode of failure:

- The theoretical V_r values of diagonal shear resistance case are the closest among the other theoretical V_r values to the values of the maximum experimental load capacity. But generally, all the theoretical values are either much higher or much lower than the experimental ones, especially the sliding values which are double the experimental V_r.
- The theoretical V_r values of flexural shear resistance case and diagonal shear resistance case are much lower than the experimental V_r values. This can lead us to the fact that the code is underestimating the actual capacity of the CMU walls to resist diagonal or flexural failures which provides more safety in the design. However, in the case of sliding shear resistance, the code appears to overestimate the actual capacity of the walls which provides less safety in the design. As mentioned previously the term accounting for the axial load results in a near doubling of the resistance.
- Sliding shear resistance values are much higher than other theoretical shear values and far away from the experimental V_r values. However, five out of eight walls appeared to fail in sliding shear. This may be due to the low axial load or the supports at the bottom or the load rate of the program may have been too high causing sliding failure to be more favourable.
- The factor of the horizontal reinforcement contribution "0.6" in the diagonal equation (eqn. 5.7) is very small and it should be larger. Miller *et al.* [2005],

in his experimental study, suggested increasing the percentage of the horizontal reinforcement contribution in shear resistance. And, according to the spreadsheet example of diagonal shear in section 5.3.3, it can be stated that if this factor for the case of the Wall-S, particularly, was increased to 0.88 and the effective depth, d_v, is taken as $0.9l_w$, the diagonal shear V_r will be exactly the same value of the experimental V_r. However, for the other walls and according to Appendix A, using these factors or larger will get the theoretical V_r values just closer to the exact values of the experimental ones. However, many tests and much research should be conducted to check the reliability of these factors before making recommendations for new factors.

- There were no compression failures at all in the results which is expected because the axial load applied on the top of the wall was small and there was no vertical reinforcement (anchorage) which caused lifting. So, the walls that apparently failed in sliding (Wall-S, G(G), G(T), E(G1), E(G2)) may actually be considered to have failed in tension due to this lifting.

5.4 Comparison with Literature Review

Table 5.4 shows a summary of the experimental studies discussed in chapter two which are related and very close to this study. All summarized studies tested masonry walls with aspect ratio 1 and under in-plane cyclic load.

Table 5.4: Summary of the Experimental Studies from L.R. Related to This Study

Author	H/L	Reinforcement Material, Type & Configuration	Lateral Capacity Increase over URM Walls
Mahmood *et al.* [2008]	1	Horizontal GFRP laminate (1.3 mm) one face	15% increment
Saatcioglu *et al.* [2005]	1	Diagonally CFRP sheet (0.16 mm) one face	3 times
Haroun *et al.* [2005]	1	Repaired with 1 layer CFRP laminate 1 face	120%,
		Strengthened with 1 layer CFRP laminate 1 face	115%,
		Strengthened with 1 layer CFRP laminate 2 faces	130%,
		Strengthened with 2 layers GFRP laminate 2 faces	128%,
		Strengthened with horizontal Strips CFRP 1 face	118%
Li *et al.* [2005]	1	Strengthened with horizontal NSM GFRP bars on 2 faces	8%
Schultz *et al.* [1998]	1	Steel ladder BJR – 3.76 mm ($\rho = 0.056\%$)	BJR feasible lateral-load resistance.
		Steel ladder BJR – 5.26 mm ($\rho = 0.11\%$)	The ratio didn't affect.
Gouveia *et al.* [2007] & Lourenço *et al.* [2008]	1	Steel truss BJR / 2nd course – ($\rho = 0.09\%$)	5% to 10%
Penna *et al.* [2008]	1	Steel truss BJR / 2nd course	60%

From the table above it can be stated that there is a variation between results among the experimental studies. However, by comparing using FRP sheets or laminates with FRP bed joint reinforcement, generally sheets and laminates are much more effective than bed joint reinforcement. One of the studies, Saatcioglu *et al.* [2005], showed that the lateral capacity of the CMU wall increased by up to three times by strengthening it with diagonal CFRP sheets on one face. However, in terms of quantity of material used, the method of sheets or laminates uses much more material than BJR and this should be considered.

In addition, steel truss shape bed joint reinforcement in the study by Penna *et al.* [2008] enhanced the lateral capacity of the masonry wall by 60%. However, in our study

the steel ladder shape bed joint reinforcement improved the lateral capacity by only 13.3%. This indicates that truss shape appears to be more effective than ladder shape.

5.5 Summary

As a summary and according to the results of the tests, it is effective to use bed joint reinforcement to improve the lateral capacity of CMU walls. The improvement was as high as 85% in some cases. However, the stiffness of the concrete masonry walls constructed with bed joint reinforcement decreased significantly and in most cases, the use of bed joint reinforcement forced the specimens to fail in sliding failure.

The energy absorption was increased significantly by using both GFRP and Geogrid materials as bed joint reinforcement. Moreover, the ductility, μ_u, was almost the same for all test walls based on the results in Table 5.2 except Wall-E(G2) which had twice the ductility of the control wall (Wall-C) which is beneficial in seismic design. There was a big difference in using bed joint reinforcement every course or every 2^{nd} course with the capacity increasing by 85% when using BJR every course and only 25% when using it every 2^{nd} course for the Geogrid material. However, the stiffness of the wall, K_e, was a little bit higher when bed joint reinforcement was present only every 2^{nd} course as shown in Table 5.2.

Furthermore, from Figures 5.5 to 5.8, it is observed that, in general, the use of bed joint reinforcement resulted in an increase in ultimate displacement and thus energy absorption capacity for the walls.

As shown in Table 5.3, shear cracking (Step Failure) occurred in the CMU walls that were reinforced with ladder shape BJR (Wall-E(L) and Wall-G(L)). However, Wall-S with steel ladder shape bed joint reinforcement was the exception, where the failure was sliding, perhaps because steel as a material is much stiffer, smoother, or has a larger cross-sectional area than the GFRP or Geogrid materials used here.

CHAPTER SIX:

CONCLUSION AND RECOMMENDATIONS

The poor performance of unreinforced CMU walls subjected to lateral loads is due to insufficient shear and flexural capacity. Therefore, the objective of this work was to investigate and evaluate the improvement of lateral capacity of ungrouted masonry walls by using different materials and shapes or configurations of bed joint reinforcement.

Eight masonry walls (1.6 m long × 1.4 m high) constructed with concrete masonry blocks were tested under cyclic lateral load. One specimen was a URM control wall and one specimen was reinforced with commonly used steel-ladder shaped bed joint reinforcement. Three walls were reinforced with different configurations of GFRP. The last three were reinforced with different configurations of Geogrid reinforcement.

The results of the tests showed how bed joint reinforcement can enhance the ability of the masonry walls to resist the lateral load resulting from earthquakes and increase the energy dissipation of the walls.

6.1 Conclusions

Based on the experimental test results in this thesis, the following conclusions can be drawn:

The seismic performance of URM walls due to cyclic in-plane loads can be enhanced by using GFRP or Geogrid materials when used as bed joint reinforcements.

However, the level of enhancement varies due to the type and properties of material and also due to the distribution on the horizontal reinforcement (every course/every 2nd course).

Based on the compressive strength tests of the prisms discussed in section 3.2.1 (13.6 ± 1.9 MPa), the coefficient of variation (COV) is about 14%. Therefore, in some cases, the apparent improvements in the lateral capacity of the specimens could be due in part to the variation in masonry and not only due to the material or configuration of the lateral reinforcement. So, both the properties of the masonry blocks and the reinforcements affected the improvement of the lateral capacity for all tested walls. Accordingly, if there were two or three more specimens of each type of the walls, the results would be more accurate.

Geogrid is a recyclable material, corrosion resistant, and is very cheap. Therefore, it has advantages over and is more economical to use than Steel or GFRP bed joint reinforcement.

Generally, using FRP, Geogrid or Steel bed joint reinforcement, will increase the cost of the walls constructed. Especially if the masonry walls were horizontally reinforced with BJR every course to get the maximum lateral capacity as shown in this study. However, the increase in cost will not be significant and must be balanced against the increased strength, ductility and energy absorption for masonry walls constructed in seismic zones.

The presence of grid shape reinforcement appeared to cause the specimens to fail in sliding. However, the specimen with steel ladder shaped bed joint reinforcement was the

exception; the failure was also sliding, possibly because steel as a material is much stiffer, smoother, or has a larger cross-sectional area than GFRP or Geogrid.

Concrete masonry walls are safe to be used for construction in seismic zones if they were constructed properly and reinforced horizontally with GFRP or Geogrid bed joint reinforcement.

6.2 Recommendations

The CSA Standard S304.1-04 provides the equation needed to calculate the diagonal shear resistance V_r:

$$V_r = \phi_m (V_m b_w d_v + 0.25 P_d)\gamma_g + \left(0.6 \phi_s A_v f_y \frac{d_v}{s} \right)$$

However, the factor of the horizontal reinforcement contribution "0.6" in the equation above is very small and this experimental study confirmed what was suggested by Miller *et al.* [2005]; that this factor should be larger (0.75 to 1) to reflect the real effect and the role of the lateral reinforcement in resisting the lateral forces, especially in squat walls. However, from this study, it is recommended that for walls with steel wire bed joint reinforcement, this factor should be increased to 0.88 and the effective depth, d_v, should be increased to $0.9l_w$ in the equation to give more accurate results. Still, many tests and much research should be conducted to check the reliability of these factors and develop recommendations for new factors. In addition, more research must be carried out to investigate these factors for the other BJR materials, GFRP and Geogrid, to get the factors that give theoretical shear values equal to the experimental values.

Based on the experimental results, using GFRP and Geogrid materials as bed joint reinforcement is recommended. The average percentage increase in the lateral capacity for both materials was 54.7%. However, in Geogrid case, using the grid shape was the best case and the ladder shape was not very effective.

More tests should be carried out to investigate the enhancement of lateral capacity of ungrouted masonry walls by using different materials such as; other types of FRP or plastics (polymers) and configurations such as; truss-ladder mix shape, same configurations with different cross-sectional areas and grid shape with smaller or larger dimensions. Further investigations where the amount of reinforcing is varied (every course vs. every 2nd course) should also be carried out to determine whether the effect seen in this study for the Geogrid material is the same for other materials as well.

REFERENCES

Blondet, M., and Garcia, G.V., 2004, "Earthquake resistant earthen buildings," *13th World Conference on Earthquake Engineering, Vancouver, B.C., Aug. 1-6, 2004*.

Corradi, M., Borri, A., and Vignoli, A., 2008, "Experimental Evaluation of In-plane Shear Behaviour of Masonry Walls Retrofitted Using Conventional and Innovative Methods," *Journal of the British Masonry Society Masonry International, Vol. 21, No. 1, (2008*) *pp. 29*-41.

CSA, 2004, "Design of Masonry Structures," *CSA-S304.1-04, Canadian Standards Association, Mississauga, Ontario, Canada.*

Drysdale, R.G., and Hamid, A.A., 2005, "Masonry Structures: Behaviour and Design," *Canada Masonry Design Centre, Mississauga, Ontario, Canada.*

ElGawady, M.A., Lestuzzi, P., and Badoux, M., 2005, "Aseismic Retrofitting on Unreinforced masonry Walls Using FRP," *2005 Elsevier Science Ltd., Part B 37 (2006) pp. 148-162*.

Fallis, G.J., 2008, Personal communication, *Vice-President Construction Technologies - Vector Construction Group*.

Foster, P.B., Gergely, J., Young, D.T., McGinley, W.M., and Corzo, A., 2005, "FRP Repair Methods for Unreinforced Masonry Buildings Subject to Cyclic Loading," *Proceedings of the 7th International Symposium of the Fibre-Reinforced Polymer Reinforcement for Reinforced Concrete Structures, Kansas City, Missouri, USA, Nov. 6-9, 2005*, *pp. 289*-305.

Gouveia, J.P., and Lourenço, P.B., 2007, "Masonry shear walls subjected to cyclic loading: influence of confinement and horizontal reinforcement," *Proceedings of the 10th North American Masonry Conference, St. Louis, Missouri, USA, Jun. 3-6, 2007, pp. 838-848*.

Guzman, M.J., 2008, "Development of a Dynamic System for Testing Structural Masonry Elements and Study of FRP Bed Joint Reinforcement," *MSc Thesis, University of Calgary, 155 p*.

Haroun, M.A., Mosallam, A.S., and Allam, K.H., 2005, "Cyclic In-Plane Shear of Concrete Masonry Walls Strengthened by FRP Laminates," *Proceedings of the 7th International Symposium of the Fibre-Reinforced Polymer Reinforcement for Reinforced Concrete Structures, Kansas City, Missouri, USA, Nov. 6-9, 2005, pp. 327-339*.

Hatzinikolas, M.A., and Korany, Y., 2005, "Masonry Design - for Engineers and Architects," *Canadian Masonry Publications, Edmonton, Alberta, Canada.*

ISIS Design Manual No. 3, Version 2, "Reinforcing Concrete Structures with Fibre-Reinforced Polymers," *September 2007, Winnipeg, Manitoba, Canada.*

Li, T., Silva, P.F., Belarbi, A., Nanni, A., and Myers, J.J., 2001, "Retrofit of Un-Reinforced Infill Masonry Walls with FRP," *Proc., CCC 2001 Composites in Construction Conference, Porto, Portugal, Oct. 10-12, 2001, pp. 559-563.*

Li, T., Galati, N., Gustavo, T., and Nanni, A., 2005, "FRP Strengthening of URM Walls with Openings – Experimental Results," *TMS Journal, Dec. 2005. Masonry Society Journal. Vol. 23, no. 1, pp. 47-58. Dec. 2005*

Lissel, S.L., Simundic, G., Page, A.W., and Shrive, N.G., 2000, "Improving the shear resistance of Masonry," *Proc. of the 12th Int'l Brick/Block Masonry Conference Madrid, Spain, June 2000, pp. 1075-1084.*

Lourenço, P.B., Vasconcelos, G., Gouveia, J.P., Haach, V., and Freitas, J.F., 2008, "Validation of Masonry System for In-plane Lateral Loading using Truss Reinforcement," *14th International Brick & Block Masonry Conference, Sydney, Australia, Feb. 17-20, 2008.*

Magenes, G., and Calvi, G.M., 1997, "In-plane seismic response of brick masonry walls," *Earthquake Engineering and Structural Dynamics, Vol. 26 (1997), pp. 1091-1112.*

Mahmood, H., Russell, A.P., and Ingham, J.M., 2008, "Laboratory Testing of Unreinforced Masonry Walls Retrofitted with Glass FRP Sheets," *14th International Brick & Block Masonry Conference, Sydney, Australia, Feb. 17-20, 2008*.

Marcari, G., Manfredi, G., Prota, A., and Pecce, M., 2007, "In-plane shear performance of masonry panels strengthened with FRP," *2006 Elsevier Science Ltd., Part B 38 (2007), pp. 887-901.*

Miller, S.C., El-Dakhakhni, W., and Drysdale, R.G., 2005, "Experimental Evaluation of the Shear Capacity of Reinforced Masonry Shear Walls," *10th Canadian Masonry Symposium, Banff, Alberta, Canada, June 8-12, 2005*.

Oan, A.F., and Shrive, N.G., 2009, "Shear of Concrete Masonry Walls," *11th Canadian Masonry Symposium, Toronto, Ontario, Canada, June 1-3, 2009*.

Penna, A., Magenes, G., Calvi, G.M., and Costa, A.A., 2008, "Seismic performance of AAC infill and bearing walls with different reinforcement solutions," *14th International Brick & Block Masonry Conference, Sydney, Australia, Feb. 17-20, 2008*.

Saatcioglu, M., Serrato, F., and Foo, S., 2005, "Seismic Performance of Masonry Infill Walls Retrofitted with CFRP Sheets," Proceedings of the *7th International Symposium of the Fibre-Reinforced Polymer Reinforcement for Reinforced Concrete Structures, Kansas City, Missouri, USA, Nov. 6-9, 2005, pp. 341-353*.

Sanada, Y., Nakamura, Y., Yamauchi, N., and Nakano, Y., 2006, "Seismic Performance of Masonry Walls Using Interlocking Units," *First European Conference on Earthquake Engineering and Seismology, Geneva, Switzerland, Sep. 3-8, 2006*, *Paper Number: 508*.

Schultz, A.E., Hutchinson, R.S., and Cheok, G.C., 1998, "Seismic Performance of Masonry Walls with Bed Joint Reinforcement," *Structural Engineers World Congress. Proceedings. Paper Number T119-4. July 18-23, 1998, San Francisco, CA, Elsevier Science Ltd., 1-7 pp, 1998.*

Shrive, N.G., 2005, "The use of fibre reinforced polymers to improve seismic resistance of masonry," *Construction and Building Materials, 20 (4), pp.269-277, May 2006.*

Soric, Z., Galic, J., and Kisicek, T., 2008, "Strengthening of masonry walls with glass fibre strips," *14th International Brick & Block Masonry Conference, Sydney, Australia, Feb. 17-20, 2008*.

Thanoon, W.A., Jaafar, M.S., Noorzaei, J., Kadir, M.R.A., and Fares, S., 2007, "Structural Behaviour of Mortar-Less Interlocking Masonry System Under Eccentric Compressive Loads," *Advances in Structural Engineering, Feb. 2007, Vol. 10 No. 1. pp. 11-24*.

Tinazzi, D., Modena, C., and Nanni, A., 2000, "Strengthening of Masonry Assemblages with FRP Rods and Laminates," *International Meeting on Composite Materials, PLAST 2000, Proceedings, Advancing with Composites 2000, Ed. I. Crivelli-Visconti, Milan, Italy, May 9-11, 2000, pp. 411-418*.

Tomaževič, M., 1999, "Earthquake-Resistant Design of Masonry Buildings," *Series on Innovation in Structures and Construction, Vol. 1., Imperial College Press, London, England.*

Tumialan, J.G., Morbin, A., Nanni, A., and Modena, C., 2001, "Shear Strengthening of Masonry Walls with FRP Composites," *COMPOSITES 2001 Convention and Trade Show, Composites Fabricators Association, Tampa, FL, October 3-6, 2001.*

Vinidiktova, N. S., Ermolovich, O. A., Goldade, V. A., and Pinchuk, L. S., 2006, "Strength of Biodegradable Polypropylene Tapes Filled with a Modified Starch," *Mechanics of Composite Materials Journal, Vol. 42, No. 3, May–June, 2006, pp. 389–400.*

Yu, P., Silva, P.F., and Nanni, A., 2007, "In-plane response of URM walls strengthened with GFRP grid reinforced polyurea," *10th North American Masonry Conference, St. Louis, Missouri, USA, Jun. 3-6, 2007*.

Yu, P., Silva, P.F., and Nanni, A., 2005, "In-plane Strengthening of Unreinforced Masonry Walls with Prestressed GFRP Bars," *Proceedings of the 7th International Symposium of the Fibre-Reinforced Polymer Reinforcement for Reinforced Concrete Structures, Kansas City, Missouri, USA, Nov. 6-9, 2005, pp*. 466-477.

Zhuge, Y., 2008, "FRP retrofitted URM walls under inplane shear – A review of available design models," *14th International Brick & Block Masonry Conference, Sydney, Australia, Feb. 17-20, 2008*.

APPENDIX A

ADDITIONAL CALCULATIONS

- **Diagonal Failure:**

For Wall-C:

$V_r = \phi_m (V_m b_w d_v + 0.25 P_d) \gamma_g + [0.6 \phi_s A_v f_y d_v/s]$

$V_m = 0.16 (2-M_n/V_n d_v) (f'_m)^{0.5}$

$\phi_m = \phi_s =$	**1**	
$f_m' =$	**12.7**	MPa
$\gamma_g = A_e/A_g =$	**0.39**	
$A_v =$	**0.0**	mm^2
$f_y =$	**0.0**	MPa
Vertical load corresp. to $V_r =$	**76000**	N
$s =$	**400**	mm
$b_w =$	**74**	mm
P_d = DL + Vertical load corresp. to $V_r =$	**80668.3**	N
$M_n =$	**72000000**	N.mm
$V_n =$	**60000**	N
$l_w =$	**1590**	mm
Experimental $V_r =$	**60.0**	**kN**

$d_v = d_{factor} * l_w$

			Reinf. factor			
d_{factor}	d_v	V_m	V_r	0.6	0.75	0.85	1
0.80	1272	0.602	**30.0**	**30.0**	**30.0**	**30.0**
0.81	1287.9	0.609	**30.5**	**30.5**	**30.5**	**30.5**
0.82	1303.8	0.616	**31.0**	**31.0**	**31.0**	**31.0**
0.83	1319.7	0.622	**31.6**	**31.6**	**31.6**	**31.6**
0.84	1335.6	0.628	**32.1**	**32.1**	**32.1**	**32.1**
0.85	1351.5	0.634	**32.6**	**32.6**	**32.6**	**32.6**
0.86	1367.4	0.640	**33.1**	**33.1**	**33.1**	**33.1**
0.87	1383.3	0.646	**33.6**	**33.6**	**33.6**	**33.6**
0.88	1399.2	0.651	**34.2**	**34.2**	**34.2**	**34.2**
0.89	1415.1	0.657	**34.7**	**34.7**	**34.7**	**34.7**
0.90	1431	0.662	**35.2**	**35.2**	**35.2**	**35.2**
0.91	1446.9	0.667	**35.7**	**35.7**	**35.7**	**35.7**
0.92	1462.8	0.673	**36.3**	**36.3**	**36.3**	**36.3**
0.93	1478.7	0.678	**36.8**	**36.8**	**36.8**	**36.8**
0.94	1494.6	0.683	**37.3**	**37.3**	**37.3**	**37.3**
0.95	1510.5	0.687	**37.8**	**37.8**	**37.8**	**37.8**
0.96	1526.4	0.692	**38.4**	**38.4**	**38.4**	**38.4**
0.97	1542.3	0.697	**38.9**	**38.9**	**38.9**	**38.9**
0.98	1558.2	0.701	**39.4**	**39.4**	**39.4**	**39.4**
0.99	1574.1	0.706	**39.9**	**39.9**	**39.9**	**39.9**
1.00	1590	0.710	**40.4**	**40.4**	**40.4**	**40.4**

For Wall-S:

$V_r = \phi_m (V_m b_w d_v + 0.25 P_d) \gamma_g + [0.6 \phi_s A_v f_y d_v/s]$

$V_m = 0.16 (2\text{-}M_n/V_n d_v) (f'_m)^{\wedge 0.5}$

$\phi_m = \phi_s =$	**1**	
$f_m' =$	**12.0**	MPa
$\gamma_g = A_e/A_g =$	**0.39**	
$A_v =$	**19.2**	mm^2
$f_y =$	**560.0**	MPa
Vertical load corresp. to $V_r =$	**75000**	N
$s =$	**400**	mm
$b_w =$	**74**	mm
P_d = DL + Vertical load corresp. to $V_r =$	**79668.3**	N
$M_n =$	**81600000**	N.mm
$V_n =$	**68000**	N
$l_w =$	**1590**	mm
Experimental $V_r =$	68.0	kN

$d_v = d_{factor} * l_w$

			Reinf. factor 0.6	0.75	0.85	1
d_{factor}	**d_v**	**V_m**	**V_r**			
0.80	1272	0.586	**49.8**	**54.9**	**58.3**	**63.5**
0.81	1287.9	0.592	**50.5**	**55.7**	**59.2**	**64.4**
0.82	1303.8	0.598	**51.3**	**56.6**	**60.1**	**65.3**
0.83	1319.7	0.605	**52.1**	**57.4**	**60.9**	**66.3**
0.84	1335.6	0.611	**52.8**	**58.2**	**61.8**	**67.2**
0.85	1351.5	0.616	**53.6**	**59.1**	**62.7**	**68.1**
0.86	1367.4	0.622	**54.4**	**59.9**	**63.6**	**69.1**
0.87	1383.3	0.628	**55.1**	**60.7**	**64.4**	**70.0**
0.88	1399.2	0.633	**55.9**	**61.5**	**65.3**	**70.9**
0.89	1415.1	0.639	**56.7**	**62.4**	**66.2**	**71.9**
0.90	1431	0.644	**57.4**	**63.2**	**67.0**	**72.8**
0.91	1446.9	0.649	**58.2**	**64.0**	**67.9**	**73.8**
0.92	1462.8	0.654	**59.0**	**64.9**	**68.8**	**74.7**
0.93	1478.7	0.659	**59.7**	**65.7**	**69.7**	**75.6**
0.94	1494.6	0.664	**60.5**	**66.5**	**70.5**	**76.6**
0.95	1510.5	0.668	**61.3**	**67.3**	**71.4**	**77.5**
0.96	1526.4	0.673	**62.0**	**68.2**	**72.3**	**78.4**
0.97	1542.3	0.677	**62.8**	**69.0**	**73.2**	**79.4**
0.98	1558.2	0.682	**63.6**	**69.8**	**74.0**	**80.3**
0.99	1574.1	0.686	**64.3**	**70.7**	**74.9**	**81.2**
1.00	1590	0.690	**65.1**	**71.5**	**75.8**	**82.2**

For Wall-G(G):

$V_r = \phi_m (V_m b_w d_v + 0.25 P_d) \gamma_g + [0.6 \phi_s A_v f_y d_v/s]$

$V_m = 0.16 (2\text{-}M_n/V_n d_v) (f'_m)^{\wedge 0.5}$

ϕ_m =	**1**	
f_m' =	**12.2**	MPa
$\gamma_g = A_e/A_g$ =	**0.39**	
A_v =	**14.1**	mm^2
f_y =	**250.0**	MPa
Vertical load corresp. to V_r =	**141000**	N
s =	**400**	mm
b_w =	**74**	mm
P_d = DL + Vertical load corresp. to V_r =	**145668.3**	N
M_n =	**126000000**	N.mm
V_n =	**105000**	N
l_w =	**1590**	mm
Experimental V_r =	105.0	kN

$d_v = d_{factor} * l_w$

				Reinf.factor			
d_{factor}	d_v	V_m	V_r	0.6	0.75	0.85	1
0.80	1272	0.590	**42.6**	**44.3**	**45.4**	**47.1**
0.81	1287.9	0.597	**43.2**	**44.9**	**46.0**	**47.7**
0.82	1303.8	0.603	**43.8**	**45.5**	**46.7**	**48.4**
0.83	1319.7	0.610	**44.4**	**46.1**	**47.3**	**49.0**
0.84	1335.6	0.616	**45.0**	**46.8**	**47.9**	**49.7**
0.85	1351.5	0.622	**45.6**	**47.4**	**48.6**	**50.4**
0.86	1367.4	0.627	**46.2**	**48.0**	**49.2**	**51.0**
0.87	1383.3	0.633	**46.8**	**48.6**	**49.8**	**51.7**
0.88	1399.2	0.638	**47.4**	**49.2**	**50.5**	**52.3**
0.89	1415.1	0.644	**48.0**	**49.8**	**51.1**	**53.0**
0.90	1431	0.649	**48.6**	**50.5**	**51.7**	**53.6**
0.91	1446.9	0.654	**49.2**	**51.1**	**52.4**	**54.3**
0.92	1462.8	0.659	**49.8**	**51.7**	**53.0**	**54.9**
0.93	1478.7	0.664	**50.4**	**52.3**	**53.6**	**55.6**
0.94	1494.6	0.669	**51.0**	**52.9**	**54.3**	**56.2**
0.95	1510.5	0.674	**51.6**	**53.6**	**54.9**	**56.9**
0.96	1526.4	0.678	**52.2**	**54.2**	**55.5**	**57.5**
0.97	1542.3	0.683	**52.8**	**54.8**	**56.2**	**58.2**
0.98	1558.2	0.687	**53.4**	**55.4**	**56.8**	**58.8**
0.99	1574.1	0.692	**53.9**	**56.0**	**57.4**	**59.5**
1.00	1590	0.696	**54.5**	**56.6**	**58.0**	**60.1**

For Wall-G(L):

$V_r = \phi_m (V_m b_w d_v + 0.25 P_d) \gamma_g + [0.6 \phi_s A_v f_y d_v/s]$

$V_m = 0.16 (2\text{-}M_n/V_n d_v) (f'_m)^{\wedge 0.5}$

$\phi_m = \phi_s =$	**1**	
$f_m' =$	**14.4**	MPa
$\gamma_g = A_e/A_g =$	**0.39**	
$A_v =$	**14.1**	mm^2
$f_y =$	**250.0**	MPa
Vertical load corresp. to $V_r =$	**116000**	N
$s =$	**400**	mm
$b_w =$	**74**	mm
P_d = DL + Vertical load corresp. to $V_r =$	**120668.3**	N
$M_n =$	**115200000**	N.mm
$V_n =$	**96000**	N
$l_w =$	**1590**	mm
Experimental $V_r =$	96.0	kN

$d_v = d_{factor} * l_w$

			Reinf.factor			
d_{factor}	**d_v**	**V_m**	**0.6**	**0.75**	**0.85**	**1**
0.80	1272	0.642	**42.0**	**43.7**	**44.8**	**46.5**
0.81	1287.9	0.649	**42.7**	**44.4**	**45.5**	**47.2**
0.82	1303.8	0.655	**43.3**	**45.0**	**46.2**	**47.9**
0.83	1319.7	0.662	**44.0**	**45.7**	**46.9**	**48.6**
0.84	1335.6	0.669	**44.6**	**46.4**	**47.5**	**49.3**
0.85	1351.5	0.675	**45.2**	**47.0**	**48.2**	**50.0**
0.86	1367.4	0.681	**45.9**	**47.7**	**48.9**	**50.7**
0.87	1383.3	0.688	**46.5**	**48.4**	**49.6**	**51.4**
0.88	1399.2	0.694	**47.2**	**49.0**	**50.3**	**52.1**
0.89	1415.1	0.699	**47.8**	**49.7**	**50.9**	**52.8**
0.90	1431	0.705	**48.5**	**50.3**	**51.6**	**53.5**
0.91	1446.9	0.711	**49.1**	**51.0**	**52.3**	**54.2**
0.92	1462.8	0.716	**49.7**	**51.7**	**53.0**	**54.9**
0.93	1478.7	0.722	**50.4**	**52.3**	**53.6**	**55.6**
0.94	1494.6	0.727	**51.0**	**53.0**	**54.3**	**56.3**
0.95	1510.5	0.732	**51.7**	**53.7**	**55.0**	**57.0**
0.96	1526.4	0.737	**52.3**	**54.3**	**55.7**	**57.7**
0.97	1542.3	0.742	**52.9**	**55.0**	**56.3**	**58.4**
0.98	1558.2	0.747	**53.6**	**55.6**	**57.0**	**59.1**
0.99	1574.1	0.751	**54.2**	**56.3**	**57.7**	**59.8**
1.00	1590	0.756	**54.9**	**57.0**	**58.4**	**60.5**

For Wall-G(T):

$V_r = \phi_m (V_m b_w d_v + 0.25 P_d) \gamma_g + [0.6 \phi_s A_v f_y d_v/s]$

$V_m = 0.16 (2\text{-}M_n/V_n d_v) (f'_m)^{\wedge 0.5}$

$\phi_m = \phi_s =$	**1**	
$f_m' =$	**14.4**	MPa
$\gamma_g = A_e/A_g =$	**0.39**	
$A_v =$	**14.1**	mm^2
$f_y =$	**250.0**	MPa
Vertical load corresp. to $V_r =$	**143000**	N
$s =$	**400**	mm
$b_w =$	**74**	mm
P_d = DL + Vertical load corresp. to $V_r =$	**147668.3**	N
$M_n =$	**120000000**	N.mm
$V_n =$	**100000**	N
$l_w =$	**1590**	mm
Experimental $V_r =$	100.0	kN

$d_v = d_{factor} * l_w$

			Reinf.factor			
d_{factor}	d_v	V_m	0.6	0.75	0.85	1
0.80	1272	0.642	**44.7**	**46.4**	**47.5**	**49.2**
0.81	1287.9	0.649	**45.3**	**47.0**	**48.2**	**49.9**
0.82	1303.8	0.655	**46.0**	**47.7**	**48.8**	**50.6**
0.83	1319.7	0.662	**46.6**	**48.3**	**49.5**	**51.2**
0.84	1335.6	0.669	**47.2**	**49.0**	**50.2**	**51.9**
0.85	1351.5	0.675	**47.9**	**49.7**	**50.9**	**52.6**
0.86	1367.4	0.681	**48.5**	**50.3**	**51.5**	**53.3**
0.87	1383.3	0.688	**49.2**	**51.0**	**52.2**	**54.0**
0.88	1399.2	0.694	**49.8**	**51.7**	**52.9**	**54.7**
0.89	1415.1	0.699	**50.4**	**52.3**	**53.6**	**55.4**
0.90	1431	0.705	**51.1**	**53.0**	**54.2**	**56.1**
0.91	1446.9	0.711	**51.7**	**53.6**	**54.9**	**56.8**
0.92	1462.8	0.716	**52.4**	**54.3**	**55.6**	**57.5**
0.93	1478.7	0.722	**53.0**	**55.0**	**56.3**	**58.2**
0.94	1494.6	0.727	**53.7**	**55.6**	**56.9**	**58.9**
0.95	1510.5	0.732	**54.3**	**56.3**	**57.6**	**59.6**
0.96	1526.4	0.737	**54.9**	**57.0**	**58.3**	**60.3**
0.97	1542.3	0.742	**55.6**	**57.6**	**59.0**	**61.0**
0.98	1558.2	0.747	**56.2**	**58.3**	**59.6**	**61.7**
0.99	1574.1	0.751	**56.9**	**58.9**	**60.3**	**62.4**
1.00	1590	0.756	**57.5**	**59.6**	**61.0**	**63.1**

For Wall-E(L):

$V_r = \phi_m (V_m b_w d_v + 0.25 P_d) \gamma_g + [0.6 \phi_s A_v f_y d_v/s]$

$V_m = 0.16 (2\text{-}M_n/V_n d_v) (f'_m)^{\wedge 0.5}$

$\phi_m = \phi_s =$	**1**	
$f_m' =$	**17.0**	MPa
$\gamma_g = A_e/A_g =$	**0.39**	
$A_v =$	**9.0**	mm^2
$f_y =$	**202.0**	MPa
Vertical load corresp. to $V_r =$	**86000**	N
$s =$	**400**	mm
$b_w =$	**74**	mm
P_d = DL + Vertical load corresp. to $V_r =$	**90668.3**	N
$M_n =$	**84000000**	N.mm
$V_n =$	**70000**	N
$l_w =$	**1590**	mm
Experimental $V_r =$	70.0	kN

$d_v = d_{factor} * l_w$

			Reinf. factor			
d_{factor}	d_v	V_m	**0.6**	**0.75**	**0.85**	**1**
0.80	1272	0.697	**37.9**	**38.8**	**39.3**	**40.2**
0.81	1287.9	0.705	**38.5**	**39.4**	**40.0**	**40.9**
0.82	1303.8	0.712	**39.2**	**40.1**	**40.7**	**41.6**
0.83	1319.7	0.720	**39.8**	**40.7**	**41.3**	**42.2**
0.84	1335.6	0.727	**40.5**	**41.4**	**42.0**	**42.9**
0.85	1351.5	0.734	**41.1**	**42.1**	**42.7**	**43.6**
0.86	1367.4	0.740	**41.8**	**42.7**	**43.3**	**44.3**
0.87	1383.3	0.747	**42.4**	**43.4**	**44.0**	**45.0**
0.88	1399.2	0.754	**43.1**	**44.0**	**44.7**	**45.6**
0.89	1415.1	0.760	**43.7**	**44.7**	**45.3**	**46.3**
0.90	1431	0.766	**44.4**	**45.4**	**46.0**	**47.0**
0.91	1446.9	0.772	**45.0**	**46.0**	**46.7**	**47.7**
0.92	1462.8	0.778	**45.7**	**46.7**	**47.3**	**48.3**
0.93	1478.7	0.784	**46.3**	**47.3**	**48.0**	**49.0**
0.94	1494.6	0.790	**47.0**	**48.0**	**48.7**	**49.7**
0.95	1510.5	0.795	**47.6**	**48.7**	**49.3**	**50.4**
0.96	1526.4	0.801	**48.3**	**49.3**	**50.0**	**51.1**
0.97	1542.3	0.806	**48.9**	**50.0**	**50.7**	**51.7**
0.98	1558.2	0.811	**49.6**	**50.6**	**51.3**	**52.4**
0.99	1574.1	0.816	**50.2**	**51.3**	**52.0**	**53.1**
1.00	1590	0.822	**50.9**	**52.0**	**52.7**	**53.8**

For Wall-E(G1):

$V_r = \phi_m (V_m b_w d_v + 0.25 P_d) \gamma_g + [0.6 \phi_s A_v f_y d_v/s]$

$V_m = 0.16 (2-M_n/V_n d_v) (f'_m)^{\wedge 0.5}$

$\phi_m = \phi_s =$	**1**	
$f_m' =$	**17.0**	MPa
$\gamma_g = A_e/A_g =$	**0.39**	
$A_v =$	**9.0**	mm^2
$f_y =$	**202.0**	MPa
Vertical load corresp. to $V_r =$	**84000**	N
$s =$	**200**	mm
$b_w =$	**74**	mm
P_d = DL + Vertical load corresp. to $V_r =$	**88668.3**	N
$M_n =$	**133200000**	N.mm
$V_n =$	**111000**	N
$l_w =$	**1590**	mm
Experimental $V_r =$	111.0	kN

$d_v = d_{factor} * l_w$

			Reinf. factor			
d_{factor}	d_v	V_m	0.6	0.75	0.85	1
0.80	1272	0.697	**41.2**	**42.9**	**44.1**	**45.8**
0.81	1287.9	0.705	**41.9**	**43.6**	**44.8**	**46.5**
0.82	1303.8	0.712	**42.6**	**44.3**	**45.5**	**47.3**
0.83	1319.7	0.720	**43.2**	**45.0**	**46.2**	**48.0**
0.84	1335.6	0.727	**43.9**	**45.8**	**47.0**	**48.8**
0.85	1351.5	0.734	**44.6**	**46.5**	**47.7**	**49.5**
0.86	1367.4	0.740	**45.3**	**47.2**	**48.4**	**50.3**
0.87	1383.3	0.747	**46.0**	**47.9**	**49.2**	**51.0**
0.88	1399.2	0.754	**46.7**	**48.6**	**49.9**	**51.8**
0.89	1415.1	0.760	**47.4**	**49.3**	**50.6**	**52.5**
0.90	1431	0.766	**48.1**	**50.0**	**51.3**	**53.3**
0.91	1446.9	0.772	**48.8**	**50.8**	**52.1**	**54.0**
0.92	1462.8	0.778	**49.5**	**51.5**	**52.8**	**54.8**
0.93	1478.7	0.784	**50.2**	**52.2**	**53.5**	**55.5**
0.94	1494.6	0.790	**50.9**	**52.9**	**54.3**	**56.3**
0.95	1510.5	0.795	**51.6**	**53.6**	**55.0**	**57.0**
0.96	1526.4	0.801	**52.2**	**54.3**	**55.7**	**57.8**
0.97	1542.3	0.806	**52.9**	**55.0**	**56.4**	**58.5**
0.98	1558.2	0.811	**53.6**	**55.8**	**57.2**	**59.3**
0.99	1574.1	0.816	**54.3**	**56.5**	**57.9**	**60.0**
1.00	1590	0.822	**55.0**	**57.2**	**58.6**	**60.8**

For Wall-E(G2):

$V_r = \phi_m (V_m b_w d_v + 0.25 P_d) \gamma_g + [0.6 \phi_s A_v f_y d_v/s]$

$V_m = 0.16 (2\text{-}M_n/V_n d_v) (f'_m)^{\wedge 0.5}$

$\phi_m = \phi_s =$	**1**	
$f_m' =$	**17.0**	MPa
$\gamma_g = A_e/A_g =$	**0.39**	
$A_v =$	**9.0**	mm^2
$f_y =$	**202.0**	MPa
Vertical load corresp. to $V_r =$	**147000**	N
$s =$	**400**	mm
$b_w =$	**74**	mm
P_d = DL + Vertical load corresp. to $V_r =$	**151668.3**	N
$M_n =$	**96000000**	N.mm
$V_n =$	**80000**	N
$l_w =$	**1590**	mm
Experimental $V_r =$	80.0	kN

$d_v = d_{factor} * l_w$

			Reinf. factor			
d_{factor}	d_v	V_m	0.6	0.75	0.85	1
0.80	1272	0.697	**43.8**	**44.7**	**45.3**	**46.2**
0.81	1287.9	0.705	**44.5**	**45.4**	**46.0**	**46.8**
0.82	1303.8	0.712	**45.1**	**46.0**	**46.6**	**47.5**
0.83	1319.7	0.720	**45.8**	**46.7**	**47.3**	**48.2**
0.84	1335.6	0.727	**46.4**	**47.4**	**48.0**	**48.9**
0.85	1351.5	0.734	**47.1**	**48.0**	**48.6**	**49.5**
0.86	1367.4	0.740	**47.7**	**48.7**	**49.3**	**50.2**
0.87	1383.3	0.747	**48.4**	**49.3**	**50.0**	**50.9**
0.88	1399.2	0.754	**49.0**	**50.0**	**50.6**	**51.6**
0.89	1415.1	0.760	**49.7**	**50.6**	**51.3**	**52.3**
0.90	1431	0.766	**50.3**	**51.3**	**52.0**	**52.9**
0.91	1446.9	0.772	**51.0**	**52.0**	**52.6**	**53.6**
0.92	1462.8	0.778	**51.6**	**52.6**	**53.3**	**54.3**
0.93	1478.7	0.784	**52.3**	**53.3**	**54.0**	**55.0**
0.94	1494.6	0.790	**52.9**	**53.9**	**54.6**	**55.6**
0.95	1510.5	0.795	**53.6**	**54.6**	**55.3**	**56.3**
0.96	1526.4	0.801	**54.2**	**55.3**	**56.0**	**57.0**
0.97	1542.3	0.806	**54.9**	**55.9**	**56.6**	**57.7**
0.98	1558.2	0.811	**55.5**	**56.6**	**57.3**	**58.4**
0.99	1574.1	0.816	**56.2**	**57.2**	**58.0**	**59.0**
1.00	1590	0.822	**56.8**	**57.9**	**58.6**	**59.7**

APPENDIX B:

ADDITIONAL GRAPHS

In Chapter 5, tabular results for values calculated for the cyclic testing hysteresis envelopes were shown in Table 5.2. The results were also plotted, with a typical graph (Wall-G(L)) shown in Figure 5.3. The graphs for all walls are shown below:

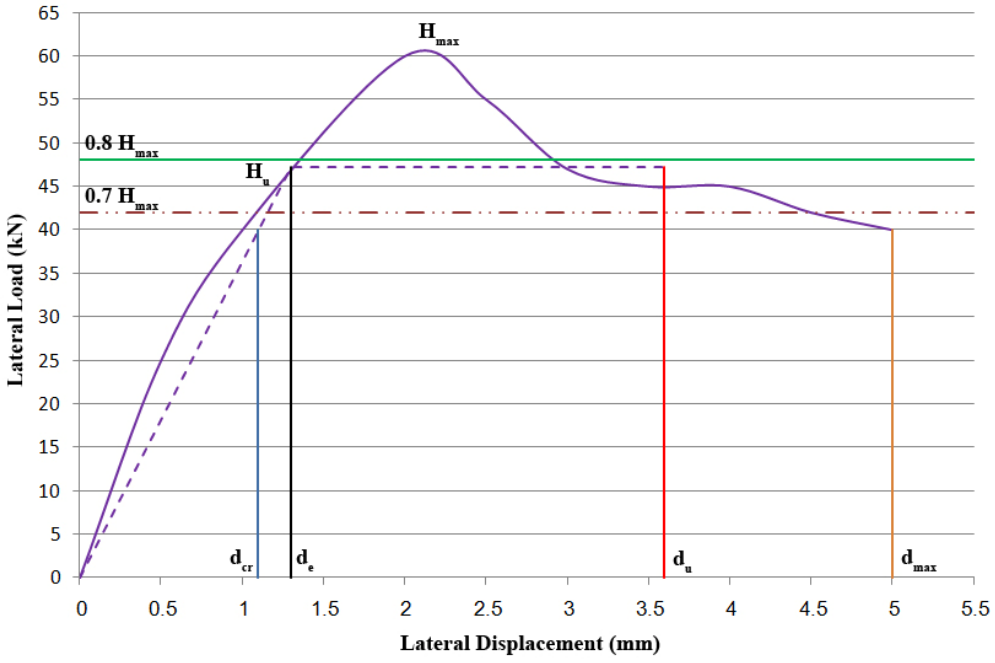

Figure B.1: Idealization of Experimental Envelope of Wall-C

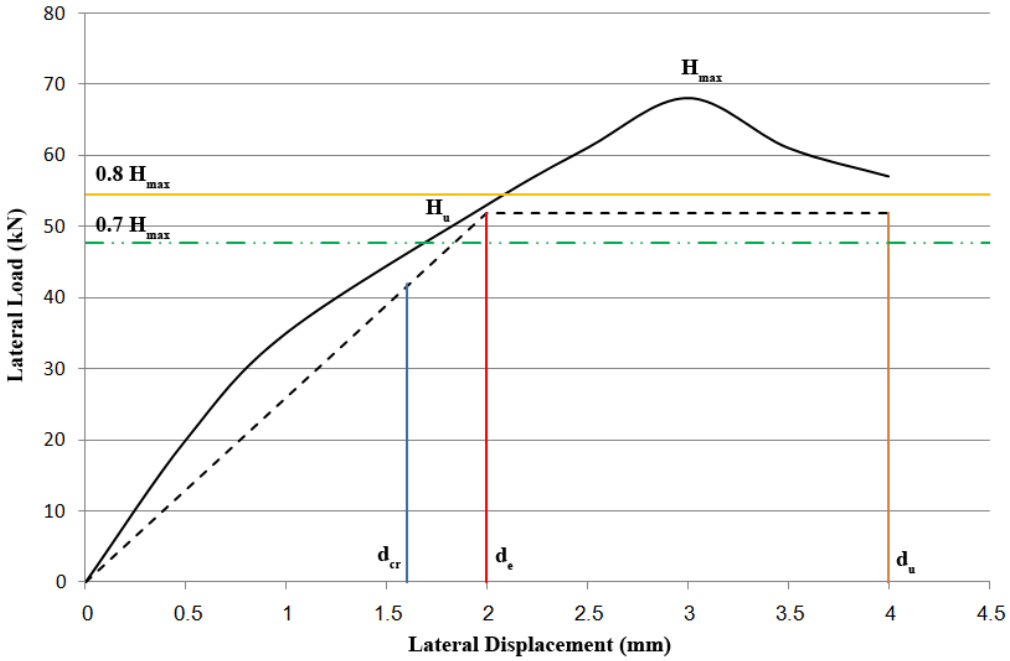

Figure B.2: Idealization of Experimental Envelope of Wall-S

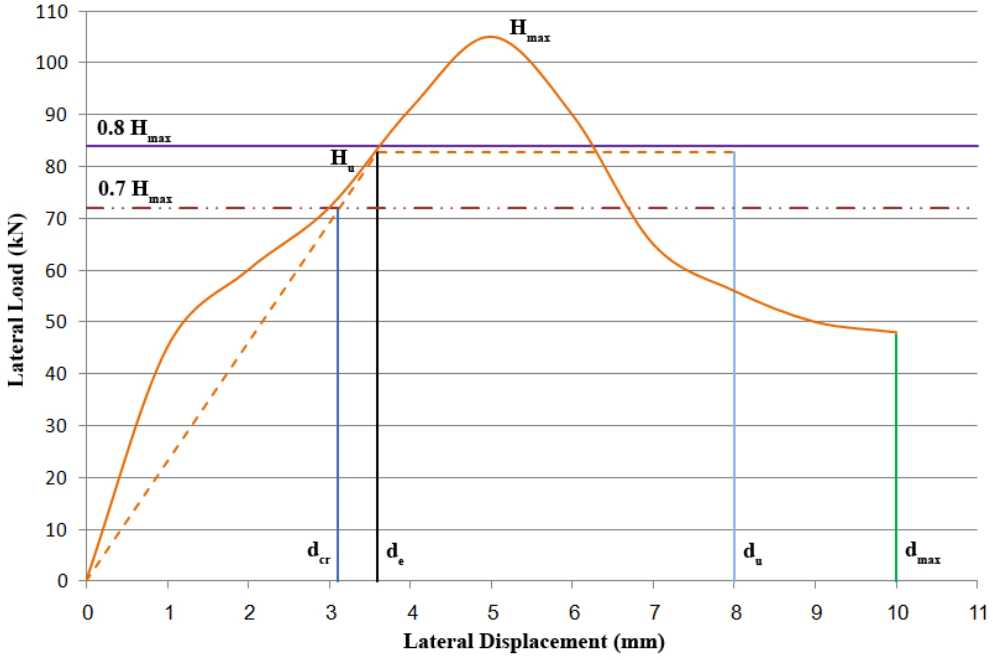

Figure B.3: Idealization of Experimental Envelope of Wall-G(G)

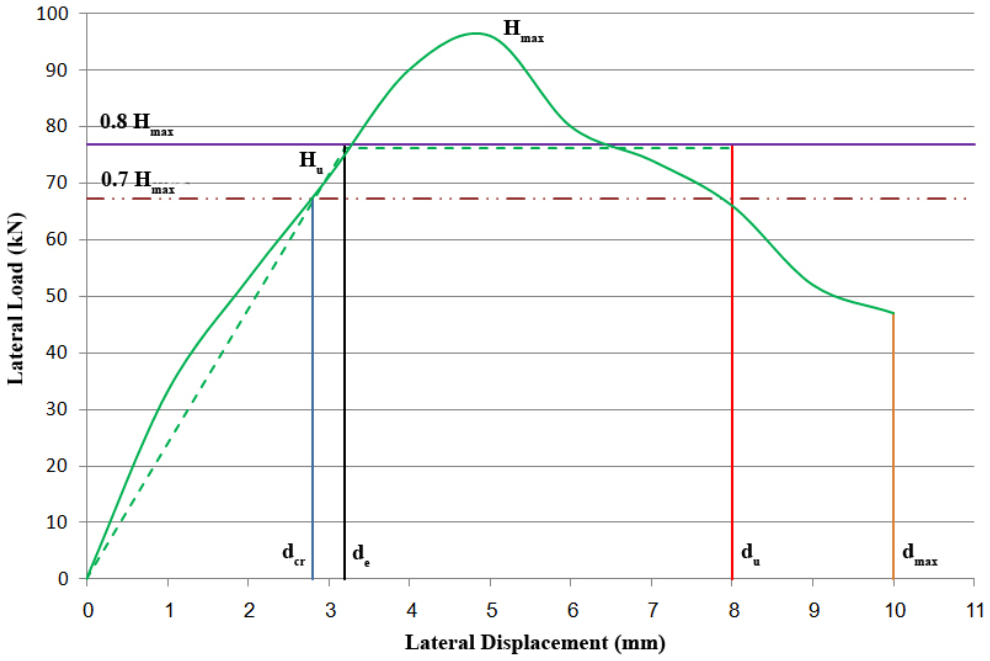

Figure B.4: Idealization of Experimental Envelope of Wall-G(L)

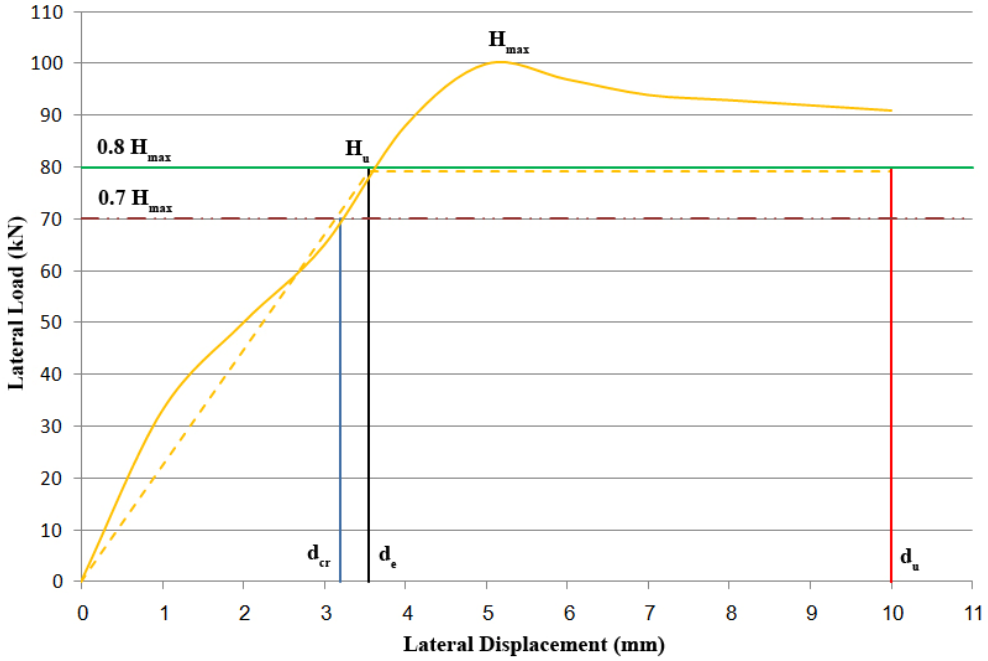

Figure B.5: Idealization of Experimental Envelope of Wall-G(T)

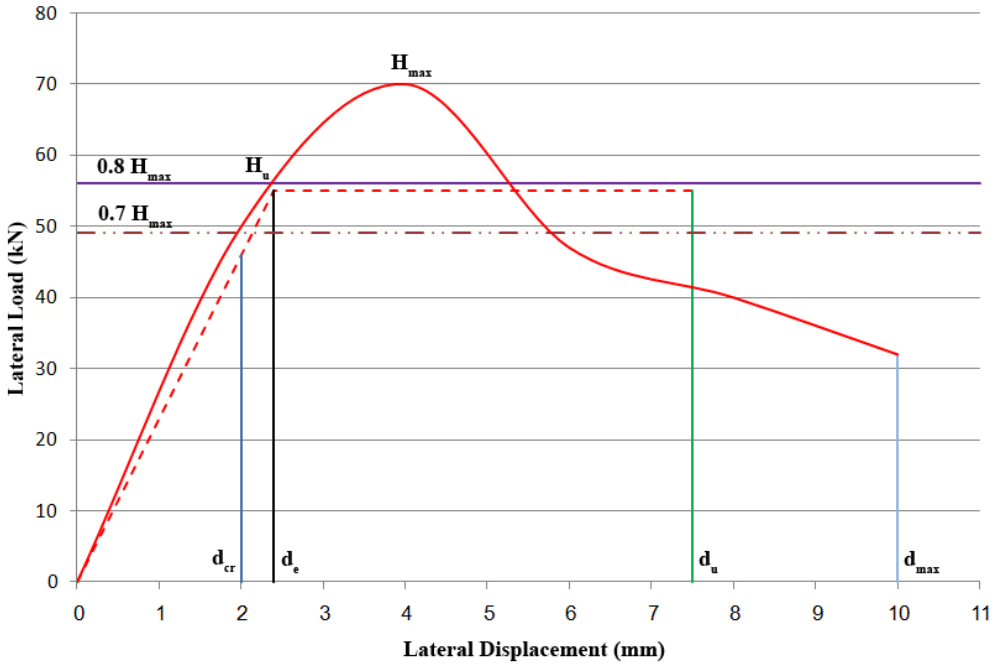

Figure B.6: Idealization of Experimental Envelope of Wall-E(L)

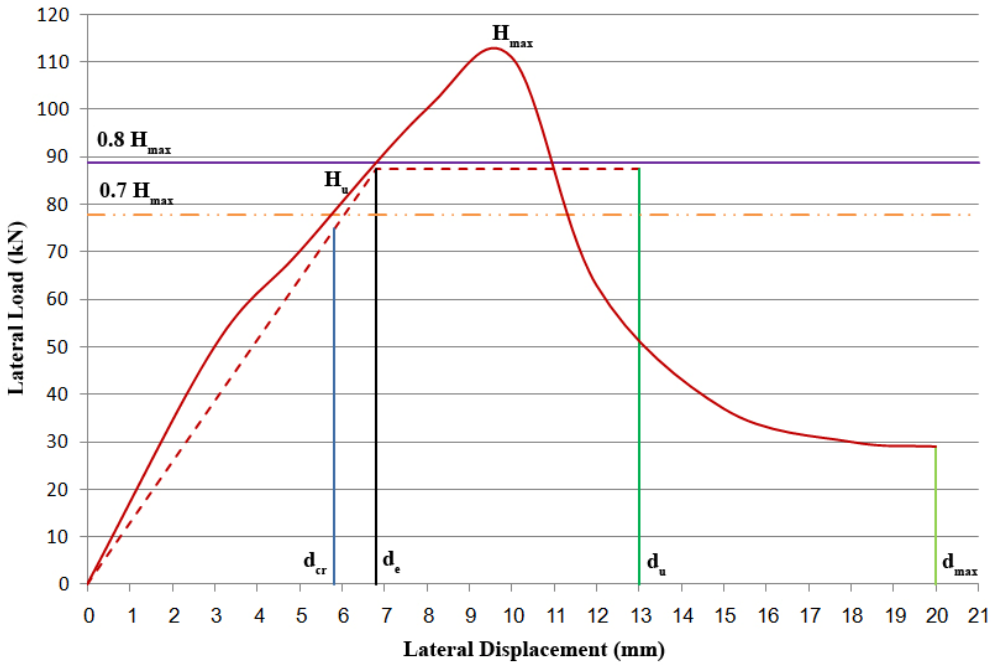

Figure B.7: Idealization of Experimental Envelope of Wall-E(G1)

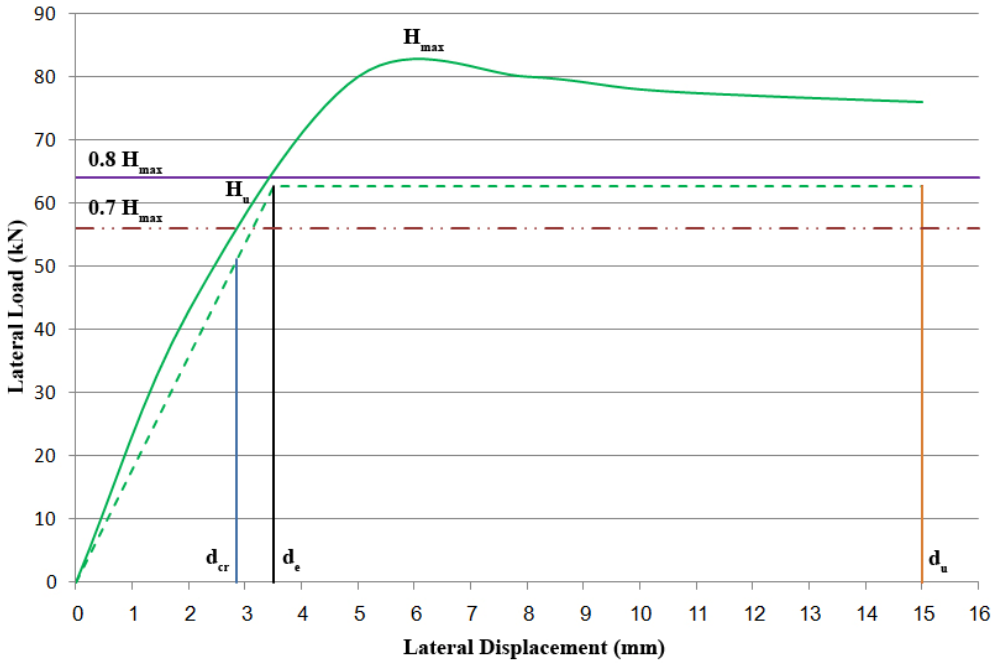

Figure B.8: Idealization of Experimental Envelope of Wall-E(G2)

APPENDIX C:

ADDITIONAL PHOTOS

Some additional photos for the test setup, constructing of walls and testing them are provided in this appendix. Most of the walls with pictures after testing are provided also.

C.1: Test Setup:


11/08/07 11:21 am

C.2: Constructing Walls & Prisms:

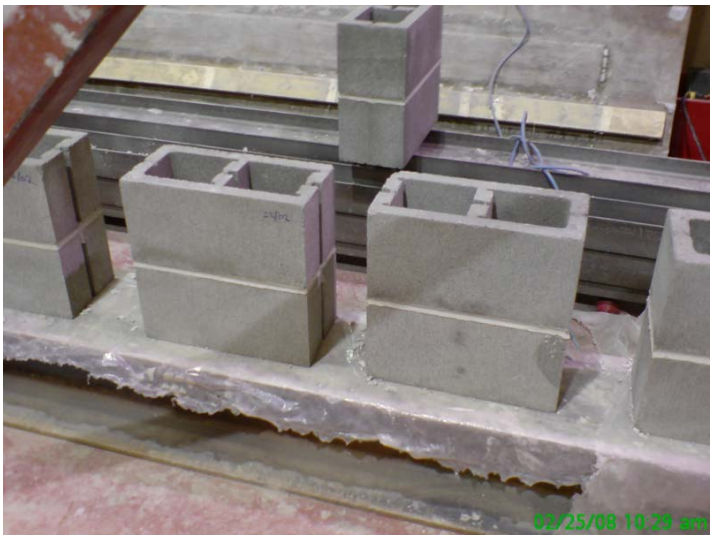
02/25/08 10:23 am


04/24/08 4:07 pm

C.3: Wall-C:

C.4: Wall-G(G):

C.5: Wall-G(L):

C.6: Wall-G(T):

C.7: Wall-E(L):

C.8: Wall-E(G1):